Master thesis : In silico model for Gel Aspiration-Ejection (GAE) process in the context of clinical peripheral nerve repair

Auteur : Pitti, Estelle
Promoteur(s) : Geris, Liesbet; 17064
Faculté : Faculté des Sciences appliquées
Diplôme : Master en ingénieur civil biomédical, à finalité spécialisée
Année académique : 2021-2022
URI/URL : http://hdl.handle.net/2268.2/14384

University of Liège - Faculty of Applied Sciences
UCL - UCL Centre for Nerve Engineering

In silico model for Gel Aspiration-Ejection (GAE) process in the context of clinical peripheral nerve repair

Master Thesis conducted by

Estelle Pitti

with the aim of obtaining the degree of Master in Biomedical Engineering

Supervisors :
Pr. Rebecca Shipley
Pr. Liesbet Geris

Academic Year 2021-2022

Acknowledgements

I would like to thank my supervisors from the UCL Centre for Nerve Engineering, Dr. Rebecca Shipley and Dr. James Phillips for their warm welcome, motivation and guidance. They made me feel like I was a member of their team. They allowed this master's thesis experience to be rich in discoveries and learning. I could develop myself in a stimulating, inter-disciplinary, and highly skilled environment. I will always be grateful for the opportunities they gave me.

This master's thesis was full of unpredictable challenges yet exciting and worthwhile. I would also like to express my sincere gratitude to Hanni Cheikh Sleiman, Simao Laranjeira Gomes, Maxime Berg, and Diana Cruz De Oliveira for their endless support, precious advise, interesting discussions, friendly attitude, and warm welcome. They all helped me in the mathematical models' exploration, the installation and discovery of FEniCS, the model implementation, troublesshooting, and scientific report writing.

In addition, I would like to thank the GAE team at the School of Pharmacy including Poppy Smith, Rebecca Powell, and Ryan Trueman for their expertise, their availability, and their enjoyable collaboration in the use and outcomes of the GAE process as well as laboratory visits. I am also grateful to the people in room 509, Sarah Abad Guaman and Giorgia Bosi who made me enjoy every single day at the office.

Furthermore, I'm grateful to Professor Liesbet Geris for her availability, her precious help, and her great motivation. She was always there to listen to me in difficult situations which helped me to keep a positive mindset and to find solutions to my problems. I'm also extremely thankful to Dominique Rensonnet for correcting the English language of this report and giving useful feedback on a complete reading.

Last but not least, I wish to thank my mother, Yannick Lejeune, my brother, Xavier Pitti, and my boyfriend, Enea Datei for their love and emotional support during this time but also all along my academic path. I also thank my flatmate Julia who was the loveliest person I met in London and my friends, Camille Pirard and Hazal Tosun for sharing with me those challenging but unforgettable moments during our Master's degree.

Thank you everyone !

Abstract

Damage caused to peripheral nerves is called peripheral nerve injury which affect about 300,000 people in Europe a year. Even if the peripheral nervous system has the ability to regenerate naturally, depending on the severity of the injury, this natural repair process is not efficient enough. In most cases, a complete recovery is prevented and leads to heavy consequences for the patient and for our society due to lifelong disabilities and refractory neuropathic pain. A promising peripheral nerve repair solution is the Engineered Neural Tissue (EngNT).

Current active research and literature works focus on identifying the optimal design of EngNT constructs to promote peripheral nerve repair. However, the manufacturing methods to produce this optimal design are also an essential factor. They consists in preparing the collagen gel then stabilising it, by expelling most of the fluid from the matrix to provide the EngNT with the desired structure and properties. There are two recent promising stabilisation processes which are the Plastic Compression (PC) and the Gel Aspiration Ejection (GAE). They are used but have not been properly studied yet leading to a lack of control and process understanding. That is why, this research work tries to provide an answer in three steps on how to build a primary mathematical model to initiate the control of the stabilisation methods to target the production of the desired EngNT design.

The first step is a background study to define the features to model. The second step identifies the mathematical model focus. Indeed, the combination of modelling and experiments is found to be a powerful tool to control the stabilisation methods. However, the current stage in this integrated approach is the implementation of a primary mathematical model which first needs a model focus. A dynamic analysis has been chosen to target the aspiration stage of the construct in the cannula during the GAE method. The third step implements the model and answers to its focus. The chosen model for this research shown that an important dissipation at the wall boundaries is present due to fluid friction during the aspiration stage of the GAE process. Excessive aspiration pressure involves high dissipation which leads to elastic failure of the construct in the cannula. In successful cases, the aspiration stage has not been found to be the origin of cell death while it might be the cause of cells' alignment on the top of the construct especially for small cannula diameters.

Through the three steps and the model implementation, this research work highlights the potential of modelling for the control of stabilisation methods, opens the path for longer studies and provides a first understanding of the aspiration process in the GAE method.

Keywords: Gel aspiration ejection, plastic compression,engineered neural tissue, peripheral nerve injury, mathematical modelling, stabilisation, collagen gel

Contents

List of Figures

List of Tables

Acronyms

ANS	Peripheral Autonomic Nervous System
ATMP	Advanced Therapy Medicinal Product
BC	Boundary Condition
BDNF	Brain Derived Neurotrophic Factor
CFD	Collagen Fibril Density
CFLD	Computational Fluid Dynamics
CNS	Central Nervous system
CPU	Central Processing Unit
DMA	Dynamic Mechanical Analysis
DMEM	Dulbecco's Modified Eagle's Medium
DRG	Dorsal Root Ganglion
ECM	Extracellular Matrix
EngNT	Engineered Neural Tissue
ENS	Enteric Nervous System
FEM	Finite Element Method
FLS	Fluid Leaving Surface
GAE	Gel Aspiration Ejection
GAE-EngNT	Gel Aspiration Ejection Engineered Neural Tissue
GF	Growth Factor
GMP	Good Manufacturing Practice
HHC gel	Hyper-Hydrated Collagen gel
HPA	Hydrophilic Porous Absorber
HUVEC	Human Umbilical Vein Endothelial
IASP	International Association for the Study of Pain
MEM	Minimum Essential Medium
MSC	Mesenchymal Steem Cell
NGC	Nerve Guidance Conduit
NGF	Nerve Growth Factor
NLSM	Nonlinear Laser Scanning Microscopy
NT-3 or NT-4	Neurotrophin 3 and 4
OCAM	Optical Contact Angle Meter

PC	Plastic Compression
PDE	Partial Differential Equation
PNI	Peripheral Nerve Injury
PNR	Peripheral Nerve Repair
PNS	Peripheral Nerve System
PPy	Polypyrrole
RAFT	Real Architecture For 3D Tissues
SEM	Scanning Electron Microscopy
TE	Tissue Engineering
TERM	Tissue Engineering and Regenerative Medicine
UTS	Ultimate Tensile Stress
VEGF	Vascular Endothelial Growth Factor

Chapter 1

Introduction

1.1 Peripheral Nerve Injury

1.1.1 Peripheral Nervous System definition

The nervous system is divided into the Central Nervous System (CNS) and the Peripheral Nervous System (PNS). The CNS is composed of the brain and the spinal cord. The PNS is defined as the nervous system outside the CNS meaning the network of nerves that connect the CNS to the sensory information [1]. More specifically, the PNS is composed of the different nervous structures involved in the sensory, motor and autonomic system [2]:

1. Cranial and spinal nerves, their sensory ganglia, and their peripheral ramifications, principally within striated muscles, skin, periosteum, bones, tendons, and joint capsules.

2. Peripheral autonomic nervous system (ANS) controlling the involuntary body functions and preparing for strenuous physical activity. This system has also a role at rest and for digestive functions thanks to the sympathic and parsympathic system.

3. Enteric nervous system (ENS).

4. Visceral afferent system which has vagal and spinal components that convey sensory information to the CNS from the viscera, glands, and blood vessels.

As defined above, the PNS consists of peripheral nerves. It is, therefore, interesting to develop the composition and hierarchical organisation of a single peripheral nerve as illustrated in figure 1.1 [3]. The first level of the hierarchy is the set of fascicles pooled together with blood vessels within a first external membrane called the epineurium around the entire nerve. The second main connective tissue layer is the perineurium which surrounds each fascicle. A fascicle can be defined as a group of axons surrounded by the endoneurium. Each axon is associated with Schwann cells and an extracellular matrix [2]. The third main hierarchical level is, therefore, the axonal units surrounded by the endoneurium. The two inner membranes are composed of collagen fibres and elastin. Indeed, the endoneurium and the perineurium are highly structured. They give the mechanical properties to the nerve, and maintain the intra-fascicle pressure. The epineurium, on the contrary, consists of dense irregular fibrous connective tissue and protects the nerve from stretching and injury [2] [3] [4].

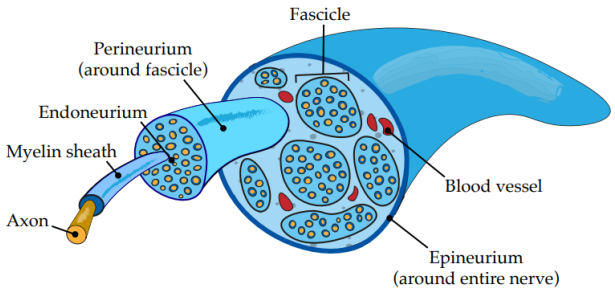

Figure 1.1: Peripheral nerve hierarchy (extracted from [3])

A neuron is composed of a cell body (soma), dendrites on one side, and the axon on the other side with the axon terminal. A peripheral nerve can be relatively long. For instance, the sciatic nerve runs all along the back of each leg from the spinal cord to the heel. Other common nerves are the sensory afferent nerves that carry sensory information from the periphery (dendrites) to the spinal cord (axon terminal). The cell bodies of those neurons are grouped together in the Dorsal Root Ganglion (DRG). At the UCL Centre for Nerve Engineering, researchers work with rat sciatic nerves or sensory nerves passing by the DRG.

The axon of peripheral nerves is accompanied by supporting cells and an Extracellular Matrix (ECM). The main supporting cells of the PNS are the Schwann cells. Those are the principal glial cells of the PNS. They are involved in many important features of the nerve such as the conduction of nervous impulses thanks to the production of myeline for myelinated neurons, nerve development and regeneration, trophic support for unmyelinated axons, production of the nerve extracellular matrix, modulation of neuromuscular synaptic activity, and immune system response [5][3]. An ECM can be defined as a complex network of macromolecules where all the components are linked together to form a structurally stable composite. It provides the mechanical properties to the tissues and is a reservoir of growth factors, bioactive molecules and other elements controlling the behaviour and characteristics of the cells in the tissues [6]. Within the endoneurium, the fibronectin, collagen fibres, and laminin from the ECM allow the axonal extension and act as a guide for nerve regeneration [7].

1.1.2 Peripheral Nerve Injury

A Peripheral Nerve Injury (PNI) is damage caused to peripheral nerves. Unlike the CNS, the PNS is not protected by the skull or the bones. It is directly exposed to external forces that create damage when those forces exceed the peripheral nerve threshold [8]. According to Gu et al, 2011 in Europe, 300,000 people suffer from PNI/year which represents a relatively high incidence [8]. Indeed, those injuries occur in around 1.5 to 3% of trauma patients [8]. Young males under 50 years old are the most targeted [9].
The causes of PNI are varied and occur in many different contexts. The most common cause is motor vehicle accidents followed by sports injuries and lacerations from metal sharp objects or machinery [7]. Other important causes of PNI are surgical procedures, falls and diabetes as well as gun shots, stabbing incidents, and military activities [3][8].

The consequences of PNI are harsh for the patients and their family as well as for the society. An injury in the peripheral nerves results in permanent loss of function. The consequences are lifelong disabilities in addition to refractory neuropathic pain which is defined by the International Association for the Study of Pain (IASP) as 'pain caused by a lesion or disease of the somatosensory nervous system'[10][11]. It is also more likely to have other pain-related conditions such as fibromyalgia and osteoarthritis [3]. The pains and dysfunctions caused by PNI often bring distress, anxiety, depression, and sleeping difficulties which considerably impact the patients' quality of life as well as their social life. The quality of life of the relatives is also impacted with a lot of socioeconomic implications. The cost of the long-term treatment and loss of productivity of the patient also has a high cost on society. A study in Sweden showed that an employee who has experienced a median nerve injury costs approximately 51,238 euros due to loss of productivity and health care fees with a median sick leave of 210 days [3].

1.1.3 Classification of injuries

Two main classification systems defines a scale of the severity of peripheral nerve injuries. These classification systems define the level of dysfunction and the possible regeneration process. Both classification systems are presented in table 1.1 extracted from Celine Kayal's publications [2] [8] [12]. The Seddon system emerged in 1943 during the second World War and divides the PNI into three categories; Neuropraxia, Axonotmesis, and Neuromesis [7][8]. The Sunderland system was implemented in 1951 and expands the classification. As a result, Sunderland proposes five types of peripheral nerve injuries (Type I to V) distinguishing the categories of PNI requiring different repair procedures and the potentiality of new techniques [7][8].

Seddon	**Sunderland**	**Description**	**Recovery**
Neuropraxia	Type I	Axon is intact Local myelin damage No degeneration process	Recovery within days without surgery
Axonotmesis	Type II	Axon affected only Degeneration process distal to the injury site	Usually full recovery
Neuromesis/ Axonotmesis	Type III	Axon and endoneurium affected Degeneration process distal to the injury site	Incomplete recovery (60-80%)
Neuromesis/ Axonotmesis	Type IV	Axon, endoneurium and perineurium affected Axon continuity lost Degeneration process distal to the injury site	Recovery failure Require surgical intervention
Neuromesis	Type V	Complete disruption of the entire nerve trunk Epineurium also disrupted Degeneration process	Require surgical intervention

Table 1.1: Classification systems of PNI (based on [2] [7] [8] [12])

1.1.4 Process of nerve injury, degeneration and natural regeneration

The PNS has the potential to regenerate itself differently than the CNS. Instead of repairing itself with scare tissues, the PNS can promote axonal growth and regenerate the nerve tissue. It is important to know the different elements that promote or prevent this nerve regeneration process after a lesion. For this purpose, based on different literature readings [2][7][8][14], I have created a diagram, in figure A.2 to explain the different events occurring after a peripheral nerve injury . As indicated in the legend, the red boxes indicate all the events involved in the trauma of the nerve due to the injury, and the green boxes correspond to the events inducing the regeneration of the nerve. It is clear that the diagram is a rough summary. They may be more or fewer impacts, or may occur at different times depending on the type of injury and the context of the lesion. The team at the UCL Centre for Nerve Engineering works on identifying the components (cells, growth factors, gene regulation, etc), their quantities, and their timing to optimise the nerve regeneration process. This is not the focus of my research work but some general key elements can still be highlighted. Firstly, the Wallerian degeneration is an axon death program distinct from apoptosis. It is a degeneration process inducing morphological and biomechanical changes at the distal side of the nerve injury. It aims at preparing the environment for axonal regeneration [2] [13] [14]. Secondly, the Bunger bands are highly aligned fibres formed by the basal lamina of the Schwann cells promoting the regeneration by guiding the axon and the growth cones to bridge the gap between the proximal and the distal ends of a peripheral nerve after a lesion [14]. And lastly, the crucial roles of Schwann cells are the development of Bungner bands as well as the proliferation, and secretion of adequate Growth Factors (GF) [14].

Depending on the type of injury as discussed in the previous section, the regeneration will be stronger or weaker compared to the trauma and this will impact the issue of the injury event. If the gap is too wide, the inflammatory components and the scar tissue dominate and prevent regeneration. This will lead to the death of the nerve in the long term and the atrophy of the muscles that are innervated by this nerve [8] [15]. Another case of failure of the nerve regeneration is when the physiological regeneration process is too slow to allow the complete nerve repair before the muscles atrophy after 12 to 18 months without being stimulated [8] [15]. Without a functional distal part, the neuronal cell bodies of the peripheral nerve die in the long term. In some cases, the nerve succeeds to regenerate leading to the recovery of some motor or sensory outcomes. However, the axon sprouts are most often misdirected and lead to inappropriate re-innervation. The consequences are limited fine motor control, disturbed sensory localisation, and pain [8] [15]. In sum, the success of the physiological regeneration process is limited leading to poor functional recovery. The main reasons for the limited repair process are a lack of mechanical support, a misappropriate surrounding environment and guiding cues as well as underlying diseases such as diabetes [8] [15].

1.1.5 Repair solutions

For peripheral nerve injuries that do not allow complete recovery (type II-type IV), a repair solution can be proposed although, currently, there is no best solution allowing the completely recovery from the lesion. We can distinguish three types of repair interventions depending on the context and the severity of the injury.

1. For small gaps (<1cm), a surgical intervention is proposed to reconnect the proximal and distal ends. Two types of surgery can be proposed; end-to-end and end-to-side. The cons of this solution are the atrophy of the muscles or the drop of the neurotrophic factors before the surgery, the long rehabilitation period, and random repairs through the injured site [7].

2. For larger gaps (1cm < gap length < 15cm), autologous nerve graft or autograft are currently the most successful repair solutions. Grafts have the advantages of being easily available and immunogenetically inert scaffolds providing mechanical support, growth factors, supporting cells and chemical cues of a peripheral nerve. However, the downsides are numerous. We can mention a double surgery, the potential morbidity of the patient, the limited nerve supply, the mismatch of the nerve sizes and sites and the risk of painfull neuroma. In addition, peripheral nerve grafts still have unsatisfactory functional recovery outcome while consequences of the surgery can bring new difficulties such as additional nerve and tissue damage at the donor site and additional pain [3][7].

3. There are some alternatives to autologous nerve grafts such as nerve transfers and gene therapy [7].

1.2 Tissue engineering

1.2.1 Basic principles of Tissue Engineering

Tissue Engineering and Regenerative Medicine, also named TERM, is the discipline of fabrication of biological replacement solutions for damaged organs as an alternative to grafts [14]. The Tissue Engineering (TE) principle is explained in figure 1.2 [14]. A scaffold is used as a supporting structure in which cells from a culture are seeded. After the addition of specific growth factors, the *in vitro* culture is inserted *in vivo* allowing nerve regeneration. The three key elements for TE are [14]:

1. Scaffold

2. Seeded cells

3. Growth factors

The scaffold provides mechanical sustenance and the right morphology for cell proliferation. It also needs to be mechanically resistant to protect the regeneration process while matching the mechanical and physical properties of the native nerve. The scaffold can be made with synthetic material or can be taken from biological tissues. In some cases, scaffolds are not used and cells arrange by self-organisation.
Concerning the seeded cells, in some cases, no cells are used and the tissue engineered matrix is acellular. However, the lack of cells has been shown to limit the regeneration

capacity of the acellular nerve construct [16]. Indeed, seeded cells are crucial for bringing biochemical cues to the scaffold to promote the regeneration [16]. As shown in section 1.1.4, it is an entire study by itself to select and optimise the seeded cells that need to be inserted into the scaffold. Among others, supporting cells are interesting glial cells providing ECM homeostasis, neuronal information processing, protection, and axonal regeneration support [8]. The principal glial cells of the PNS are the Schwann cells playing a key role in promoting axonal regeneration by changing its phenotype as explained in section 1.1.4. The different seeded cells used in the GAE-EngNT constructs produced at the UCL Centre for Nerve Engineering will be presented later on in section 2.2.4. As shown in figure 1.2, the seeded cells come from cellular culture. Culture of cell lines are preferred because of a better availability and the ease to use [17]. Starting from few cells, a large volume can be produced in a simple and controlled way which is really convenient for experimental research [17]. It is also appreciable to control cell lines differentiation during the cell culture aiming at producing a volume of cells similar to a targeted cell and with a specific phenotype when inserted in the tissue engineered construct. On the contrary, primary cells are harvested from a donor and so are less favourable than cell lines when it comes to the PNS as harvesting primary cells causes donor morbidity.
The last component of TE are the GFs which are neurotrophic factors most of which being small proteins and peptides produced by specific cells, for instance, Schwann cells. Those factors promote the growth and cell survival response [18]. Four categories of GFs can be mentioned for the PNR [18]:

1. Nerve growth factor (NGF): Gradient of NGF modulates neuronal behaviour and neurites respond.

2. Brain derived neurotrophic factor (BDNF): it promotes the survival of motoneurons and the growth of motor as well as sensory neurons.

3. Neurotrophin 3 and 4 (NT-3 and NT-4): they act respectively for the maintenance of the adult nervous system and the regeneration process in serious PNI.

4. Vascular growth factor: The most important one is the Vascular endothelial growth factor (VEGF). It promotes vascular permeability and basement membrane degradation during the initial stages of angiogenesis. It also acts as a mitogen for endothelial cells and affects the rate and directionality of endothelial cell migration.

The delivery method and the spatiotemporal arrangement of GFs in the matrix are crucial. A lot of research is still ongoing in this field [8].

Different combinations of these three key elements are possible with different shapes, types and arrangements of scaffolds, with or without one or several populations of seeded cells, and with different combinations of GFs. There is still a lot to explore and to optimise in order to promote nerve regeneration and to obtain successful outcomes [8][14]. For now, the TE solution is not efficient enough yet. The gold standard in clinical use is still the autologous nerve graft or autograft. However, the potential of TE is high and is currently the subject of active research [8].

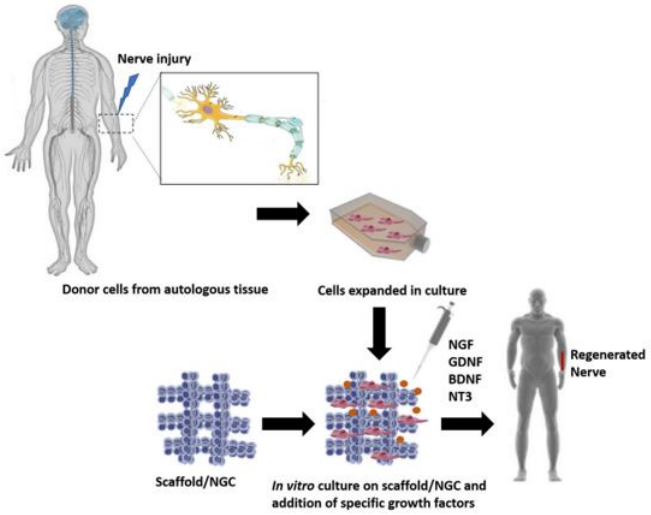

Figure 1.2: The classic Tissue Engineering model (extracted from [14])

1.2.2 Nerve Guidance Conduit

The Nerve Guidance Conduit (NGC) is a tubular structure used as a TE scaffold and designed to be implanted into the injury site and to guide the neurite growth from the proximal to the distal side of the axon to bridge the lesion gap. NGCs aim at providing an adequate mechanical and chemical support for the nerve regeneration by mimicking the architecture of the nerve with the properties of the ECM [8]. Furthermore, NGCs need to be compatible with *in vivo* implantation meaning being biocompatible, biodegradable, permeable to gas and nutriments, and having appropriate stiffness and flexibility [8].
The materials of the NGCs range from synthetic polymers such as PCL and PLGA [8] to biopolymers such as type I collagen and fibrin [14]. The shape is usually tubular but different shapes can also be designed for different purposes. For instance, the creation of density gradients or the ability to enrapture drugs and GFs has already been implemented [8]. The basic NGC is a hollow conduct providing space for free nerve regeneration and supporting structure aligned in one direction to promote the axon regeneration longitudinally. The process of nerve regeneration in the hollow NGC is illustrated in five steps in figure A.1 taken from the Cristiana R. et al publication [14].

Alternatives from hollow NGCs to improve the efficacy in case of large gaps can be built by adding filler materials. Additionally, different designs of the tube can be used providing more specific chemical and physical cues for the regeneration. Examples of different options such as hydrogel filling, freeze-dried technique, unidirectional aligned micro- or nano-filaments, magnetically aligned cells and fibres, and multi-lumen can be found in the literature [14] and [8]. Illustration of NGCs can be found in figure 1.3 from Huiquan Jiang's publication [75].

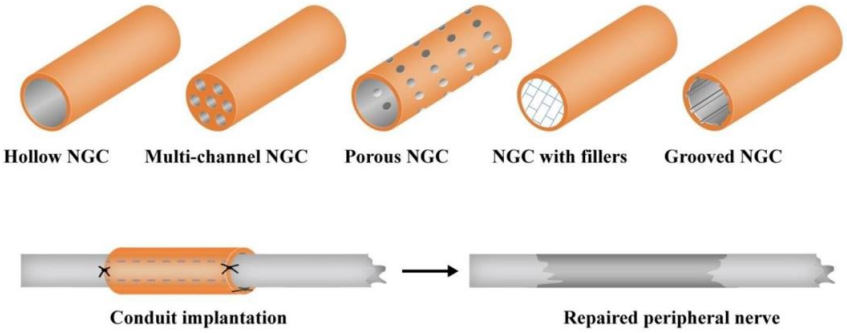

Figure 1.3: Nerve Guidance Conduits (extracted from [75])

1.2.3 Engineered Neural Tissue

Another strategy of TE is the implementation of an Engineered Neural Tissue (EngNT). Used as a scaffold, the EngNT consists of an aligned collagen matrix hosting columns of elongated therapeutic cells, typically Schawnn cells [19]. The aim of this living structure is to support and guide the axonal regeneration thanks to a matrix that resembled natural endoneurium (aligned fibrils of type I collagen) and elongated aligned Schwann cells with pro-regenerative phenotype or other important seeded cells promoting the regeneration [20]. An illustration of an EngNT from James B. Phillips 's publication [19] is shown in figure 1.4.

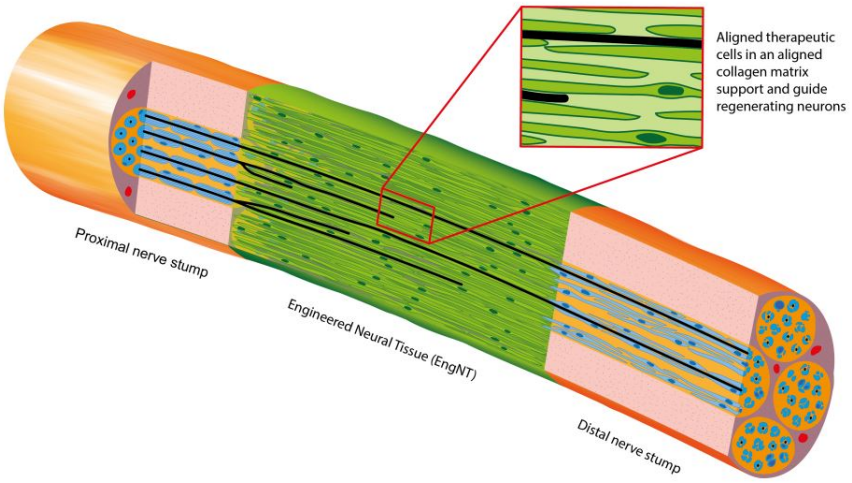

Figure 1.4: Structure of an EngNT (extracted from [19])

This engineered neural tissue has large scientific, commercial, and clinical potentials despite some obstacles to clinical applications at the current stage [19]. Indeed, EngNT is now well known, pre-clinical efficacy has been proved and active research is still ongoing [19]. The main benefit of EngNT is its capacity of creating the aligned cellular and extracellular matrix architecture associated with nerve grafts by mimicking the ECM anisotropy which is critical for the nerve [20]. EngNT would fill a gap for PNR when autografting is failing for long gap injuries. EngNT could also be used for short gap injuries where autografts are not justifiable or where expertise, infrastructure, and time are insufficiently available to allow autografts [19]. Furthermore, this potential can be

easily extended to the treatment of optic nerve and spinal cord injury. Indeed, EngNT can be used in combination with a range of cell types and hydrogel matrices, providing a versatile approach for clinical use [19]. Concerning the commercial potential, the low number of constructs produced for the early clinical trial stage can be easily scaled-up and automated thanks to the use of basic components of EngNT such as - Human Umbilical Vein Endothelial Cells (HUVEC), collagen type I, and simple production methods. The expansion of the Advanced Therapy Medicinal Product (ATMP) sectors with rising knowledge, use and abilities such as cryopreservation, makes EngNT suitable for clinical-grade manufacturing [19].

The two main components of the EngNT are a collagen type I hydrogel and some seeded cells. As explained just above the tissue is versatile and will be slightly different depending on the manufacturing methods or on the seeded cells used.
To manufacture those Engineered Neural Tissues, the desired collagen hydrogel needs to be produced using essential medium (Sigma-Aldrich), collagen type I (for instance type I rat tail collagen), sodium hydroxide and the cell culture [8][21]. Afterwards, the gel needs to be cast in a specific mould or well-plate. After approximately 30 minutes, the gel sets but it is still hyper-hydrated. Indeed, the solution in the mould or the plate contains more than 95% of fluid [22]. One of the main consequences is the change of the mechanical properties compared to the ECM matrix. Indeed, the collagen concentration appears to be extremely low (less than 2 mg/mL) which affects, among others, the stiffness of the matrix. The main goal of the EngNT to mimic the key mechanical features of the endoneurium to match the hosted nerve tissue is compromised [20][22]. Additional consequences of the hyper-hydration are the difficulty to shape the EngNT into the peripheral nerve repair geometry and the instability of the material making it difficult to manipulate and keep its integrity [20][22]. Therefore, stabilised methods need to be implemented to expel the majority of the fluid in the hydrogel and shape the stabilised gel into a construct for PNR.
The first technique would be to create cross-links using some enzymes or irradiation. Another way is to use electrospinning. However, both methods alter the structure of the matrix and add signaling. This causes the change of the matrix properties and makes it hard to understand and predict a particular density gradient or neurite behaviour for the construct [8]. The two promising methods to produce EngNT are the Plastic Compression (PC) and the Gel Aspiration Ejection (GAE). The first one applies simply a compressing force on the top of the hydrogel expelling the fluid and deforming in a plastic way the construct into sheets which are then rolled into tubular structures [20][22][23]. On the other side, the GAE method consists in aspirating the hydrogel into a narrow cannula thanks to an angioplasty device and then ejecting the GAE-EngNT construct out of the cannula reversing the pressure in the syringe [21][24].

This thesis will explore in detail these two manufacturing techniques as well as the collagen gel and the different seeded cells used. Indeed, the EngNT for PNR is a recent, promising, and active research field on which the UCL Centre for Nerve Engineering is currently working and to which I added my little contribution.

1.3 Motivation

Peripheral nerve injuries have a relatively high occurrence but have especially a high cost for the patient, the relatives, and the entire society. The research for PNR is particularly important to allow the recovery of the functionalities and the autonomy of the patient. It is also important to reduce the pain and to enable the patient to recover some productivity to start again his working life. In this way, PNR can have a big impact on the health and well-being of 300,000 patients but also on their relatives, and the entire society. The potential of the PNR field is high thanks to the ability of the PNS to regenerate naturally. The process of repairing the lesion of a peripheral nerve does not start from scratch but the process needs to be promoted and optimised. There are already different solutions but with significant drawbacks and limited to short lesions. This scientific gap makes way for the high potentiality of TE.

The UCL Centre for Nerve Engineering aims at finding solutions to clinical nerve repair problems. The research group is launched in 2017 by Professors James Phillips and Rebecca Shipley. It brings physics and life sciences together to engineer new solutions in Tissue Engineering for repairing nerve lesions. The collaboration between life scientists and modellers enables the study and the design of NGCs. More recently, the research team has been focusing its work on EngNTs. Starting from the collagen gel preparation, two stabilisation methods are possible to produce the EngNT construct. This workflow is illustrated in figure 1.5. Most of the current active research and literature focus is studying the EngNT design to optimised its skills to promote nerve regeneration (second step indicated in orange in figure 1.5). However, the production process to obtain the desired design of EngNT is also important in the workflow and proper dedicated studies are missing. The need to control those techniques in order to target the production of the desired EngNT design arises.

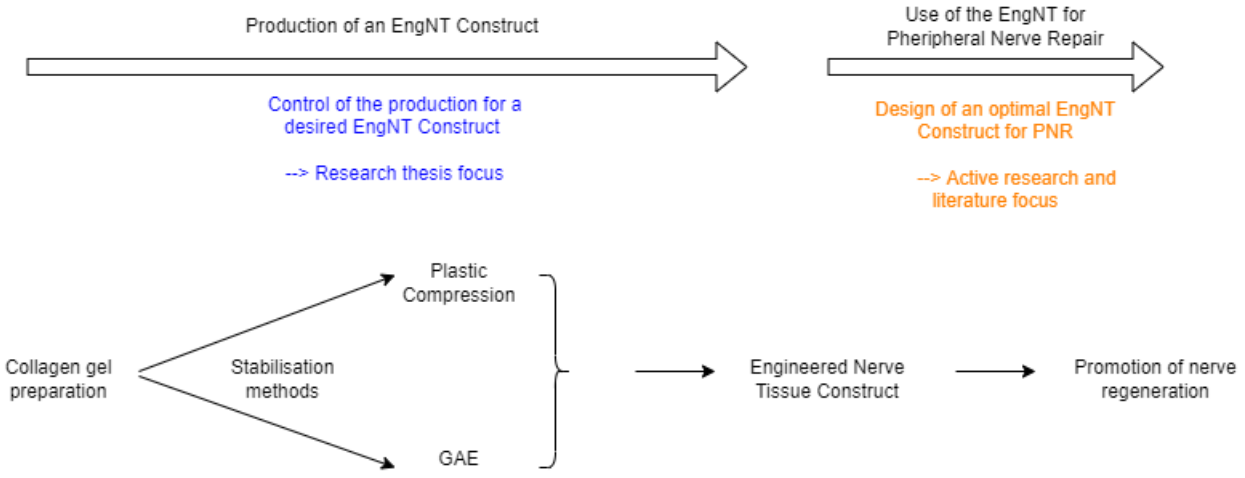

Figure 1.5: Workflow of the production of EngNT constructs

Therefore, this research work is studying the potential of the two stabilisation methods, identifying the challenges, and introducing the need for a mathematical model to control those production methods. Indeed, knowing the design that allows optimal nerve repairs is an important focus. However, the way to produce this desired design and the certitude of the impact of the production method on the properties and the quality of the construct is also fundamental. This current situation has lead to the formulation of the research question for this research work:

"How to build a primary mathematical model to initiate the control of the stabilisation methods to target the production of the desired EngNT design?"

1.4 Organisation of the thesis

The identification of mathematical model needs, the construction of a framework for *in silico* models, and the proposal of a primary mathematical model of the GAE method have been the targets of this research work. Starting from scratch, with the limited time period allotted for this research work, the proposed model is far from representing the entire experimental reality nor giving a complete answer to the need to control the production methods. However, it allows to open and give first insights into the challenging topic of understanding and optimising the EngNT especially processed by the GAE method. The PC stabilisation method is part of the investigation as it is one of the manufacturing techniques. However, this research work put the focus on the GAE method which is the most recent and most promising technique currently used at the UCL Centre for Nerve Engineering. To answer the research question formulated previously, this research work follows the organisation presented in figure 1.6.

The first chapter was developed here above and presented the context of Peripheral Nerve Injuries and Engineered Neural Tissues. It is important to introduce the reasons and the importance of the development of EngNTs as well as the existing alternatives. From this introduction arises the presentation of the two stabilisation methods. A quick state of the art motivated the focus of this research work and brought the research question. Entering the core of the project to answer this question, chapter II presents the experimental context. A background study of the collagen gel, its mechanical properties, the PC method, and the GAE technique is conducted. This chapter aims at defining the framework essential to be able to develop mathematical models on the stabilisation methods. Afterwards, the third chapter develops the need for mathematical models as well as some ideas for future longer studies of mathematical models coupled with specific experiments to improve the control of the stabilisation methods. As the focus has been put on the GAE technique, the first part of the chapter shows the specific experimental challenges of this process and the potential of mathematical modelling. In addition, the current stage for *in silico* representation and the future perspective of integrated approach strategy is presented. After that, an explanation of the primary model focus for this research work is provided. The second part of the chapter explores rapidly mathematical modelling ideas for the PC method. The fourth chapter presents the primary model for the GAE process. Since no *in silico* representation can be found in the literature, the model proposed in this chapter is a primary model entirely implemented. Therefore, the method with the development of the theoretical framework is presented followed by the results. A discussion

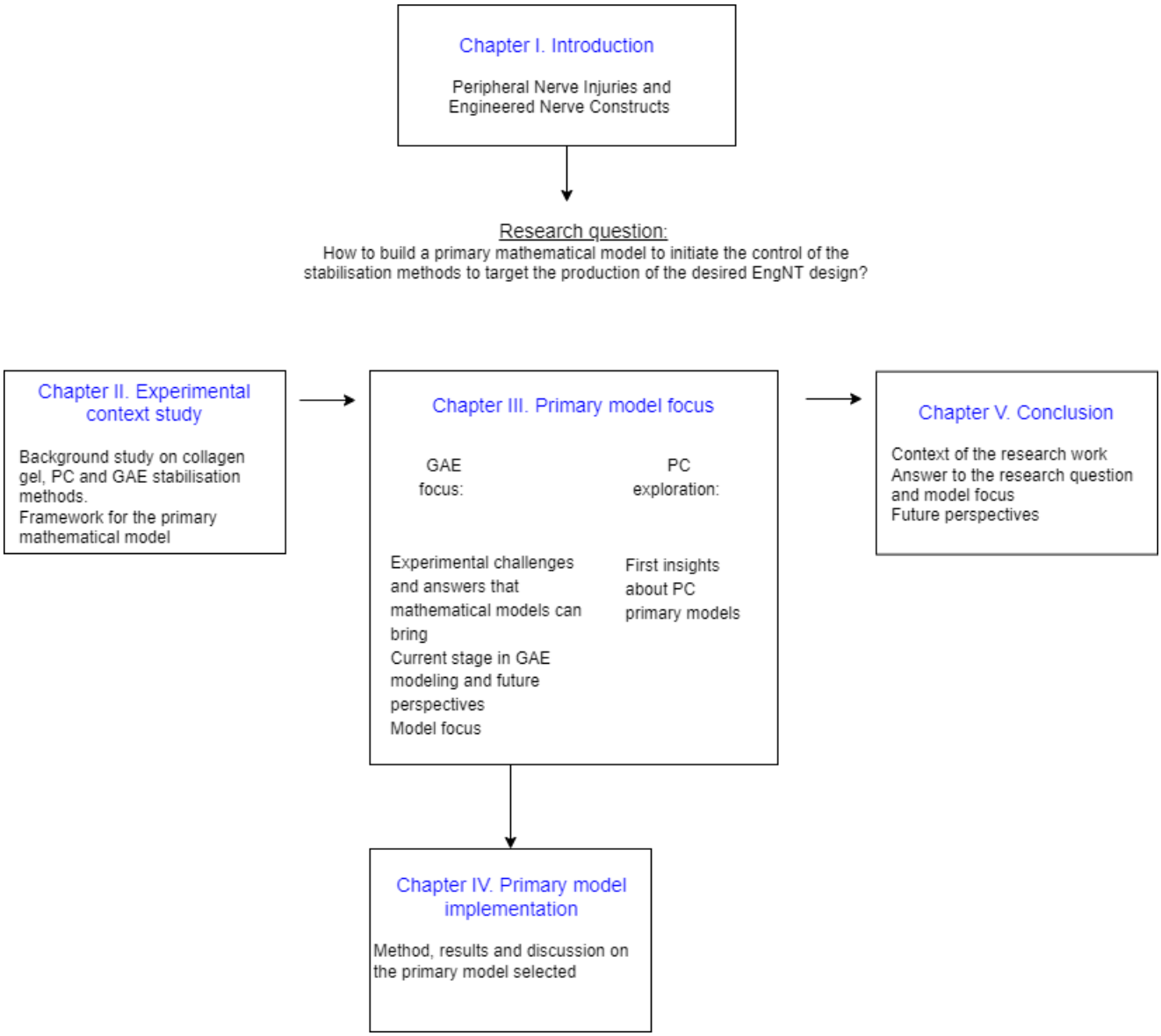

Figure 1.6: Organisation chart for the research work

on the results and the comparison with the experimental features notified in the previous chapters are performed in order to answer the model focus formulated in chapter III. The limitations and future developments are also discussed. Finally, a conclusion closes the research work by providing an answer to the research question. A conclusion on the primary model focus is also provided. In addition, the context of the research work and the important highlights are reminded before a quick discussion on future perspectives.

Chapter 2

Experimental context study

The first step to build a primary mathematical model for the stabilisation methods of EngNT constructs is to study the collagen gel and the two stabilisation processes. The modelisation of the production methods of EngNT involves the modelling of the main component of the construct which is the collagen hydrogel. Therefore, a preliminary study of this hydrogel and its mechanical properties is necessary. For this purpose, an overview of the mechanical tests is useful in order to understand the characterisation of the collagen gel exposed in the second section. The different mechanical tests and the main quantities which define the mechanical properties of a material are presented before being applied to the collagen gel of EngNT. The section on mechanical tests is followed by a detailed study of the collagen hydrogel. A description of the choice of collagen type I hydrogel and its composition is provided followed by an investigation on the mechanical characteristics of this gel. A quick words is also dedicated to the seeded cells and their behaviour as they are influenced by the mechanical characteristics of their substrate, the collagen gel. Afterwards, the Plastic Compression method is explained as well as its potential, limitations and different techniques. The last section of this chapter explains the GAE process, the equipment and the current variability in use and failure cases. It is important to identify the current stage in the use of the method and to report its outcomes.

2.1 Mechanical test

2.1.1 Class of material

Mechanical tests are important to study the response of a material to different applied loads. Depending on its behaviour, the material will be identified in different classes [8]:

- An elastic material has the characteristic to recover its shape and size after loading. This is due to the storage and restitution of the energy during and after loading. The tendency to resist deformations within the elastic range is called the elastic modulus or the Young's modulus. This quantity is denoted by E and characterises the stiffness of the material. It is defined as $E = longitudinal\ stress/strain$.
  - The stress-strain curve of linear elastic materials is therefore linear.
  - In the case of a non-linear stress-strain curve, the material is considered hyper-elastic if it shows three characteristics. It has a highly non-linear stress-strain curve, it responds to large elastic deformation, and it is nearly incompressible.

Elastomers, rubbers, and some biomaterials such as muscles, are typically identified in this class [25].

- Viscoelastic material can store and dissipate energy. The dissipation enables the semi-permanent change of shape with some elastic and plastic deformation. The stress-strain curve depends on time.

Different loading conditions enable the identification of different material properties. To fully characterise a material, different mechanical tests need to be performed. Three major categories of mechanical tests can be carried out; static mechanical tests, Dynamic Mechanical Analysis (DMA) and rheometry [8].

2.1.2 Static mechanical tests

Static mechanical tests are typically creeping tests and stress relaxation tests. They evaluate the behaviour of the material respectively under constant applied stress and constantly applied strain condition.

2.1.3 Dynamic Mechanical Analysis

Regarding DMA, sinusoidal stress is applied to the material which induces a sinus strain of the material that is measured. The delay between the applied force and the measured displacement is a direct evaluation of the viscoelasticity of the material. This phase shift named δ ranges between 0 and 90 degrees corresponding respectively to a purely elastic or purely viscous material. The amplitude of the applied stress σ_0 and the measured strain ϵ_0 is also evaluated. At the UCL Centre for Nerve Engineering, DMA tests are performed with BOSE-ElectroForce 3200 instrument. A typical result is illustrated in figure 2.1 extracted from Celine Kayal's thesis [8].

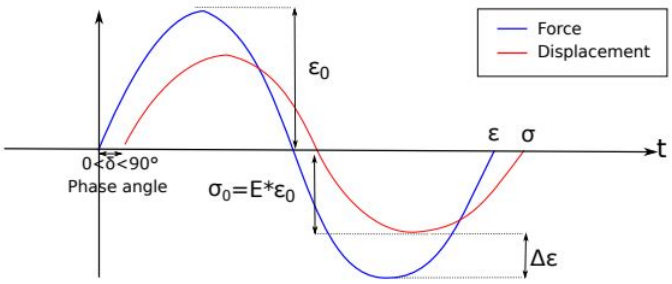

Figure 2.1: Typical force-displacement sine wave from an DMA test (extracted from [8])

The collected data enable to evaluate two moduli:

- The storage modulus defines the elastic respond of the material. It corresponds to the energy stored per cycle and it can be obtained using the following relationship:

$$E' = \frac{\sigma_0}{\epsilon_0 cos\delta} \tag{2.1}$$

- The loss modulus defines the viscous response of the material. It is the energy dissipated per cycle and it can be obtained using the following relationship:

$$E'' = \frac{\sigma_0}{\epsilon_0 sin\delta} \tag{2.2}$$

Those two moduli can be combined in a complex number defining the complex modulus. It can be defined as the complex viscoelastic response of the material as it represents the resistance of the material under dynamic deformation. Its formula is:

$$E^* = E' + jE'' \tag{2.3}$$

With j, the imaginary number.
The module of this complex number is the elastic respond of the material. Therefore, it gives the Young's modulus of the material:

$$E = \frac{\sigma}{\epsilon} = |E^*| = \sqrt{E'^2 + E''^2} \tag{2.4}$$

The relationship between the the elastic and the viscous modulus, related to the tangent of the phase shift, is defined as the damping. This quantity is the energy dissipation of the material under cyclical stress:

$$tan\delta = \frac{E''}{E'} \tag{2.5}$$

Dynamic mechanical analysis tests can be performed by applying a sinus compressive force or inversely tensile force as shown in figure 2.2 extracted from Celine Kayal's thesis [8]. The result can be largely different depending on the deformation modes chosen for the analysis; compression or tension.

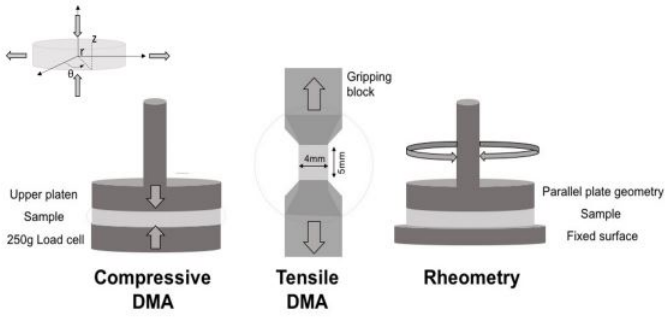

Figure 2.2: DMA and rheology tests (extracted from [8])

2.1.4 Rheology study

Rheology studies the relationship between the shear stress, the deformation and the flow. It also enables to deduce the viscoelastic properties of the material [27]. Rheology tests are performed thanks to a rheometer. It tests the material behaviour under rotational oscillations as illustrated in figure 2.2 [8]. It controls the torque ($M(t)$), the angular displacement ($\theta(t)$), and the angular velocity ($\omega(t)$) and provides values for the material's viscosity (η) and the shear modulus (G). There are three geometries of rheology study but the results collected for this research work use the parallel plate geometry to study

the collagen hydrogel of an EngNT. The viscosity (η) is defined from the measured shear stress (τ) and the shear rate ($\dot{\omega}$) as follows:

$$\eta = \frac{\tau}{\dot{\omega}} \tag{2.6}$$

The viscoelastic properties are evaluated thanks to the measurement of the resulting stress τ after application of a sinusoidal strain γ at an angular frequency ω [8]

$$\gamma(\omega, t) = \gamma_0 sin(\omega t) \tag{2.7}$$
$$\tau(\omega, t) = \tau_0 sin(\omega t + \delta) = G'\gamma_0 sin(\omega t) + G''\gamma_0 cos(\omega t) \tag{2.8}$$

Where G' and G'' are respectively the storage modulus of elastic energy and the shear loss modulus of the viscous dissipation [8].

Frequency sweep tests consist of describing the time-dependent behaviour. DMA or rheology tests are performed. The typical results are the diagram of the storage modulus and the (shear) loss modulus over the frequency which is the frequency of the oscillating compressive/ tensile force/deformation applied or angular velocity.
To allow comparison between rheometry and DMA results, the relationship below is commonly used involving the Poisson's ratio ν

$$G = \frac{E}{2(1+\nu)} \tag{2.9}$$

2.2 Collagen hydrogel

As mentioned earlier, collagen hydrogel is a key element in this research as it represents the material processed by the GAE and PC method to manufacture the EngNT. Modelling the manufacturing methods of EngNT requires a preliminary study of the collagen gel. The production of GAE-EngNTs is recent and mainly studied in two research laboratories. The definition of the collagen gel for EngNTs is based on the research works of those two main laboratories which are the UCL Centre for Nerve Engineering and the Canadian research team from McGill University.

2.2.1 Choice for the collagen gel

The EngNT scaffold aims at mimicking the ECM structure and properties. This is a key feature as the ECM supports nerve function throughout the entire life [8]. For this reason, animal material is preferred to synthetic hydrogel [19]. Indeed, synthetic polymers are popular scaffolds because they are easy to handle, often clinically approved, and relatively strong [23]. However, naturally derived collagen gel contains by nature the major ECM proteins in connective tissues, bones, and nerve tissues [8]. Nevertheless, native biopolymer scaffolds such as collagen, fibrin, hyaluron, and fibronectin have manufacturing challenges, weak cell-seeded possibility and limited control in the assembly [23]. In addition, the materials such as collagen are derived from animal sources, which carries additional challenges around source, consistency, infection risk and ethical as well as cultural issues. The solution to those limitations is the use of Engineered Nerve Tissues with collagen type I gel scaffold [23]. It has the advantage of animal-based material

with a seeded collagen type I from animal origin. However, the collagen gel is produced *in vitro* to get a controlled scaffold. The animal collagen type I engineered scaffold is biocompatible, biodegradable, highly available, highly versatile, easy to use [8], and able to produce stable cross-linked networks [28]. The collagen type I substrate also provides structural support and guidance cues. This influences cell proliferation, differentiation, and migration [8], and the natural aspect of this substrate makes the interactions with the seeded cells easy [28]. All those advantages of animal origin collagen type I engineered scaffold make it a primary choice not only for peripheral nerve repair but also for bone and skin reconstruction as well as drug delivery.

2.2.2 Collagen type I

Collagen gel is a dominant option for the EngNT scaffold. The type of collagen chosen for this scaffold is collagen type I because it is the most abundant fibrillar protein. It accounts for 90% of the collagen in the body [29]. It has a major importance in tissue structure, cell signaling, and modulation of cell behaviour [29]. Collagen type I is composed of three polypeptide chains (two a1 and one a2 chain). Those form a single right-handed triple helical structure [30]. These triple-helical monomers assemble with a precise structure, into collagen fibrils [30]. In the body, collagen fibrils are cross-linked by the enzymes to form a collagen fibre. This composition of collagen type I is illustrated in figure 2.3 extracted from the publication of Tanaya Walimbe et al [29].

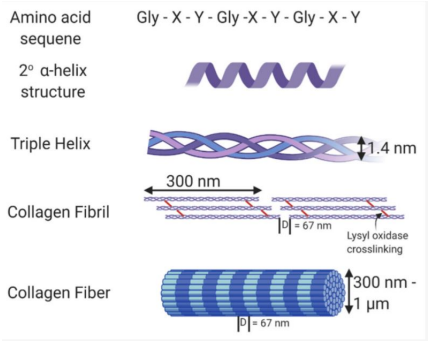

Figure 2.3: Structure of the collagen type I (extracted from [29])

2.2.3 Composition

The collagen gel for the peripheral nerve repair scaffold has mainly the same composition in all the literature from the two laboratories considered. In general, the collagen gel is produced by adding 80 % volume of the final volume of acid-solubilised type I collagen solution (*Co* mg/mL in 0.6% acetic acid) with 10% volume of the final volume of 10×Minimum Essential Medium (MEM) and 5% volume ratio of Dulbecco's modified eagle's medium (DMEM) [8]. Finally, 5% volume of sodium hydroxide is added to the solution aiming at neutralising the acidic collagen type I solution. It also enables to achieve physiological pH [8]. In addition, this last step aims at inducing the collagen gelation [8]. Indeed, the acidic collagen solution is mainly composed of monomers of collagen that can not aggregate. At physiological pH and temperature, the collagen fibrils aggregate, forming an organised rod network, after approximately 30 min. This network gives a

structure to the collagen solution which makes it less liquid and more viscous [22]. The resulting gel can be summarised as a two-phase material consisting of collagen nano-scale fibrils filled with a large excess of interstitial fluid. The fluid phase is usually more than 99.5% of the solution [22][33]. Figure 2.4 illustrates the production of the collagen type I for EngNT manufacturing. The percent volumes of the components in the final volume are indicated in blue. On the contrary, the features subjected to variations between the works considered in this research work (Co, c, V, Vp), are indicated in orange.

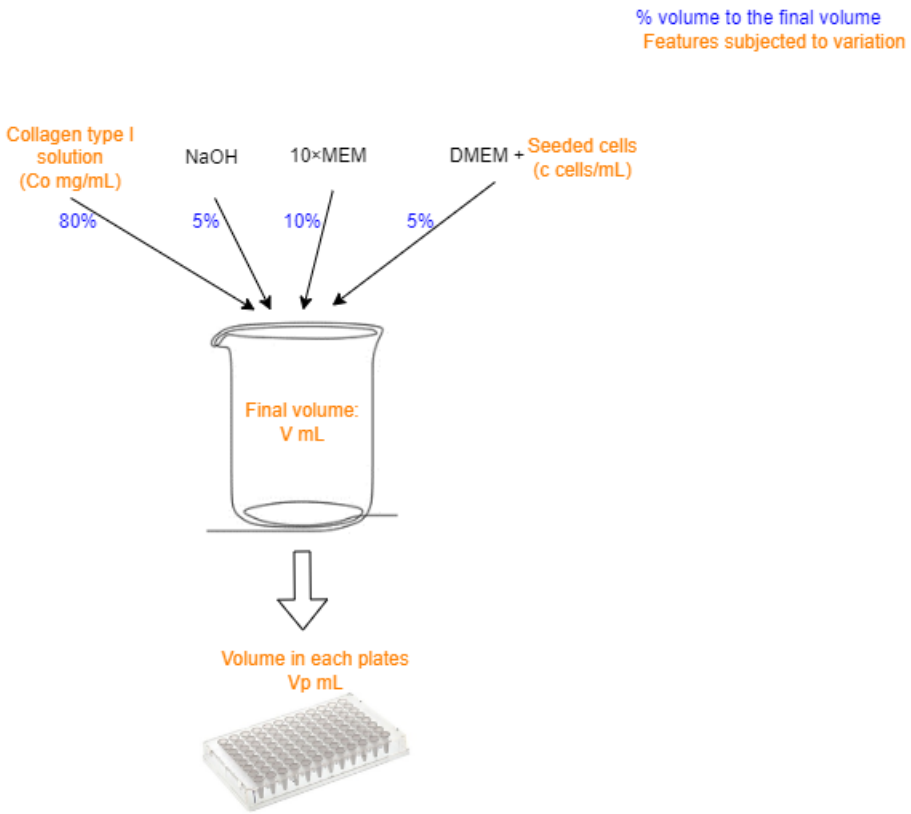

Figure 2.4: Composition of the collagen gel for EngNTs (based on [8] [21] [24] and interviews)

The first variation concerns the origin of the animal collagen type I. The UCL Centre for Nerve Engineering uses a rat tail collagen type I [8][21] because some *in vivo* experiments are conducted in the sciatic nerve of rats. The Canadian team of Neysan O. Kamranpour [24] uses sterile bovine dermis-derived type-I collagen. The latter has the advantage to be used in clinical trials. This parameter does not seem to influence the main properties of the collagen gel but it's more important for the compatibility with the *in vivo* or clinical use. On the contrary, the concentration of this collagen type I is a parameter that has a predictable effect on collagen gel properties. The UCL Centre for Nerve Engineering uses 2 mg/mL [8][21] while the Canadian team of Neysan O. Kamranpour [24] uses 6 mg/mL [24]. It is important to notice that those values are the Co parameters in figure 2.4 and decrease slightly when preparing the final volume of gel depending on the percentage of the collagen gel solution that has been added to the final volume. An additional difference is the type of final container as well as the volumes for the use of the hydrogel. The latter varies also between different works within the same team. A last difference concerns the types and the concentrations of seeded cells as well as a combination of added particles

relevant for the research study. While this last feature will be discussed in the next section 2.2.4, the differences in the composition of the collagen hydrogel in the different research works considered in this project are summarised in table 2.1 [8][21][24]. A quick overview of each work will be provided in section 2.4.

Work of	**Origin of the animal collagen type I**	**Concentration of collagen type I = Co**	**Final volume = V**	**Type of final shape**	**Volume in each sample Vp**
Canadian team	Sterile bovine dermis derived type-I collagen	4mg/mL[1]	Not stated	48-well plate	1,5mL
Celine Kayal	Rat tail tendon collagen	2mg/mL	Not stated	96-well plate	0.1 to 0.3 mL
				24-well plate	0.8 to 1.5 mL
Papon Muangsanit	Rat tail tendon collagen	2mg/mL	Not stated	48-well plate	1mL
				92-well plate	0.075 mL
				EngNT mould	0.4 ml
Poppy O.Smith	Rat tail tendon collagen	2mg/mL	3.5 mL	48-well plate	1mL
Rebecca Powell	Rat tail tendon collagen	2mg/mL	1ml<V<4.5ml	48-well plate	1mL
Ryan Trueman	Rat tail tendon collagen	2mg/mL	3.5mL	48-well plate	0.6mL

Table 2.1: Specificities of the different research works for the production of collagen gel intended to EngNT manufacture (based on [8] [21] [24] and interviews)

2.2.4 Seeded cells

As mentioned in Chapter 1, the subject of many research works is to determine the optimal combination of seeded cells and other added particles in the construct. The final aim is to target nerve regeneration. Depending on the focus of the research, different types of cells or components are added to the hydrogel. The table 2.2 summaries the main types of cells or components added to the collagen gel preparation as well as the cell density. The latter feature is parameter c in figure 2.4. It is highlighted in blue in table 2.2. Some of those works have focused on identifying the optimal cell density in a specific context based on specific criteria of nerve regeneration. The values exposed in the table are supposed to be the optimal ones, reported in completed works or still under investigation for ongoing works. This research project focuses on the GAE method, therefore, table 2.2 presents the data found in the literature only for this stabilisation method. A similar table can be created for the PC method but the literature is richer and would require a deeper study.

[1]Added to 75% volume of the final volume instead of 80%

The first type of cells used mainly by Papon Muangsanit and Poppy 0. Smith are HUVECs. They are a variety of endothelial cells. The potential of HUVECs in nerve repair construct arises because Schwann cells have been shown to migrate along with endothelial cell capillary-like structures. These structures bridge the nerve gap of a nerve lesion and allow the Schwann cells to act for nerve repair. Secondly, the Schwann cells can also be used as seeded cells. They are well-proven important type of cells for nerve repair. They give mechanical and chemical cues for nerve regeneration as explained in Chapter 1. The third type of cell is NG108-15, used to assess neurite growth *in vitro*. Contrarily to the UCL Centre for Nerve Engineering, the Canadian team of Neysan O. Kamranpour [24] has been working with Mesenchymal Stem Cells (MSCs). They look at how those multipotent cells [31] differentiate in the construct that has been processed with the GAE method. MSCs can differentiate into a variety of cell types, including osteoblasts which is the focus of this team [24][31]. Some specific particles such as Polypyrrole (PPy) nanoparticles can also be added to the collagen gel solution. Those particles add electrical conductivity properties to the gel. After stabilisation, the gel might respond to electrical stimulations and promote more or less nerve regeneration. Ryan Trueman is currently working on this topic.

	HUVEC	SCL4.1/F7	NG108-15	MSCs	Polypyrrole (PPy) nanoparticles
	Human umbilical vein endothelial	Rat Schwann cell line	Rat neuronal cell line	Mesenchymal stem cells	Conductive components
Canadian team				With GAE $0.2 * 10^6$ cells/mL	
Papon Muangsanit		With GAE $2*10^6 cells/ml$			
		Co-culture (NG108-15 or DRG) with GAE-EngNTs (F7) $2 * 10^6$ cells/ml			
Poppy O. Smith	With GAE $0.5 * 10^6$ cells/mL				
Rebecca Powell		Differentiated Schwann cell precursors and differentiated Schwan cells $1 * 10^6$ cells/mL			
Ryan Trueman		With GAE $1 * 10^6$ cells/mL			Added within the 10XMEM solution

Table 2.2: Types of seeded cells used in the EngNTs in the different works of the two research laboratories considered (based on [8] [21] [24] and interviews)

2.2.5 Mechanical characteristics

It is important to identify the mechanical properties of the collagen gel to target correctly the mathematical model for the material processed by the GAE or the PC method. The presence and density of the seeded cells developed in the previous section do not influence the main mechanical characteristics of the gel. Those are mainly given by the collagen fibrils and the liquid phase trapped into the network.
Depending on the production and the stabilisation method, the collagen fibrils in the gel will be aligned or have a random orientation [8][16][21][24]. The hydrogel can therefore be considered respectively as an anisotropic or an isotropic material.
The goal of the stabilisation method is to remove the majority of the liquid phase from the hydrogel to acquire some micro-structural control and strengthen the mechanical properties of the hydrogel [8][20][22]. Indeed, expelling the majority of the liquid from the hydrogel increases the collagen concentration in order to fully mimick the highly organised components of the native ECM. The collagen gel has therefore a slightly different behaviour as Hyper-Hydrated Collagen (HHC) gel or after stabilisation.

Hyper-Hydrated Collagen gel

The analysis of the properties of the HHC gel explored in this section is not only based on publications by the two research laboratories considered until now. In general collagen hydrogel shows a non-linear poro-viscoelastic behaviour due to its two-phase composition of liquid trapped within a collagen fibril network [32]. However, different types of mechanical tests highlight different properties of the HHC gel. Mostly, to extract the relevant characteristic values from the mechanical tests, theories have to be used to fit the experimental data curves [32][33][34]. Different models can be used, pointing out different aspects of the collagen gel. Due to its complex behaviour, the HHC gel is challenging to characterise. It is therefore, a topic that has been studied for many years by a lot of research groups. This work does not aim to present all the properties of the hyper-hydrated gel that has been studied. However, the major key results are reported giving a primary overview of the hydrated collagen gel's mechanical characteristics. Because these properties vary depending on the composition of the collagen gel, table 2.3 summarises the type of gel used in the different works presented below. This table comes separately from table 2.1 because the collagen gel composition considered in this research work is one of the two laboratories working on the potential of the GAE method. On the contrary, the literature concerning the HHC characterisation is broader and is composed of dedicated research for the identification of the hydrogel mechanical properties.

Work of	Origin of the animal collagen type I	Final collagen concentration [2]	Volume used Vp
Velegol and Lanni	Vitrogen 100 Type I collagen = purified, pepsin-solubilized bovine dermal collagen	2.3 mg/mL	rectangular capillary tubes (ID 0.20 mm, inner width 2 mm, and length 5 cm)
Knapp et al.	Vitrogen 100 type I collagen	2mg/mL	Not stated
Busby et al.	rat tail tendon and hydrogels	2, 3 and 4 mg/ml	24-well plates (1mL)
Castro et al.	Type I bovine collagen	2, 3 and 4 mg/ml	20 mm diameter,1 mm height
Brooks A.Lane	Bovine corium	2,3 and 4 %w/w	10mm diameter, 3.5mm height
Frank Sauer et al	bovine skin type 1 and rat tail type 1	3mg/mL	Not stated
Robert A. Brown et al	Rat tail type I collagen	2.16mg/mL	rectangular mould (33X13X4) mm

Table 2.3: Types of collagen gel used in the different works for HHC gel mechanical characterisation (based on [32] [33] [34] [35] [36] [38] [40])

The evaluation of the shear and viscous behaviour is a key feature to assess the biomechanical properties of soft tissues and hydrogels. For this purpose, rheology is one of the most commonly used techniques [32]. Among other studies, Velegol and Lanni have determined a shear modulus for their HHC gel, constantly around 80 Pa over the frequency range. The storage modulus and the shear loss modulus both slightly increase with the frequency respectively in the range of 50-60 Pa and 5-10 Pa [35]. Those results were obtained by performing frequency sweep tests thanks to laser trap microrheometry. A major linear Hookean behaviour up to 10% strain has also been determined [35].

However, rheological tests are dynamic and the fluid in the collagen network is not able to instantaneously move through the porous solid [32]. Therefore, the characterisation is monophasic, focusing only on the solid part of the hydrogel. To account for the interphase drag of biphasic materials such as hydrogels, rheology needs to be coupled with confined compression tests [32]. Knapp et al.[34] conducted this study performing creep tests, ramp tests, and dynamic tests. Critical results obtained are presented in table 2.4 [34]. However, confined compression provides inhomogeneous deformation. The biphasic continuum theory was used providing the constitutive model required to analyse the rheology data [34]. It shows that the HHC gel exhibits Maxwell fluid behaviour in both shear and compression [34]. Similarly, Busby et al. [33] performed ramp tests determining peak stress, aggregate modulus, and permeability for collagen gel with different collagen concentrations. The results matched the results of Knapp et al. [34]. Additionally, Busby et al. [33] have shown that the mechanical properties of collagen are highly influenced by the collagen concentration.

[2] Concentration in the final volume. Not to be compared with the Co parameter

Creep tests	Compliance over time ranges between 0 and 0.06 Pa^{-1}. Highly linear evolution in compression while fast increase before stabilisation in shear.
	Drag coefficient= $6.43 * 10^9$ $Pa.s.m^{-2}$
	Aggregate viscosity= $6.63 * 10^4$ Pa.s
	Aggregate modulus= 6.32 Pa
Ramp tests	Drag coefficient= $1.23 * 10^9$ $Pa.s.m^{-2}$
	Aggregate viscosity = $3.13 * 10^4$ Pa.s
	Aggregate modulus 318.3 Pa
Dynamic tests	Shear modulus G' (30-80 Pa) and G'' (5-8 Pa) over strain rate. Both storage and loss moduli increase slowly with increased frequency. The loss modulus is approximately 20 % lower of the corresponding storage modulus.

Table 2.4: Major results from Knapp et al. study on mechanical characteristics of the HHC hydrogel (based on [34])

Besides, all the studies in which confine compression coupled with rheology is performed, have faced difficulties in obtaining a stable creep deformation. This is due to the high compression rates generating fast fluid exudation, which is hardly measurable [32]. For this reason, combining experimental and numerical approaches with FEM brings a larger range of behaviour [32][37]. In this idea, Castro et al. [32] present an experimental and numerical framework for the biomechanical characterisation of HHC hydrogels with different concentrations. The experiments have provided comparable results to the previous studies while using a non-linear poroelastic approach for the FEM model. This approach neglected the viscoelasticity due to long-term compression rates during the experiments. Instead, a compressible Neo-Hookean model is coupled with the van der Voet model. The latter was applied to describe the strain-dependent permeability [32]. Another research group, Brokes A. Lane [36], carried on uniaxial unconfined compression tests to collect the strain corresponding to a compressing stress level. The result was the evaluation of a stress-strain curve. Different elastic behaviour models have been tested to see which one would fit the best experimental data curves. It appears to be the General-Blatz-Ko hyperelastic material model [36]. Frank Sauer et al. [40] affirmed the collagen networks exhibit a viscoelastic power-law behaviour in a frequency range not accessible by classical rheology. Therefore, they performed microrheological tests to measure viscoelastic dispersion. They fit the experimental data with a power-law rheological behaviour [40].

Concerning the Poisson's ratio, even if the overall domain of most soft tissues is almost incompressible, biological hydrogels tend to adopt a Poisson's ratio between 0.20 and 0.30 for the solid part [32][38].

Stabilised collagen gel

When the gel is stabilised, its mechanical characteristics change. As mentioned earlier, this work focuses on the two stabilisation methods (GAE and PC) and their use by the two research laboratories which are the UCL Centre for Nerve Engineering and the Canadian team from McGill University.

On the one hand, Celine Kayal from UCL has conducted mechanical tests on collagen type I gel stabilised by Plastic Compression without tethering [8]. As will be discussed in section 2.3.1, the non-tethering nature of the PC keeps the random organisation of the collagen fibrils and describes the properties of a stabilised isotropic material. Firstly, she characterised the fluid expel process using an optical contact angle meter (OCAM). She measured the change in height (thickness) due to the plastic compression [8]. Keeping the area constant, the change in hydrogel volume can be deduced. Finally, the ratio between the mass of collagen in the initial HHC gel and the final stabilised volume gives the new density of collagen in the stabilised gel. A table containing those data for different well-plates and initial volumes has been implemented by Celine Kayal [8]. Secondly, compressive DMA testing and rheometry have been conducted at a constant frequency of 5 Hz. It appears that the elastic and the viscous moduli (E' and E'') of the collagen gel are independent to the strain applied up to a critical strain level. It means that the collagen gel behaves as a linear viscoelastic material until a limit of 2% strain [8]. Thirdly, frequency sweep tests in tension, compression, and rheology allow to obtain the evolution of the storage, the loss, and the complex moduli ($E'/G', E''/G''and E^*/G^*$) over the frequency as well as the tangent of the phase shift ($tan\delta$) over the frequency [8]. Under uniaxial compression, the stabilised gel has a viscoelastic behaviour with an E'' increasing with the frequency from 10 to 40 kPa, consistently approximately 2.5 kPa higher than E' [8]. Under tension, the elastic modulus predominates staying constant at around 100 kPa. On the contrary, the viscous modulus always stays close to zero kPa for all the frequencies [8]. Concerning the rheometry measurements, the viscous modulus was lower than the elastic modulus for all frequencies and 2.6 times softer than under compression. However, this value is still not negligible, which indicates a viscoelastic behaviour [8]. In sum, the $tan\delta$ clearing shows a viscoelastic behaviour in compression with $tan\delta > 1$, an elastic behaviour in tension $tan\delta$ close to 0 and a viscoelastic with elastic dominance behaviour for rheology. In addition, the relationship between the complex modulus and the frequency has been evaluated [8]. The stabilisation method used by Celine Kayal is the Levis'method which will be explained later on in section 2.3.4. However, literature not coming from the two laboratories needs to be considered to characterise the mechanical properties of the collagen gel stabilised by Brown's method. Robert A. Brown et al [23][41] evaluate the stress-strain curve of the final cylindrical construct in tension. The typical stress–strain curve demonstrates a toe, linear, and failure region with maximum stress around 0.6 MPa and a modulus of 1.5 MPa.

On the other hand, Papon Muangsanit from UCL [16][21] and the Canadian team of Neysan O. Kamranpour [24] have dedicated a part of their research to the mechanical characteristics of the collagen gel stabilised by the GAE method. Papon Muangsanit has conducted tensile frequency sweep tests with a cylindrical GAE-EngNT construct of 10 mm in length and 1.2 mm in diameter due to the use of a cannula gauge 16 [16][21]. The equipment used for the GAE process will be explained in section 2.4. The first result was the evaluation of the linear viscoelastic limit to 1% strain. Indeed, a constant evolution of the E' and E'' over the strain can be observed until their values drop after this limit [16][21]. The second result was the E' and E'', constantly ranging respectively around 0.9 MPa and 0.1 MPa for all the frequencies. In addition, the loss tangent ($tan\delta$) stays around 0.18 showing a viscoelastic behaviour of the GAE-EngNT construct with an elastic dominance [16][21]. Those three results allow to conclude similar viscoelastic mechanical behaviours of the GAE-EngNT construct compared to rat sciatic nerves [16][21]. This re-

sult could also be valid for the strain-stress curve at low strain. Furthermore, some tensile tests under a strain rate of 0.17 mm/s were performed showing lower values of Ultimate Tensile Stress (UTS) (0.219 MPa), ultimate strain (0.681), and Young's modulus (0.351 MPa) compared to rat sciatic nerve data [16][21].

Concerning the work of the Canadian group, Neysan O. Kamranpour et al.[24] characterised the GAE-EngNT construct produced with different cannula sizes. Four needle gauge numbers were considered 8G, 10G, 12G, and 14G corresponding respectively to internal cannula diameters of 3.43, 2.69, 2.16, and 1.60 mm . In each case, the collagen fibril density (CFD) in percent weight, has been evaluated. The collagen gel concentration in the GAE-EngNT construct can be deduced from the volume of each construct dictated by the cannula size [24]. In terms of mechanical characterisation, the research team conducted quasi-static tensile tests enabling to obtain the different stress-strain curves for the four different cannula sizes. The apparent modulus values depending on the CFD, and the UTS over the collagen fibril density were also computed. The four stress-strain curves show truly different profiles. A more curved profile is shown for the 8G cannula. A linear behaviour for a not too large strain appears for the 10G and 12G cannulas. Finally, a hyperelastic behaviour is presented for higher needle gauge numbers [24]. Regarding the apparent modulus and the UTS, both increased exponentially with the CFD, respectively ranging from 0.15 MPa to 3.2 MPa, and from 0.0015 MPa to 0.45 MPa [24].

The properties listed above are summarised in table 2.5 and will be used to define the mathematical model approach in Chapter 3.1.3

2.2.6 Mechanobiology

The set of mechanical tests explained in the previous section is important to characterise the properties of the hydrogel of an EngNT. Some seeded cells are also added to this gel bringing cues to guide the axonal regeneration in the engineered construct. The hydrogel is therefore the substrate of those seeded cells. Consequently, the cells' behaviour in the engineered construct need to be studied in association with the mechanical characterisation of collagen gel and of the manufacturing process. Indeed, the mechanical and structural properties of the substrate as well as the forces applied to it, are proved to have a wide influence on the behaviour of the cells. For instance, their differentiation, migration, neurite branching, and orientation can be modified. The study of this relationship is called the mechanobiology [8]. Besides, the neural and glial cells' behaviour in response to their mechanical environment is called the mechanotaxie. Similarly, the chemotaxis and the haptotaxis are the responses of neural cells to respectively chemical and topographical cues [8]. An additional particularly interesting cell behaviour is the durotaxis. This term refers to the ability of the cells to sense and respond to the stiffness gradient of their substrate. As described in the literature [8][26], the cells tend to move towards stiffer ECM.

Cells can respond to stress in various ways. If some stress types and levels activate a specific cell behaviour, others types and levels activate cell death. Fluid shear stress has been shown to influence cell functionality in vivo (Wittkowske et al. [56]) and *in vitro* (Pedersen et al. [57] and Silvani et al. [58]). A high shear stress level, beyond physiological ranges, decreases cell viability. The limit shear stress level range of values depends

<table>
<tr><td>HHC gel</td><td colspan="2">Globally more elastic behaviour than viscous
The shear moduli (storage and shear loss) has a dependence on the frequency but the evolution is quite slow
Porous solid and power-law rheological behaviour were used as models to extract the evolution of the shear modulus over the frequency
FEM models are used for in-silico representations of the performed mechanical tests. They used mostly hyperelastic materials for the HHC gel</td><td>Order of magnitude for the characteristics of the gel varies with the temperature and with the final concentration of collagen. Therefore, slight variations can be noticed but the results of the different works stay coherent and some order of magnitudes lower than for the stabilised gel</td></tr>
<tr><td rowspan="3">Stabilised gel by PC</td><td>Compression</td><td>Linear viscoelastic behaviour under 2% strain with viscous dominance</td><td rowspan="4">Order of magnitude for the characteristics of the gel depends a lot on the stabilisation determining the final collagen concentration</td></tr>
<tr><td>Tension</td><td>Elastic behaviour. Stress-strain curves with a toe, a linear and a failure region</td></tr>
<tr><td>Rheology</td><td>Linear viscoelastic behaviour under 2% strain with elastic dominance</td></tr>
<tr><td>Stabilised gel by GAE</td><td>Tensile tests only</td><td>Linear viscoelastic behaviour under 1% strain with a elastic dominance. Stress-strain curves with different profiles depending on the cannula size but all with a linear region</td></tr>
</table>

Table 2.5: Conclusion on the mechanical characterisation of the collagen gel (based on [8] [16] [20] [21] [22] [24] [32] [33] [34] [35] [36] [38] [40])

on the simulation context and the type of cell. A lot of studies have been conducted concerning this topic with endothelial cells as they form the inner membrane of blood vessel directly subjected to the blood flow. However, the limit of shear stress levels in this context can not be used in the GAE process because the endothelial cells are moving with the flow of the construct within the tube during the aspiration and ejection stage. Even if no quantitative study can be done, a qualitative analysis could be performed between the stress level simulated in the construct during the GAE process and the cell viability data collected by analysis of the GAE-EngNT.

2.3 Plastic Compression

2.3.1 General principle

Plastic compression is used as a stabilising method for the collagen gel. Its goal is to produce the final EngNT construct aiming at promoting and guiding nerve regeneration. PC manufacturing method is performed in three steps.

1. Collagen gel preparation. Following the composition and the explanation in section 2.2, the collagen gel is produced *in vitro* by adding different constituents and the seeded cells to the collagen type I solution. The resulting gel needs to achieve physiological pH and temperature in order to allow the gel to set [20][22]. However, the solid phase of the gel is weakly spread and the CFD stays low. This feature gives instability to the gel but the ability to compress with large deformation [22].

2. Stabilisation by plastic compression. The idea is to compress the gel to expel the majority of the fluid phase of the collagen gel which undergoes large and plastic deformation due to the specific setup of the method. This approach allows the fluid to leave the construct and not to return when the compression stops [20][39]. There are three slightly different techniques to perform this step and that will be explained hereafter [39]. The stabilisation of the collagen gel by expelling approximately 95% of the interstitial fluid, leads to an increase of the collagen density and micro-layering of the collagen fibrils [23]. The mechanical properties of the EngNT construct are tuned in a controllable way without any cell participation while keeping a high cell viability [23].

3. Spiral assembly. The sheet of EngNTs obtained after plastic compression is structurally stable enough to be rolled in a silicone cylinder for early-stage experimental studies whereas for more translational studies a degradable collagen outer tube is used. Therefore, the EngNT construct acquires the proper geometry of the nerve to be repaired as shown in figure 2.5 extracted from Melanie Georgiou et al publication [20]. *In vivo* experiments, suture the silicon cylinder containing the EngNT construct to both ends of the damaged nerves.

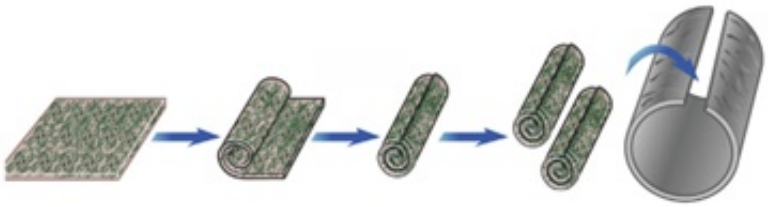

Figure 2.5: Spiral assembly step for EngNT construct manufacturing with the PC method (extracted from [20])

2.3.2 Potential

The key point of PC is its ability to control the mechanical properties of the EngNT construct. The method adjusts the collagen fibrils concentration thanks to the command of the percentage of fluid being expelled. Indeed, the construct is strengthened and has mechanical properties more comparable to soft human tissues without the use of chemical cross-linking agents [20]. At the same time, because the EngNT construct hosts seeded cells, the characteristics of the environment for those cells are controlled to promote cell proliferation, cell migration, and cell interactions [22]. Besides, the method provides mechanical integrity to the hydrogel that allows to shape it. This enables the implantation of the construct to the nerve lesion site for *in vivo* experiments. During the compression, the deformation is plastic because the collagen gel does not re-hydrated and it preserves the structural features of the collagen fibril network and the cell viability [8][23]. The latter point has the advantage of seeding the collagen gel with seeded cells before stabilisation. This process is easy and fast with a limited risk of cell death [39]. Furthermore, the PC method is standardised, not experience-dependent, and rapid as it takes around 40 minutes (without tethering that will be explained later on) to produce the EngNT through the three steps mentioned earlier [8]. A last strength of the PC method is that it controls the mechanical properties of the collagen gel without any physicochemical driver. Indeed, the act of plastic compression which stabilises the gel does not require cell participation which also eliminates a major source of variability [22]. Plastic Compression is a potential method to produce EngNT efficiently.

2.3.3 Limitations of the method

However, two limitations can be pointed out. Firstly, the potential excessive packing of collagen fibrils at the primary Fluid Leaving Surface (FLS), might prevent extra fluid to flow out of the construct during the PC process. This feature limits the efficiency of the technique [22]. Secondly, the PC is not able to provide any alignment to the original random orientation of the collagen fibrils in the hydrogel while the anisotropy of the EngNT construct is a key feature to promote nerve regeneration. To overcome this issue, tethering steps can be performed preliminary to the plastic compression with the requirement of using contractive cells. This will be developed in the next section.

2.3.4 Different methods

Brown's method

Different Plastic Compression variants show different setup and fluid expelling techniques. The first method was developed by Professor Brown and his team in 2005. It consists of an unconfined compression where the gel is placed in between a series of nylon and stainless steel meshes to prevent adhesion. Blotting filter papers on the bottom were collecting the expelled fluid and an additional load was compressing the entire system providing the required plastic compression. This setup can be found in figure 2.6A extracted from Brown et al publication [39]. The process is the application of a load of 120 g for 1 min [20]. The applied load, in addition to the self-compression of the collagen gel by the weight of the matrix swollen with fluid, creates a downwards flow of fluid. The expelled water is absorbed by the paper pad underneath [39].

Robert A. Brown et al [23] studied the resulting collagen gel after the PC method. The main results were exposed in the previous section to define the collagen gel mechanical properties. The decrease percentage in gel wet mass was measured for different compaction regimes. To reach 90% of fluid loss, a load of at least 50 g needs to be applied for 1 min. The outcome of using Brown's method is evaluated by the quality of the EngNT in terms of its ability to promote nerve regeneration. For this purpose, Umber Cheema et al [22] have studied the change of collagen gel properties and the cells respond to this change during PC. Cell proliferation rate depending on the initial collagen density and durotaxis of the cell moving towards a stiffer substrate has been evaluated.

Levis' method

The major drawback of Brown's method is the unconfined nature of the compression process inducing an uncontrolled and messy fluid loss in various directions [39]. Indeed, the Brown's method has a greater potential for the production of aerosols and particulates [39]. Another limitation is the difficulty to scale up the technique for easy production of multiple constructs [39]. Therefore, Levis et al. in 2015 [39] adapted the method to fulfil the requirements of the Good Manufacturing Practice (GMP) standards. The goal is the production of cell therapy and the improvement of the repeatability to suit clinical application [39]. The team developed the Real Architecture For 3D Tissues (RAFT) process which is commercially available as RAFT kits. The collagen gel is now confined in a container. Rolled filter paper absorbers and other blotting elements are placed on the top surface of the collagen hydrogel and a similar compressing load to Brown's method is applied for 15 min [39]. In contrast to Brown's technique, there is an upward flow of the fluid phase of the collagen hydrogel which is illustrated in figure 2.6B. The outcome of both methods is quite similar which confirms the potential of Levis'method. Indeed, it provides an equivalent PC method, as well as conforming to GMP standards and clinical applications. The only parameter significantly different was the thickness of the RAFT construct. It appears to be thicker with the unconfined compression. process [39]. However, a change in this property did not adversely affect the function of the construct to host cells [39].

Levis et al improved the technique using a Hydrophilic Porous Absorber (HPA) and no more compressive load [39]. It aims at minimising contamination risks, being time-effective, increasing the repeatability, and using equipment compatible with clean rooms. Therefore, the process is no longer a proper compression. The water is absorbed through an upward flow capillary action into the HPA with only the minimal weight of the HPA itself applied as a load on the collagen gel as can be seen in figure 2.6C. This method was used by Celine Kayal and Papon Muangsanit in their research works [8][16].

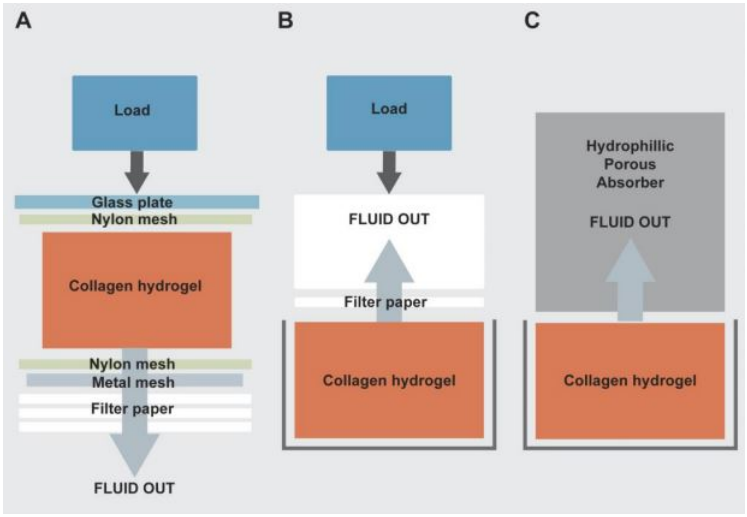

Figure 2.6: Three different Plastic Compression techniques (extracted from [39])

PC tethered with Levis'method

One of the main limitations of PC methods, which was pointed out just earlier, is the disability to align the collagen fibrils in the construct to replicate the anisotropy of ECM. To overcome this issue, Melanie Georgiou et al [20] explained the tethered technique shown in figure 2.7.

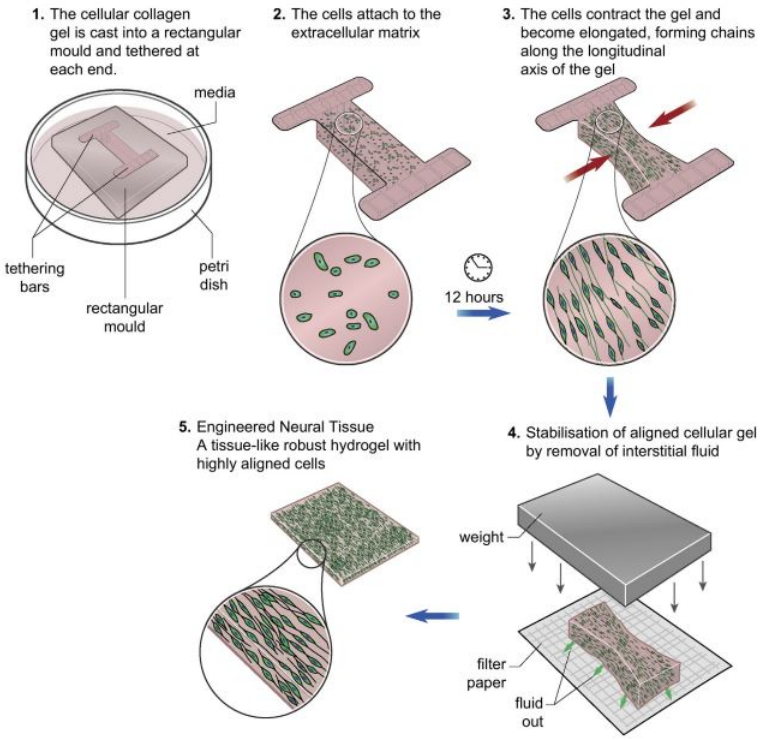

Figure 2.7: Stages in the fabrication of EngNT with the PC tethered method (extracted from [20])

The manufacturing process of the EngNT with this method is performed in five steps instead of three initially.

1. Collagen gel preparation: This step is the same as the general PC principle. A crucial aspect of the gel preparation is the seeded cells used. Those need to have the ability to contract such HUVEC or SCL 4.1/F7 used by the UCL Centre for Nerve Engineering.

2. Cast of the hydrogel in tethered moulds: Instead of being cast in well-plates, the hydrogel is placed in a mould containing tethered bars at the extremities as can be seen in figure 2.8 extracted from Papon Muangsanit publication [16]. The collagen fibrils in the gel will be tethered to the bars at the two ends of the mould during the gelation process of the hydrogel.

Figure 2.8: Tethered mould (extracted from [16])

3. Contraction of the gel by the seeded cells: Thanks to their contraction ability, the seeded cells attach to the matrix (via integrins) and the cytoskeleton contracts, applying inward forces on the collagen fibrils. The tethering means that the gel is restricted from contracting along the longitudinal axis thanks to the tetherinb bars at both extremities of the rectangle. Tension develops and the collagen fibrils align following the specific profile shown by the dotted line in the right part of figure 2.8 [16]. After 12 hours of seeded cells action, the collagen gel is now an anisotropic material containing aligned collagen fibrils and aligned cells following the matrix alignment [20].

4. Stabilisation by PC: Despite its alignment, the hydrogel is still composed mostly of liquid which makes it unstable. This step of fluid removal from the hydrogel by plastic compression is the same as explained in section 2.3.1. Celine Kayal and Papon Muangsanit decided to use the RAFT process in their work as can be shown in the figure 2.9 from Papon Muangsanit thesis [8][16].

Figure 2.9: Manufacturing equipment for EngNT with the tethered PC method (extracted from [16])

5. Spiral assembly: In order to use the construct *in vivo* to promote nerve regeneration, cylindrical geometry needs to be acquired by rolling the EngNT sheets as explained in section 2.3.1.

The outcomes of this technique were studied through different research works producing EngNTs using the PC tethered method. However, the aim of the entire works was not to study this technique in detail [8][16] but mostly to improve features of EngNT constructs to promote nerve regeneration. Quick important results of two works at the UCL Centre for Nerve Engineering can be explored in this section. Firstly, Papon Muangsanit determined the variation of the contraction ability of HUVEC cells, and the pattern of cellular alignment regarding cell density. Thanks to this tethered technique, HUVEC cells and collagen fibrils form tube-like structures that have the essential roles of promoting vascularisation and guiding Schwann cells in the primary steps of nerve regeneration [16]. It was proved that the cell alignment and the cell viability were preserved after stabilisation while the tube-like structures were mostly disrupted during the plastic compression [16]. Secondly, Celine Kayal [8] focused on the seeded cells which behave according to the mechanical characteristics of their environment. Migration of NG108-15 cells following an increasing stiffness gradient in the EngNT construct produced by the RAFT PC tethered method has been modelled mathematically.

2.4 Gel Aspiration Ejection

2.4.1 Equipment

The Gel Aspiration Ejection stabilisation method, as its name suggests, consists of aspirating the hyper-hydrated gel into a small cannula. This process stabilised the gel due to the change of shape imposed by the small cannula size [21] [24]. Afterwards, the gel is ejected to achieve a GAE-EngNT. In order to develop this process in the next section, preliminary explanations of the equipment are essential.
As illustrated in figure 2.10 extracted from Papon Muangsanit et al [21], the GAE system is composed of four principal elements:

(i) Angioplasty inflation device: Initially used for angioplasty surgical intervention to open up a blocked or narrowed artery around the heart [43], the device is here used in another context. It is made up of a handle (white extremity) and a screw bar (elongated white solid cylinder) which plays the role of the piston in the guiding chamber (clear cylinder). A locker (green) prohibits the translational movement of the screw bar. Indeed, by turning the handle upwards, the piston is screwed up in the locker which aspirates the media of the system in the guide body. A pressure gauge at the bottom of the clear body indicates the aspiration pressure level the device is applying [21][24].

(ii) Luer lock valve(s): This particular device is composed of three valves. The first one joins the flexible tubing, itself linked to the angioplasty device. The second is connected to the cannula (iii) and the third lock is linked to the fluid transfer syringe (iv). The valve is positioned to occlude one of the three inputs. For the aspiration, the valve blocks the air room input (no fluid transfer syringe used during the aspiration) and therefore directs the flow of the system media from the cannula to the flexible tubing. This aspirates the construct in the cannula. Conversely,

during the ejection, the fluid transfer syringe is connected to the system and its input is open while the flexible needle input is closed and the downward pressure applied by the syringe allows the ejection of the construct out of the cannula. Two Luer lock valves can be used but always with the same basic principle playing with the opened and closed inputs to allow the aspiration and ejection.

(iii) Cannula: This cannula is a blunt hypodermic needle gauge number conventionally used in microfluidics [42]. It is a sterile and standardized cannula with a geometry specified by the needle gauge number [42]. The latter indicates the inner and outer diameters decreasing with increasing gauge number ranging from 7G to 34G. Table 2.6 below presents the geometry specifications for the cannulas used for the GAE method [42]. This targeted range has been chosen because the production of GAE-EngNT was not possible in too small cannula diameters (needle gauge numbers > 16 G), while the use of larger cannula sizes (needle gauge numbers < 8 G) yielded collagen fibril density with values < 5 wt%, which is too small to fit the GAE-EngNT requirement of mimicking mechanical properties of the native nerve tissue. [24][44].

Needle gauge number	Outer diameter (mm)	Inner diameter (mm)
8G	4.191	3.429
10G	3.404	2.692
12G	2.769	2.159
14G	2.108	1.600
16G	1.651	1.194

Table 2.6: Corresponding dimensions of the needle gauge numbers (based on [42])

(iv) Fluid transfer syringe: It is a syringe with the bottom tip attached to the Luer lock. It is connected to the GAE system only for the ejection phase. That's the reason why it is not represented in figure 2.10. During the ejection, this syringe applies a downward pressure on the construct to eject it from the system [21].

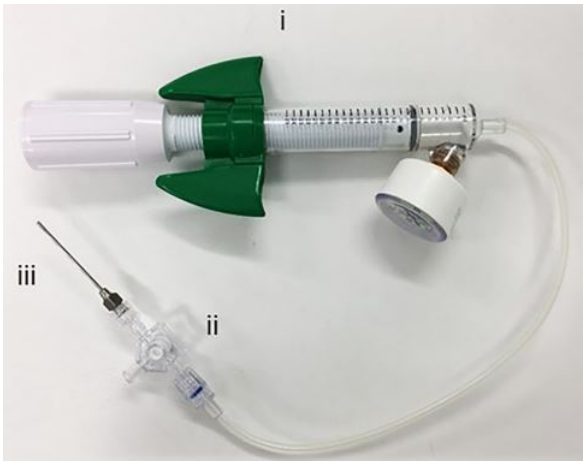

Figure 2.10: GAE equipment (extracted from [21])

2.4.2 Process

It is interesting to look at the process of the GAE method not only to implement the mathematical model as close as possible to the reality but also to identify the different ways to use the GAE technique and to give the first insights for automating the method. Indeed, the GAE process is not standardised or automated yet. The research groups working with it have been mostly focusing on using the GAE method to produce GAE-EngNT and optimising those constructs for nerve regeneration in terms of chemical, mechanical and structural cues *in vitro* and *in vivo*. The GAE process is therefore the production step in their study and the target is to succeed in the production and not the way to do it. Consequently, there are some variations in use between researchers using the GAE method. An explanation of the GAE process and its use will be given including the differences noticed between the laboratories considered of the UCL Centre for Nerve Engineering and of the Canadian team from McGill University [16][21][24].

GAE process explanation

The first step in the GAE process is the preparation of the collagen gel. Following the composition described in section 2.2, the collagen gel is made by neutralising the combined collagen type I solution and 10x MEM to a final volume of 10%, with NaOH. Once neutralised, the cells are added to the collagen gel solution which is then cast into the cylindrical moulds of a well-plate chosen for the research study, before being incubated at 37°C for 30 min to complete gelation [21][24]. At this stage already, there are some variations between research works in terms of the type of collagen type I, the initial concentration of collagen, the volumes and the geometries used. Those have already been presented in table 2.1. The goal of each research study working with the GAE method requires the production of different numbers of constructs. While some researchers produce low quantities of GAE-EngNT per setting (<10), others need to maximise the number of GAE-EngNT produced by stetting. Also concerning this feature, some variations arise among different researchers. Some reach 36 constructs in one setting while other users are limited to 12 constructs per setting. The reason why there is a limit on the number of GAE constructs which can be made in one sitting is related to the endurance of the experimentalist. In parallel, it has been reported that there is no limit in the number of GAE-EngNT constructs that can be produced with the syringe pump in one setting.
Once the hyper-hydrated collagen gel is ready to be processed by the GAE stabilisation method, the gel is detached from the edges of its container. The gel becomes independent of the container by breaking the links with the edges due to gelation.

To be able to process this prepared collagen gel, the GAE experimental setup shown in figure 2.11 needs to be built in a laminar flow hood used for sterility purposes. For the setup of the GAE process, some researchers prefer working with some supports as we can see in figure 2.11. A scissor lab-lift platform enables the adjustment of the vertical position of the well-plate containing the collagen gel samples. Another support called the micromanipulator clamp holds the cannula of the GAE equipment so that it is placed perfectly at the concentric surface centre of the collagen gel sample and it is plunged to approximately 1 mm deep into this sample [21][24]. The precision of this position has human variability which is relatively coarse at the mm scale. A repeatable technique is used by some researchers to control the seal between the gel and the cannula when plunging the cannula into the HHC gel. When using media in the GAE system, a slight downward

rotation of the handle of the angioplasty device release one drop of the system fluid at the end of the cannula. Once this drop starts to flatten at the surface of the collagen gel, the micromanipulator clamp is moved half a turn downwards so that the immersion of the cannula at 1mm depth in the gel is controlled. Another support that can be used is the clamp and stand to hold the angioplasty device tilted around 30 degrees from the vertical, which is not a precisely controlled value. Some researchers with large hands are able to hold all the GAE equipment in one hand and prefer to work without any support while others use some but not all the supports presented here above.
The cannula size is also part of the variability of the setup and the influence of this parameter on the GAE-EngNT construct characteristics has been studied especially by the Canadian group of Neysan O. Kamranpour et al [24]. Their main results will be explained in the next section. On the contrary, the UCL Centre for Nerve Engineering [16] [21] always use a 16G cannula as it has proved to be the optimal cannula size to match the mechanical properties of natural nerves.
Another feature that varies depending on the research work is the use of physiologic liquid or air inside the angioplasty device with the flexible needle and fluid transfer syringe for the ejection. The Canadian team of Neysan O. Kamranpour et al [24] uses air for the aspiration and a sterile incompressible fluid (e.g., water, phosphate-buffered saline, culture media) for the ejection. According to the feeling of the experimentalists, for aspiration, the absence of air increases the magnitude of pressure which can be built up. Therefore, it requires fewer manual turns of the handle of the angioplasty device to fully aspirate the gel which can have consequences that we will see later on. On the contrary, a system that is too sensitive a little handle turn leads to the failure of the process. Therefore, there is a lot of inter-user variability concerning this feature. Indeed, depending on the experience of the researchers, they have a better successful rate using mostly liquid with air in a part of the system making the aspiration more gentle. Other ways use liquid only or air only during the aspiration and/or the ejection.
The last setup difference is the use of the classic angioplasty device with manually screwing the piston turning the handle or the use of a pump which is the first step towards an automated system. For now, all the experiments that have led to published results were obtained with the manual angioplasty device [21][24]. Indeed, the syringe pump has been used to try producing the GAE-EngNT in a more standardised and automated way but the setup with the pump still needs to be optimised in order to rapidly produce the construct for the research studies. The use of a syringe pump would allow complete control of the applied pressure (constant or a time-dependent pressure profile), the duration of the aspiration or ejection as well as the volume rate of the aspiration or ejection. That information is coarse or has not been provided by the publications on the GAE method with the manual angioplasty device so far [21][24]. Usually, researchers use all supports with the syringe pump since hand-held is not possible.

Once the GAE system is set up, the aspiration process can start. The piston must be completely inserted into its chamber to allow screwing it outwards [24]. Before the cannula is inserted into the gel, the piston is set to as low as it can go in the chamber. The piston is then locked so it is unable to move to equilibrate pressure within the system and the surroundings. This permits pressure to be built up in the system when the piston is turned. The immersion of the cannula in the HHC gel during the setting allows a part of the collagen gel to enter into the cannula wall. This air-tight seal between the cannula and the gel is a key pre-aspiration step. Depending on the researcher using the method, a

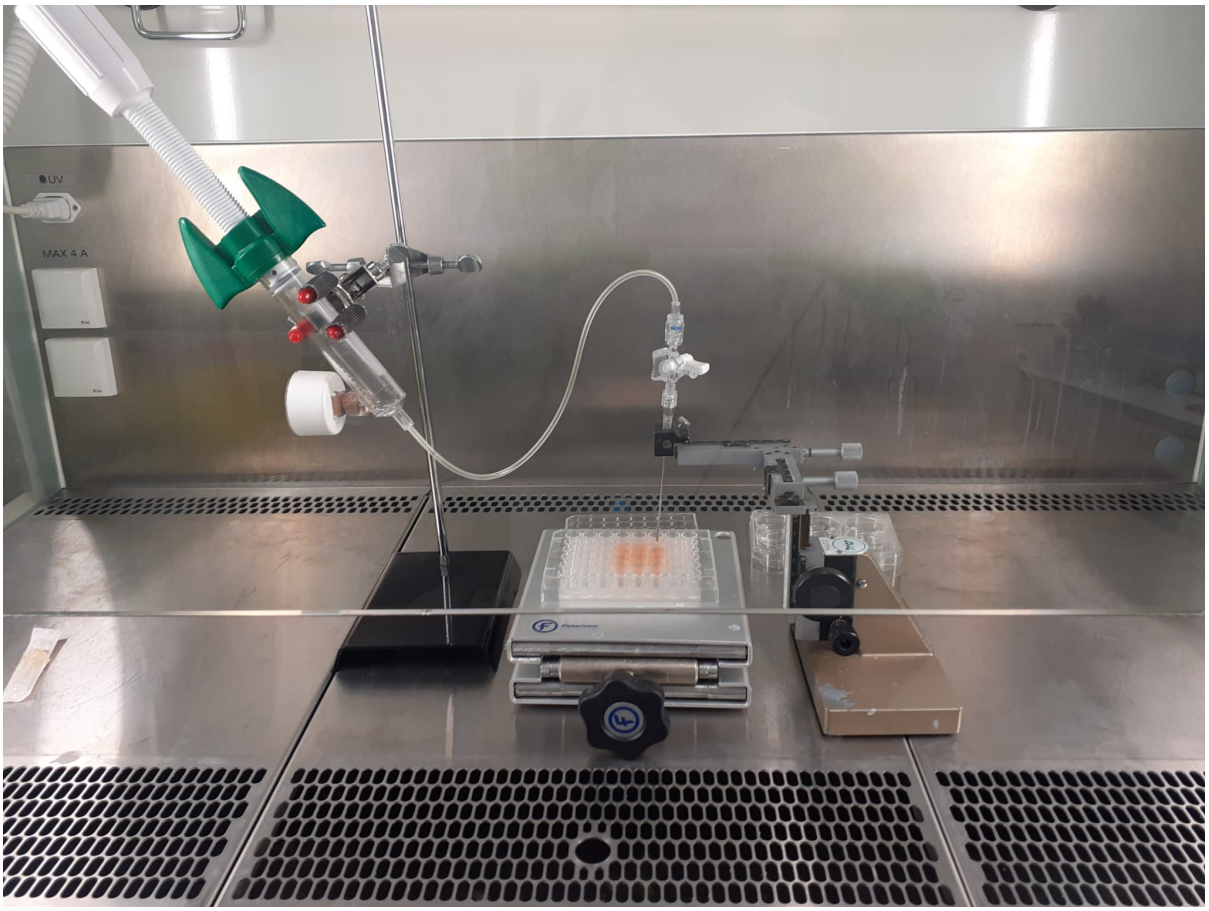

Figure 2.11: GAE experimental setup (provided by Poppy O. Smith)

primary turn of the handle is done before waiting a few seconds (around 10 s) until the gel has correctly set into the cannula to ensure this pre-aspiration step. The aspiration process is performed by gently retracting the piston to generate negative pressure and draw the HHC gel into the cannula [24]. The HHC gel is therefore squeezed and remoulded to fit into the narrow cannula [21][24]. Only the collagen matrix, the embedded seeded cells and other chemical particles to promote regeneration are rising in the cannula while the fluid phase is ejected and collected by the initial collagen gel container.
When using the manual angioplasty device, the applied pressure is only possible stepwise. Indeed, the human wrist has a limited rotational angle. Each turn will draw the piston for a Δx which applies a suction force on the collagen gel that moves upwards into the cannula replacing the pressure drop created by the previous screw turn. This operation is repeated until the entire gel is aspirated into the cannula. Only estimated values of the applied pressure are provided by the Canadian team of Neysan O. Kamranpour et al [24] using about $5 * 10^{-}3$ MPa with the 8G cannula and about 0.1 MPa with the 14G cannula. These values only depend on the user of the method because they depend on how much the wrist of the user rotates the handle, which will apply a higher or lower suction force on the construct for each aspiration time step. On the contrary, the syringe pump applies a constant known pressure on the collagen gel.
When using no support and holding the GAE system in hand, the researcher can help the stabilisation process by creating contacts between the HHG gel that is being aspirated and the edges of the container. This action allows attracting the liquid phase that was already on the surface of the HHC gel to get up and separate from the collagen gel.

In some cases observed during experiments, when the applied suction force is not high enough, for instance when using air in the system and not liquid, a lot of turns of the handle are required to aspirate the gel. In this context, the screw bar can reach the maximal longitudinal displacement. The solution is to reset the system using the Luer lock valve input connected to the fume hood air during the aspiration because no fluid transfer syringe is connected. The lock system closes the cannula input and allows the air from the angioplasty device to flow out which allows the piston to be completely inserted into its chamber. This enables resetting the aspiration system positioning the Luer lock valve down in its chamber and continuing the aspiration screwing the piston upwards. This stage allows not to start the experiment again due to a too short piston. However, it adds a lot of interfering events that add variability in the method and can alter the results.

The aspiration process is stopped when the gel is almost fully drawn into the cannula [21][24]. Approximately 2 mm in the length of the gel is left out of the cannula[21]. Some intermediate steps before the ejection depend on the user. Some researchers do not use any transfer syringe and simply reverse the direction of screwing the piston of the angioplasty device. However this method can damage the constructs for certain experiments. In the case of using only one Luer lock valve, the third input is connected to the room air during the aspiration. Once the construct has been aspirated the system can be opened to the air to equilibrate the pressure in the system. Afterwards, the fluid transfer syringe is placed at this third input of the Luer locker valve. The system is therefore ready to eject the GAE-EngNT by drawing down the syringe and the air or the fluid can flow from the syringe to the cannula to eject out the GAE-EngNT. When two Luer lock valves are used, a primary step before the ejection is to close the vacuum line by locking the distal Luer lock valve. This step prevents the aspirated gel from entering the angioplasty device and keeps the compacted hydrogel in the cannula [21][24]. The fluid transfer syringe already attached to the proximal Luer lock valve, is taking an open setting between this syringe and the angioplasty device. Afterwards, the two Luer lock valves are adjusted manually to open the pathway directly between the cannula and the angioplasty device in order to start the ejection [21][24]. In both scenarios, the fluid transfer syringe needs to be filled with air or fluid beforehand. The output is a cylindrical GAE-EngNT construct with the same cross-section area as the cannula. The final construct is usually ejected on a clean surface to measure it or in a well-plate with physiological liquid to conserve it and be able to analyse it later on [21][24].

Concerning the timing of the GAE method, a well-known result is that the ejection is always faster than the aspiration. The measured time required for a complete aspiration is different among the researchers performing the GAE method because it depends on the size of the cannula, the suction force applied, and the rate at which the force is applied. As explained previously, this applied force is thought to vary a lot depending on the researcher performing the aspiration using the manual angioplasty device. The Canadian team of Neysan O. Kamranpour et al [24], that has succeeded at giving an estimation of the force applied, also has provided a timing estimation for the aspiration of around 10 s for an 8G cannula and 100 s for a 14G cannula. At the UCL Centre for Nerve Engineering, the timing of the aspiration has also been reported by Rebecca Powell estimating the aspiration to be 270 s. The ejection time has never been precisely reported even if the total time from aspiration to ejected gel has been evaluated by Rebecca Powell to 360-420 s. The use of a syringe pump allows a faster global process because it applies

the suction pressure continuously with a controlled application rate. Indeed, the pump is not limited to the wrist's ability to turn the handle. This feature is aligned with the timing measurement of Poppy O. Smith who performed the entire production process in 15 minutes with the manual angioplasty device while the GAE-EngNT were produced in less than 5 minutes using the syringe pump.

Failures

The GAE method is not always successful. Besides, there are a lot of variations between users in the estimation of the percentage of the number of successful constructs per total number of trials for one setting as can be seen in table 2.7. Indeed, the value is only an estimation and is dependent on the way to perform the GAE process with all the variabilities exposed here above. Due to the non-automated aspect of the method, the failure rate is also dependent on the experience of the user. It has also been reported that the percentage of success is higher with the syringe pump than with the manual angioplasty device especially at the beginning when getting used to the GAE method. A complete and precise statistical study would be useful to understand the added value of the syringe pump and the automated system.

Work of	Number of success construct per total number of trials for one setting (%)
Poppy O. Smith	50-60% with manual angioplasty device 90% with the syringe pump
Rebecca Powell	100%
Ryan Trueman	>90%

Table 2.7: Report of the percentage number of successful construct per total number of trials for one setting estimated by the three GAE researchers of the UCL Centre for Nerve Engineering (based on interviews)

Typical causes of failure of the method during experiments at the UCL Centre for Nerve Engineering have been identified. The first failure case is when the air-tight seal between the cannula and the gel is not tight enough during the pre-aspiration step described earlier in the GAE process explanation section. This failure can occur due to the low quality of the seal between the gel and the cannula or a primary turn that is not adapted, causing an inadequate primary pressure value and application rate. An air leakage in the GAE equipment could also decrease the ability of the system to provide a sufficient suction for the pre-aspiration stage. This failure can also occur when the cannula is not well-positioned at the surface centre of the gel and is slightly immersed. The immersion needs to be sufficient but not too large to allow a part of the HHC gel to be pushed into the cannula before the aspiration. When the GAE system is used hand-held, shaky hands provide poor positioning of the cannula and dislodge the gel which causes pressure to break. The consequence is an HHC gel that is not captured enough into the cannula to be aspirated.

A failure of the production of the GAE-EngNT can also occur during the aspiration when a part of the collagen has already been aspirated but gets stuck in the cannula and

is not able to be aspirated any further. This can be due to a leakage in the GAE system which decreases the suction force on the construct in the cannula or shaky hands with the manual angioplasty device used without support which potentially dislodge the gel and causes pressure to break. In addition, a wrong application of the suction force in terms of value and application rate leads to a failure of the GAE process.

The ejection itself rarely fails. Indeed, once the applied pressure and application rate are controlled it is relatively easy to eject the construct. Only pressure that is too high and not applied gently enough could break the construct while ejecting it.

Sources of heterogeneity

The above explanations show a large variability between users of the GAE method. The way to process the HHC gel to produce GAE-EngNT is therefore highly user-dependent which can have a relative influence on the GAE-EngNT characteristics and potential for peripheral nerve regeneration. Table 2.8 aims at summarising the sources of heterogeneity in the GAE process which could be used as parameters for mathematical models.

Gel preparation	Animal origin of the collagen type I
	Composition of the collagen gel
	collagen concentration in the final HHC gel solution
	Volume and geometry of the HHC gel solution
	Type of seeded cells
	Concentration of seeded cells in the final HHC gel solution
Setup	Use of supports (which ones) or hand-held technique
	Position of the cannula regarding the HHC gel before the aspiration
	Cannula size
	Use of air or media or a combination of both in the GAE system during the aspiration and/ or the ejection
	Use of one or two Luer lock valves
Aspiration	Manual aspiration or syringe pump • Applied pressure value (pressure profile) • Applied pressure rate • Timing of the process
	Technique for the pre-aspiration step to capture the gel into the cannula
Ejection	Ejection on a surface or in a container filled with media
General process	Experience of the user

Table 2.8: Source of variability expressed in terms of parameters

2.4.3 Outcomes of the GAE method: GAE-EngNT study

The two research laboratories working on the GAE method have been studying the properties of GAE-EngNT constructs and their ability to promote nerve regeneration. The main relevant results of the GAE technique are presented in this section. However, entire studies on EngNT constructs using GAE to promote nerve regeneration are still ongoing and can be found in the literature of the two research teams [16] [21] [24].

The first outcome that can be reported is the geometry of the final GAE-EngNT. It is a cylinder of the same diameter as the cannula [16]. Concerning the length of the construct, the values reported by the different research works are different depending on the initial volume, the cannula size, the stabilisation process, the applied pressure value, and the aspiration application rate. For these reasons, these values are only estimations. Indeed, starting with an initial volume of the HHC gel of 1.5mL, the Canadian team of Neysan O. Kamranpour [24] measured the length of the GAE construct for the different cannula sizes and the results are reported in table 2.9. The data were extracted from the images of the publication of Neysan O. Kamranpour et al. [24] in figure B.1 in the appendix, using an online tool of picture measurements [45]. Starting with 1mL of the initial volume, the UCL Centre for Nerve Engineering obtained constructs of approximately 12 mm long.
Secondly, the Neysan O. Kamranpour publication [24] reported the CFD which can be found in table 2.9. These values were extracted from the figure B.2 in the appendix, using the online tool of picture measurements [45]. The CFDs were calculated by weighting the gel before and after freeze-drying following the formula [21]:

$$CFD\ (wt\%) = \frac{W_{dry}}{W_{wet}} * 100$$

Team	Needle gauge number	Length of the construct (mm)	CFD (wt%)
Canadian team Initial CFD: 0.8 wt%	8G	8	6
	10G	8.75	8
	12G	9.58	12.5
	14G	10.33	18
UCL centre for nerve engineering	16G	12	Not reported

Table 2.9: Measured lengths and CFD values of the GAE-EngNT construct regarding the cannula size (based on [16] [21] [24] and interviews)

The increase in the CFD is a key feature in the GAE method as it leads to a change in the mechanical properties of the GAE-EngNT. The main results of this study conducted by Neysan O. Kamranpour et al. [24] and by Papon Muangsanit et al. [16] [21] were explained previously in section 2.2.5.

Furthermore, the GAE method is able to align the collagen fibrils during the stabilisation stage due to the volume change in the cannula. The microstructure is therefore tuned and can be observed using Scanning Electron Microscopy (SEM), Nonlinear Laser Scanning Microscopy (NLSM) imaging, and ImageJ edge directionality algorithm [24]. Those techniques aim at quantifying the fibrillar orientation [3]. It has been observed by Neysan O. Kamranpour et al [24] that the fibril orientation is aligned with the longitudinal axis of the cannula. The alignment of the fibrils in the construct can also be assessed by looking at the distribution of the deviation angle which indicated the dispersion, i.e. the scattering in the orientation of individual fibrils from the mean orientation. Only Gaussian distributions are observed by Neysan O. Kamranpour et al [24]. The curves are narrower gradually from 8G to 14G. Indeed, increasing needle gauge numbers mean decreasing the inner diameter of the cannula. Therefore, the driving force to fit the cannula shape is higher for a higher needle gauge number leading to a better alignment of the fibrils. In addition, all mean deviation angles of GAE-EngNT are lower than the one obtained with non-tethered PC but the fibrils are more dispersed than native tissue. Moreover, the stress-strain curve of the 14G cannula indicates an anisotropic matrix. Indeed, the presence of a clear toe region is associated with fibrillar realignment in the direction of the applied stress [24]. On the contrary, the 8G, 10G, and 12G lack of the initial toe region is a typical feature of randomly oriented constructs. The UCL Centre for Nerve Engineering, for its part, evaluates the alignment of the cells inside the GAE-EngNT construct. Generally, the cells follow the collagen fibrils' alignment because they are trapped in the network. However, in some specific conditions, a poor cell alignment is observed while the collagen fibrils are well-aligned. Another particular observation is an alignment of the cells which is not homogeneous within the construct. Moreover, the region with the best alignment varies depending on the research work. Indeed, Papon Muangsanit et al. [16] [21] evaluated that the alignment was greater in the regions that were aspirated first compared with the leading end which was aspirated later. Oppositely, Poppy O. Smith and Rebecca Powell observed that the cells are nearly not aligned for the firstly aspirated gel part while the most aligned cellular arrangement is found in the middle or at the end of the construct, i.e. the part lastly aspirated. Intuitively, the cells that are in the firstly aspirated part of the gel travel further within the cannula. Therefore, they are exposed to the resultant forces of the diameter reduction over a longer duration than the cells in the last part of the gel to enter. This may not be the only effect to cause the alignment.

Another important feature to evaluate the GAE method is the cell viability. Papon Muangsanit et al [16] [21] evaluated that 24% of F7 seeded cells died just after the GAE, which is a higher death rate than for the PC method. However, the produced GAE-EngNT environment promotes cell activity and the percentage of cell death reduced significantly after 24 hours. Also for this characteristic, inhomogeneities along the construct have been noticed. The cell viability has always been higher in the firstly aspirated part. It can also be mentioned that the cell density increased as the volume decreased following the volume folds.

The bulk hydraulic permeability has also been assessed through a small mathematical model by Neysan O. Kamranpour et al [24]. It depends on porosity, pore size, interconnectivity, and orientation of the fibrils. It enables to control seeded cellular responses. In addition, the anisotropy of the construct is proved by a ratio between the permeability in the two main directions, different than one.

The final goal of the GAE-EngNT is to provide an optimised environment to promote nerve regeneration. It is, therefore, crucial to study the seeded cells' response in the constructs, which is the aim of numerous projects conducted using the GAE method. Depending on the focus of the research, different seeded cell behaviours are targeted such as the cell differentiation of mesenchymal stem [24], the ability to produce tube-like structures with a co-culture of F7/HUVEC or current conduction by PPy nanoparticles. The research study can also assess the efficiency of the GAE-EngNT in terms of revascularisation or during *in vivo* experiments. Promising results are found for GAE-EngNT to bring mechanical, chemical, and structural cues for peripheral nerve regeneration.

2.4.4 Potential of GAE

The GAE method has a large potential for peripheral nerve regeneration as its outcome has been proved to mimick ECM properties thanks to its stabilisation ability [21]. Indeed, promising results show the ability of GAE-EngNTs to provide chemical, mechanical, and structural cues to promote nerve regeneration after a lesion. However, the optimisation of the GAE-EngNT is still an active research topic adapting the parameters of the HHC gel and the GAE technique to enhance the ability to promote nerve repair.

One of the strengths of the GAE process is its suitability for a large number of diverse projects using different seeded cells, different volumes targeting different properties and behaviours of the GAE-EngNT. A quick overview of the different works at the UCL Centre for Nerve Engineering is a good illustration. A first project conducted by Poppy O. Smith consists in producing GAE-EngNT constructs seeded with endothelial cells. The GAE is used to simultaneously stabilise, align the hydrogel-based nerve repair construct and allow the formation of tube-like structures by after in the GAE-EngNT. While the PC method disrupts those structures due to the stabilisation, the GAE method allows for stabilising the gel before its formation. Those tube-like structures are proved to help the migration of Schwann cells to bridge the gap in a nerve lesion. Another different project is the one of Ryan Trueman working on promoting nerve regeneration with electrical stimulations. In this case, the GAE method allows to simultaneously stabilise and align a collagen gel containing seeded cells and conductive components such as Polypyrrole (PPy) nanoparticles. As for Rebecca Powell, she used the GAE method to stabilise and align a collagen gel seeded with induced pluripotent stem cells. The optimisation of this construct with differentiated Schwann cells is under investigation.

The GAE method has a real added value compared to other stabilisation methods as it provides the three properties explored in table 2.10 at once [24] [44].

	Electric and magnetic fields or microfluidic devices	PC	Crosslinkers	GAE
1. Anisotropic construct: Autograft presents columns of aligned Schwann cells embedded within an anisotropic extracellular matrix (ECM). This particular organisation provide structural and mechanical cues for nerve regeneration.	YES	NO (except with pre-step of tethering)	NO	YES
2. Collagen Fibril Concentration similar to ECM	NO	YES	NO	YES
3. Strengthening of the collagen gel: Stiffness similar to biological tissue	NO	YES	YES	YES
4. Cylindrical geometry: Direct product of the correct shape for in-vivo ejection	NO	NO	NO	YES

Table 2.10: Potential of the GAE method compared to alternative techniques (based on [24] and [44])

The last characteristic is a real added value of the GAE method as it makes it an easy and fast method without pre-or post-processing steps to create the aligned construct with the corresponding cylindrical shape for *in vivo* experiments. No use of silicon support is required nor complex surgical interventions, which make the GAE a less invasive technique [24][44].

All those advantages also make the GAE method much faster. Less than 15 minutes are needed to produce the final GAE-EngNT construct from the HHC gel compared to approximately one hour for the PC method.

In addition, an automated GAE system could bring a fine control on many important parameters of the engineered nerve tissue such as the CFD, the cell density, the cell distribution, the alignment, the length of the construct, the cell behaviour, cell differentiation, drugs delivery, and the optimisation of the construct by addition of new particles [24][44].

The GAE method has therefore a large scientific added value but also a clinical, and industrial potential. Indeed, the technique is suitable for large scale productions thanks to the automation. It can also provide an easy and fast way to directly eject the construct at the lesion site in vivo which promises great clinical success.

2.4.5 Limitations of the method

However, the GAE method has some limitations to the definition of the process itself. Firstly, the GAE-EngNT provides a good inner component of nerve conduits, but these may ultimately require strong outer sheath materials that match the mechanical properties of the epineurium [24]. Another limitation is the high side effects of the important changes of shape when entering the cannula. Together with the aspiration/ejection forces, the entry inside the cannula can lead to some cell adverse behaviour or high cell death rate at the end of the process [24].

Chapter 3

Primary model focus

The second step to build a primary mathematical model for the stabilisation methods of EngNT constructs is to define the focus of the *in silico* representation. On one hand, the model focus is developed in detail for the GAE process since this research work targets this technique as a priority. Firstly, the experimental challenges are presented with the pros and cons of mathematical modelling to bring solutions to those challenges. Afterwards, the multi-disciplinary approach is shown as a good perspective to answer the experimental challenges by combining experiments and *in silico* simulations. The current primary stage in this integrated strategy is also presented. To initiate this workflow, five ideas of primary model focus are explained. Finally, the selected GAE model focus is presented. On the other hand, the primary model for the Plastic Compression method explores some ideas about parallel modelling of both stabilisation methods, specific PC technique insights, and a coarse primary model.

3.1 Gel Aspiration Ejection focus

3.1.1 In silico model need

Experimental challenges

Besides its internal limitations, the GAE process is not yet optimised. While discovering the potential of this method, a lot of questions and challenges arise and still need to be answered. Firstly, the lack of clear and well-defined protocols for the GAE method brings a lot of intra- and inter-operator variability. Moreover, a high inter- and intra-operator variability is also observed in the final GAE-EngNT construct properties. The origins of this variability in the results are not yet identified. These features show the need for automating the GAE process. However, the parameters and the strategy for this automation are still lacking. Furthermore, some GAE outcomes presented in section 2.4.3 can not find any explanation yet such as the inhomogeneity in the cell alignment and cell viability along the construct or the cell alignment which does not follow the collagen fibrils in specific cases. Indeed, the GAE process is not yet fully understood. Therefore, its impact on the final construct needs to be investigated. In addition, the GAE process has different stages and the importance of each process step are not yet known. In some cases reported in section 2.4.2, the GAE process fails and any construct can be produced. As it costs time and money, the process should be controlled to ensure the best successful rate. As far as the maximum length of a produced construct is concerned, it is currently 12 mm. In order to be an interesting alternative to autografts, the length of the EGNT should be

around 15 mm. Some silicon conduits are used for ejecting the GAE-EngNT in large nerve gaps but the method should be optimised to produce constructs with the desired length directly [24]. Additionally, the full potential of the GAE is not yet completely explored as the outcomes of GAE-EngNT are not yet comparable to autografts in terms of nerve repair. Optimisation of the method would allow the production of GAE-EngNTs which would promote even more nerve regeneration than the existing current alternatives. The last disadvantage pointed out by the experimentalists is the lengthy setup to attenuate the variability. In addition, to avoid the use of supports and to increase the rapidity of production, the hand-held technique is used which is particularly uncomfortable.

Pros and cons of mathematical modelling

The conclusion of the experimental challenges listed above is the need for a better understanding of the GAE method. The goal is to control the process aiming at producing the targeted GAE-EngNT construct design. Mathematical models have a key role in this current need as they can help to answer each experimental challenge. They can bring a real value to optimise the GAE method, identify the best parameter values to automate the system and exploit the full potential of the method by simulating desired outcomes. One of the key added value of mathematical modelling is the ability to deal with a large number of parameters and requirements. Indeed, in order to use an optimal method to produce the desired GAE-EngNT promoting nerve regeneration, experimentalists need to deal with a lot of variables. In addition, the biomedical field of nerve repair also requires a large number of requirements such as sterilised equipment, cost-effective processes, and clinical uses [39] [46]. Besides the design process, mathematical models offer a way to standardise, provide streamlines, and accelerate the nerve construct development workflow [8] [46]. Indeed, they are able to bring the parameter values to automate the process and be compatible with clinical use. Additionally, *in silico* models often bring a better understanding of the production process of EngNTs or the effect of some variables on the final construct. This understanding is a key feature to develop new ideas about nerve repair constructs, testing, and selecting promising solutions. Furthermore, mathematical models are a cost-effective method in terms of time, money, and equipment. They also align with the "3R approach" to reduce, remove or refine the use of animals for scientific experiments [46] [47].

However, those *in silico* models have their own limitations such as the need for quality and quantity of data to allow the parametrisation of the model and the need for experiments to validate it [3][8] [46]. Another important issue of mathematical models is the ability to target only a part of the EngNT process or design due to simplifications and assumptions. This leads to some aspects of the model being relatively far from the *in vitro* and *in vivo* reality. By definition, a mathematical model focuses on some specific aspects of the process to answer a specific experimental challenge. It would be wrong to pretend to model the entire process. Indeed, a model is a simplification of reality and largely depends on the choice of the initial theory.

3.1.2 Multi-disciplinary approach

An integrated approach combining *in vitro* experiments and mathematical models is the best approach to deal with the limitations and take advantage of each to provide the best effective solution to clinical needs. An integrated workflow is proposed by Rachel H.

Coy et al.[46] for the EngNT design but that can be adapted to the design of the GAE method targeting the desired construct. The adapted version of the diagram is presented in figure 3.1. Beforehand, the potential of the GAE method needs to be discovered by experiments and used in nerve construct studies. This is the actual current stage for the GAE. Challenges of the experimental approach appear and the need for *in silico* model emerges. A primary mathematical model is built targeting the simulation of the method *in silico*. A good understanding of the process, the equipment, and the material used is essential for choosing an appropriate approach. This was the focus of chapter II. As explained earlier, every mathematical model has its limitations in terms of simplification of the physical reality and the assumptions. It is therefore essential to define the purpose of the model and the characteristics on which it focuses while neglecting other aspects. This design loop can be repeated with different models focusing on different aspects of the process. On the focused features, the mathematical model needs to best fit the experimental reality, therefore, targeted experiments need to be conducted to identify the parameters to feed the *in silico* representation. Depending on the target of the model, simulations are run varying some parameters in a dedicated range of values which explore different designs of the GAE method [8] [46]. After that, experiments can be conducted following the design results of the *in silico* simulations. Some *in vitro* or *in vivo* data enable to validate or feed the model with new data for refinement [8] [46]. Like experiments, mathematical models are neither bad nor good, they aim to be useful and this cannot be achieved immediately. Trials, refinement, validation and targets need to be performed in an experimental-theoretical feedback loop as shown in figure 3.1 [8] [46].

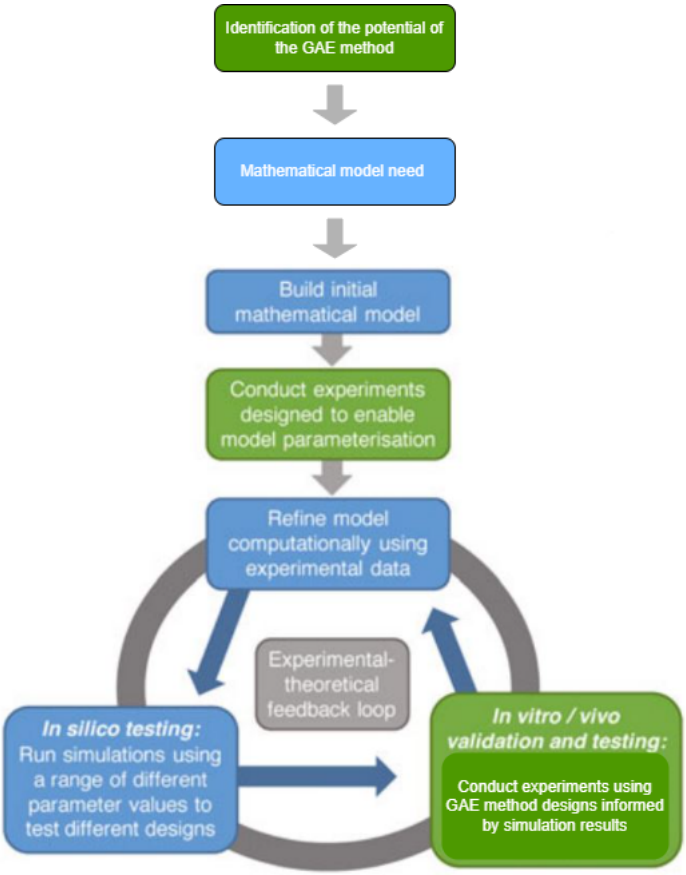

Figure 3.1: Experimental and theoretical integrated approach workflow (based on [46])

This integrated approach to the GAE design process should be the subject of a wider study spreading over a long period of several years. The current stage is the discovery of the potential of the GAE and of the challenges that require the need for mathematical models. This research project has been focusing on this stage and proposes a primary mathematical model to initiate the control of the GAE method on one aspect. The selection of the model focus is discussed in the next paragraph.

3.1.3 Ideas of model focus exploration

To date, no model has been proposed for the GAE method. Moreover, any kind of processing and behaviour of a similar collagen gel has not yet been modeled in the literature. Therefore, the choice of a primary mathematical model focus starts from scratch. As explained in section 3.1.1, mathematical models always focus on specific aspects of the process. The stage of the GAE method and the background theory are chosen for the *in silico* model and define its focus. Different approaches are explored as can be seen in figure 3.2. A quick overview of each model focus is provided with its modelling aim and its limitations. The final choice is the fifth approach, defined as the dynamic analysis. Looking at the limitations of the other approaches, the fifth one appears to be the best choice also considering the time and experimental data available for this research work. However, it could be interesting to consider the other approaches in a longer integrated study.

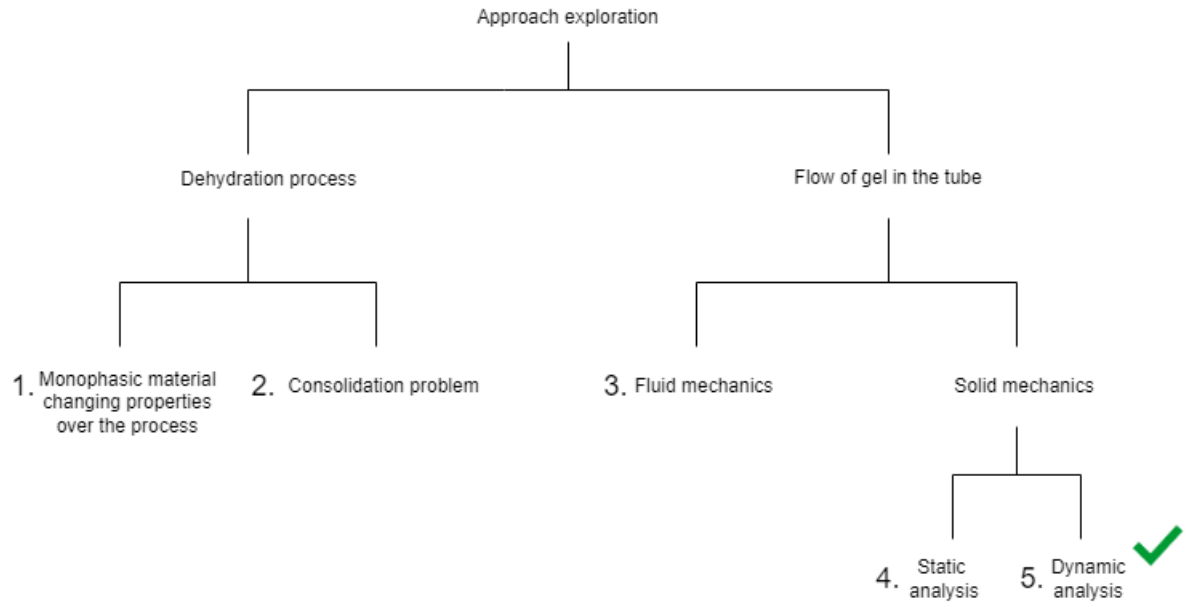

Figure 3.2: Chart of the approach selection for the GAE initial mathematical model

At first, two big categories of focus for the GAE model can be distinguished. On one hand, the GAE method can be seen as a stabilistion process of a hyper-hydrated gel that undergoes large deformation and expels the majority of the fluid out of the collagen gel. On the other hand, the mathematical model can focus on the progression of the collagen construct inside the cannula during the aspiration and the ejection of the GAE process. In this case, no large deformation, water expelling, or guidance of the gel into the cannula is considered. A major part of the GAE process is, therefore, neglected. However, these

models aim at determining the impact of the aspiration and the ejection of a dense collagen gel inside a narrow cannula testing different process parameters such as the applied pressure and the application rate or the dissipation due to contact with the cannula walls. Focusing on modelling of the stabilisation process, two different approaches can be chosen.

1. Monophasic material changing properties over the process

The approach is to use fluid mechanics to model the HHC gel as a monophasic fluid flowing from a mould into a narrow cannula. The stabilisation process would be modeled in terms of changing mechanical properties of the material such as the viscosity when entering into the cannula. The outcome of the model would be the velocity profile of the material from the inlet to the outlet and the stress distribution. The focus of the model is therefore on the effect of this change of shape when entering the cannula, on the outcomes of the approach. However, no deformation profile is shown as a result.

Even if this approach seems intuitively related to the physical process, it has a lot of limitations. Indeed, the losing part of the HHC gel while entering inside the cannula is not modelled due to the monophasic consideration. In addition, the gel needs to be considered as a fluid which is not particularly the case when looking at the mechanical properties of the collagen gel in section 2.2.5. Indeed, the storage and loss moduli are only slightly varying over the frequency range. Moreover, the storage modulus is nearly always higher than the loss modulus. In parallel, no fluidic rheological data required to model the flow of the gel from the well-plate to the cannula can be found. There is, therefore, no similar data for the change of properties when entering inside the cannula. In addition, no similar model could be found in the literature and therefore, this approach has been disregarded.

2. Consolidation problem

This approach considers the poroelasticity theory which deals with soft soils as porous medium [48]. Those materials, such as sand and clay are small particles, and the pore space between the particles is filled with water [48]. The deformation of such porous media depends upon the stiffness of the porous material, and upon the behaviour of the fluid in the pores. The consolidation theory studies the simultaneous deformation of the porous material and the flow of the pore fluid [48]. This approach is well suited for the GAE method as it considers the collagen gel as a biphasic porous material with a material behaviour highly compressible allowing deformations as large as several percent, whereas the constituents, particles and fluid, are very stiff [48]. It has also the advantage of studying the hydraulic and mechanical behaviour of the collagen gel during the stabilisation process. Another key feature is having a solid framework to start with and adapt to the nerve engineering context.

The poroelasticity theory holds in a set of equations that form with the usual variables: p, u_x, u_y *and* u_z . On one hand, there are the equations of conservation of mass and on the other hand, the equilibrium equations in terms of displacements. The assumptions of this poroelastic theory are the use of linear material, the linear compressibility of the solid particles, and the fluid, the validity of Darcy's law and static deformations only, i.e. disregarding inertial forces [48]. More complicated situations can be found in poromechanics theory.

A well-known basic model to start within this field is the Terzaghi consolidation problem. A confined soil sample is immersed in a container filled with water. The sample is loaded by constant vertical stress at its upper surface which is fully drained. On the contrary, the lower boundary is impermeable [48]. This problem is called the confined compression test or the oedometer test and is represented in figure 3.3 extracted from Arnold Verruijt's book [48].

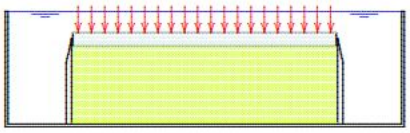

Figure 3.3: Terzaghi's problem (based on [24] and [48])

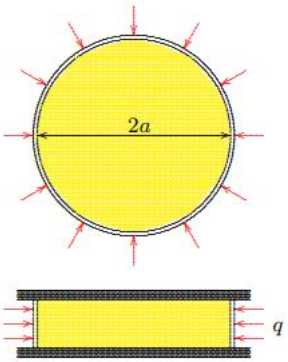

Figure 3.4: Leeuw's problem (based on [24] and [48])

The results are expressed in terms of the pore pressure evolution in time and in the vertical axis along the material [48]. Thanks to the vertical strain, the vertical deformation U can be computed over time [48]. The linear elasticity assumption enables the extraction of the stress distribution in the material over time relatively easily as well. The type of results that this approach can deliver are interesting for the GAE model. The pore pressure evolution would indicate the dehydration level over time, the stress distribution would give an indication of the stress level to which the seeded cells inside the construct are subjected providing some cues about cell viability, alignment, and behaviour during the process.

Naturally, the Terzaghi model on its own is not suited for modelling the PC and even less the GAE process. Indeed, a lot of assumptions need to be adapted such as the 1D problem, the linear elasticity and the isotropic material [48]. The idea for the stabilisation production method model is to adapt the Terzaghi model in 2D, starting with a linear elastic material and adds step by step complexity by considering hyperelastic material and anisotropy, finishing by trying some elasto-visco-plastic theory to deal with the large collagen gel deformation. To be able to represent the GAE process, the boundary conditions need to be adjusted which is the most challenging part. Some ideas would be to get inspiration from existing alternatives to Terzaghi's problem such as De Leeuw's model [48]. The same framework is used but different boundary conditions and geometries are considered as shown in figure 3.4 from Arnold Verruijt's book [48]. Even if this approach seems promising, a lot of challenges and limitations lead to let this approach for further and longer study. Indeed, the Terzaghi model is a good simple model to start with but several adaptations into 2D or types of material need to be done. For instance, the hyperelasticity model defines the stress-strain relationship with a strain energy function while the initial Terzaghi model is written with an explicitly stress-strain relationship.

An important and challenging adaptation is also to consider large plastic deformation. As seen earlier, the specific boundary conditions to fit the reality of the GAE process is also a challenge for this approach. Lastly, this point of view proposes a static resolution. Consequently, no dynamic simulation of the stabilisation method is possible particularly interesting for the evolution of the gel inside the cannula during the stabilisation in the GAE process. Dynamic effects could be considered by adding extra complexity, for instance by adding an inertia term. However, the Darcy law may no longer apply.

The focus is now driven to the modelling of the progress of the collagen gel inside the cannula during the aspiration and the ejection of the GAE process. Three different approaches can be considered, one in fluid mechanics and two in solid mechanics.

3. Fluid mechanics

This approach was inspired by the extrusion-based bioprinting of specific hydrogels [49]. The idea is to consider the hydrogel as a fluid flowing into the cannula from an inlet to an outlet. Computational Fluid Dynamics (CFLD) models are used to simulate complex flow behaviours and complex nozzle geometries [49]. The most common type of fluid that can be considered in this situation is an incompressible, non-Newtonian fluid material (at constant temperature) with steady laminar flow [49]. This leads to the use of a rheological model to simulate the flow behaviour as a power-law relationship [49] [50]. This approach is particularly interesting with shear-thinning fluids. This approach seems interesting as it could compute the shear stress and the velocity profile of the fluid material in the cannula with different geometries which can be related to important properties of the final EngNT construct. It also enables to perform a sensitivity analysis to determine which geometrical parameters or applied pressure profiles impact the most the cell viability and alignment along the construct.

However, the viscosity curve over the shear rate would be required in order to identify two parameters (the consistency index and the flow behaviour index) to feed the model [49] [50]. Those data are really hard to find in the literature even for the hyper-hydrated gel. Therefore, the question that arises is "Is this theory applicable for the collagen gel inside the cannula of the GAE method ?". Indeed, even the HHC gel can not be clearly considered as a fluid because the loss and the storage moduli vary slightly over the frequency with a storage modulus nearly always higher. The only viscosity value found in the literature is for the HHC gel around $6 * 10^4 Pa.s$ which is extremely high for a fluid. Indeed, the viscosity of fluid material ranges in the order of magnitude of mPa.s [34] [50]. In addition, no study about the mechanical characteristics of this collagen gel (stabilised or hyper-hydrated) notified this gel as a shear-thinning material. Naturally, this approach can be adapted with another types of fluid material with particular properties. However, it was a difficult task to find a proper CFLD models for the GAE process of the collagen gel with the low amount of information and knowledge about this gel and this method. Moreover, this approach would be applied only on the cannula of the GAE system where the collagen construct is not properly flowing but it's more progressing few millimeters upwards and then downwards during respectively the aspiration and the ejection.

4. Static analysis

The idea of this approach is to consider the collagen gel construct inside the GAE cannula at a particular snapshot of the aspiration process. Indeed, the static approach would use the theoretical background of static solid mechanics [51]. Therefore, the collagen gel construct is considered as a solid material with a suction force applied on the top surface and constrained on the side walls by a zero displacement condition. The situation would represent an intermediate stage during the aspiration when the experimentalists starts a new rotation of the handle of the angioplasty device but the friction forces of the gel at the walls are too strong to allow any upward movement of the construct into the cannula. The static analysis will study only the deformation of the construct in this intermediate step during the aspiration. Naturally, this approach can be also used to simulate the same situation but during the ejection. Starting with the simple model of small linear elastic deformations, the strategy would be to add step by step complexity for instance, considering hyperelasticity and viscoelastic materials. The outcome of the model would display the deformation of the material and the stress distribution over the material volume. The interesting feature would be to look at the direction of the deformation vector which could give some cues about the alignment of the collagen fibrils or seeded cells. The shear stress and major principal stress level could indicate the stress applied on the seeded cells during those intermediate aspiration steps which could show risk for the cell viability. It would also be interesting to correlate the orientation of the major principal stress with the displacement vector and the cell alignment.

This approach is classic and easily validated. However, it is a bit less interesting as the results would be difficult to relate to real alignment or cell viability results after the entire GAE process. Indeed, only an intermediate step during the entire aspiration is modelled which neglects most of the GAE process. In addition, this approach can not be used when considering the automated approach with a continuous aspiration and ejection which is the current development direction for the GAE method. Moreover, it would be challenging for this model to represent the reality of the intermediate stage during the aspiration process as there are more than one intermediate aspiration stages with different volumes of gel in the cannula. It is also difficult to evaluate with precision the value of the suction pressure applied at those snapshot stages since the applied force has to be just not enough to cause the motion of the construct upwards. Finally, due to no time dependency, the viscoelasticity property of the GAE-EngNT is not modelled. For all the reasons cited above, this approach is also disregarded.

3.1.4 Selected GAE model focus

The selected approach is the dynamic analysis to model the progression of the GAE-EngNT construct inside the cannula. During the GAE process, different phenomena take place. However, in order to understand the role and the importance of each, it is interesting to isolate each stage and identify its effects. Therefore, this model approach neglects the stabilisation process and the large deformation due to the entrance of the construct in the cannula. On the contrary, it focuses on the construct when it's already inside the cannula. The progression of the GAE-EngNT construct due to the aspiration pressure and the interaction with the cannula walls are studied. This approach is only using solid dynamics theoretical background [52] [53]. A differential pressure is applied between the bottom and the top part of the *in silico* construct in order to simulate the

suction force during the aspiration and the pulling force during the ejection. The material is also constrained horizontally at the walls of the cannula. Thanks to the applied pressure in the dynamic framework, the movement of the collagen construct inside the cannula is simulated. The final displacement reached depends on the pressure level applied, the stiffness and density of the material as well as the consideration of friction forces at the wall boundaries. The dynamics analysis is, therefore, the momentuum equilibrium of the construct inside the cannula considering its inertia, its elasticity, damping effects and applied external forces [53]. The equation to solve is a differential equation in time and in space. The basic model of solid dynamics considers a linear elastic material, however [53], the complexity is easily added considering a viscoelastic material [52].

The goal of this approach is to understand the mechanical features and the energy balance occurring inside the cannula during the aspiration process. The target of the model is firstly to provide an explanation for the failure of the GAE process during the aspiration. The appropriate applied pressure value and the magnitude of the dissipating process are identified to avoid this failure for different gauge sizes. In addition, the major principal stress distribution and orientation could provide some cues about the impact of the aspiration stage in the cannula on the direction of the cells and the collagen fibrils. The shear stress distribution would also be relevant to observe the stress level to which the cells are subjected during the aspiration. This shear stress distribution and peak identification can be a good indicator of inhomogeneities of the cell viability along the construct. In conclusion, the research question the selected dynamic model tries to answer is:

"What is the impact of the dynamic aspiration of the GAE-EngNT construct inside the cannula, on the success of the GAE process, the cell viability and alignment?"

3.2 Plastic Compression modelling exploration

3.2.1 Parallel modelling of the GAE and the PC method

In the two first chapters, two stabilisation methods for the production of Engineered Neural Tissues have been studied. Even if the focus of this research work holds on the Gel Aspiration Ejection method, the PC stabilisation technique has also been used in previous works at the UCL Centre for Nerve Engineering. The GAE process appeared by after as a good alternative to this PC method. However, neither of them has been modelled and studied in an integrated approach as explained earlier. Both methods follow the same principle which is expelling the majority of the fluid phase from the hyper-hydrated collagen gel to produce engineered nerve constructs which have similar properties as the natural nerve tissue. They share a lot of common features in the collagen gel composition but also in the experimental challenges. Therefore, it is interesting to model them in parallel using the same theoretical approach and be able to compare their results and phenomena. Consequently, during the entire literature research process for the theory of the mathematical model, both processes were kept in mind even if the focus was given to the GAE method.

3.2.2 Specific PC modelling insights

Concerning the experimental context study, the same collagen gel is used with the GAE and the PC method. Indeed, those two techniques have simply two different ways to stabilise the same HHC gel. However, depending on the research study, different seeded cells or other particles are used. Since the literature is richer for the PC method, a proper literature study is essential to create a table similar to table 2.2.

Furthermore, the PC process is also different from the GAE, and therefore, specific experimental challenges arise. A proper study of the process as the one presented in section 2.4.2 is also essential. A similar conclusion of the need for mathematical modelling also holds for the PC method. The integrated approach strategy is also presented as the future perspective for longer studies focusing on the PC process design.

Concerning the focus of the model, the flow of gel in the cannula is obviously not adapted for the PC. This method focuses, therefore, on the stabilisation process. The consolidation approach (approach 2 in figure 3.2) seems the most adapted for the PC process. While it appears clearly a challenge to represent the GAE process with realistic boundary conditions, the Plastic Compression method is relatively similar to the Terzaghi model with compression and drainage at the top surface, considering the first Levis' process shown in figure 2.6B. In this situation, the plasticity characteristics of the deformation could be represented using a permeability that depends on the applied pressure. It would be interesting to investigate in a deeper and longer research study the adaptation of this well-known soil mechanics problem to the PC method.

3.2.3 Primary model for PC method

As it will be explained in section 4.1.3, the *FEniCS* software is used for the resolution of the GAE mathematical model. Beforehand, some tutorials have been practiced to explore the different ways to represent specific well-known theories in *FEniCS* [51] [52]. Specifically, the Poisson equation, the heat transfer problem, the linear elastic beam, and the Navier-Stokes equations are problems explained in the *FEniCS* documentation useful to get used to this software. In order to put into practice, the features learned during the tutorials, a primary model of the Plastic Compression method has been implemented. Obviously, this model is not representative enough of the PC model to be exposed entirely in this research work but an overview is provided in appendix E. This primary model aimed at training to build a model from scratch targeting the PC framework.

Chapter 4

Primary model implementation

After the study of the experimental features and the selection of a primary model focus, the next step is the implementation of the primary model of the GAE stabilisation process. The method developed for this model explains in detail the theoretical and numerical framework as well as the software used for the resolution and the preliminary calculations for the parameter identification. The strategy of the simulations is also presented. Afterwards, the results are generated and presented in five different sections. The simulations are oriented to bring an answer to the model focus formulated in the previous chapter. A discussion is proposed after the results to highlight the interesting features of each computation, finding an answer to experimental challenges on which the model focuses. Putting in parallel the experimental context study and features of the model, the discussion tells the story of the mathematical model implementation and the answer it is able to bring to initiate the understanding and control of the GAE process. Limitations and future developments conclude the chapter opening the way for further study on this interesting and challenging topic.

4.1 Method

4.1.1 Theoretical framework

To keep a low computational time for a primary GAE model, the 2D approach has been preferred to 3D. The focus of the model is the GAE-EngNT progression inside the cannula. Therefore, the geometry is a rectangle of the length of the construct and the width is the inner diameter of the cannula, as it can be seen in figure 4.1.
The selected approach to model the displacement of the construct is the dynamic analysis. The standard balance of linear momentum problem [52] with the boundary conditions for the GAE-EngNT construct defined by the volume Ω can be written as follow:

$$\nabla\sigma + \rho\mathbf{b} = \rho\ddot{\mathbf{u}} \qquad in\ \Omega \times I \tag{4.1}$$

$$u_x = 0 \qquad on\ \delta\Omega_{walls} \times I \tag{4.2}$$

$$\sigma_{top} \cdot \mathbf{n_{top}} = \mathbf{p2} \qquad on\ \delta\Omega_{top} \times I \tag{4.3}$$

$$\sigma_{bottom} \cdot \mathbf{n_{bottom}} = \mathbf{p1} \qquad on\ \delta\Omega_{bottom} \times I \tag{4.4}$$

$$\sigma_{walls} \cdot \mathbf{n_{walls}} = \mathbf{T_v} \qquad on\ \delta\Omega_{walls} \times I \tag{4.5}$$

$$\mathbf{u}(x, y, 0) = (0, 0) \qquad in\ \Omega \tag{4.6}$$

$$\dot{\mathbf{u}}(x, y, 0) = (0, 0) \qquad in\ \Omega \tag{4.7}$$

With σ, the stress tensor, $\mathbf{u}$ the displacement vector of the construct and u_x the x component of this vector. $\dot{\mathbf{u}}$ and $\ddot{\mathbf{u}}$ are respectively the velocity and the acceleration of the construct. ρ is the density of the material, $\mathbf{b}$ is the body force and $\mathbf{n_i}$ are the normal vectors to the surface i. $\mathbf{p_1} - \mathbf{p_2}$ is the differential of aspiration pressure and $\mathbf{T_v}$ is the viscous stress provided by the lubrification layer. In addition, Ω is the volume of the GAE-EngNT construct modelled and $\delta\Omega_i$ is the boundary surface of the construct at the specified location i. Finally, I is the time interval of the dynamic analysis, which is $[0; T]$.

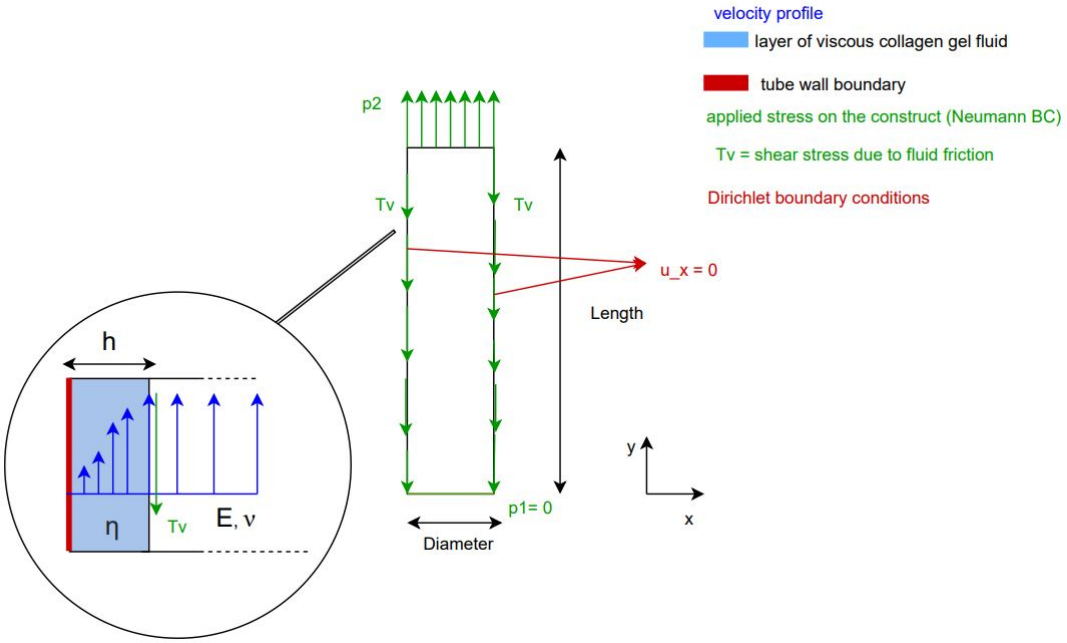

Figure 4.1: GAE process *in silico* representation

The first equation is the equilibrium of linear momentum. Beforehand, the body force term "$\rho\mathbf{b}$" is assumed equal to zero as the body forces are neglected. Indeed, the weight of the construct is negligible compared to the order of magnitude of the applied stresses. In addition, no other force applied on the entire volume Ω is present in the system. Coming back to the equation 4.1, it is extracted from the elastodynamic theory [53] but adapted to a viscoelastic material [52]. The material properties are captured in the σ term defined as

$$\sigma = 2\mu\epsilon + (\lambda \ \ trc(\epsilon) + 2\ \eta_{GAE}\ trc(\dot{\epsilon}))\ \ \mathbf{I} \tag{4.8}$$

Where η_{GAE} is the loss coefficient, linked to the viscous behaviour of the GAE-EngNT material referred to as the damping ($tan\delta$) in the equation 2.5. tr is the trace of the tensor, $\mathbf{I}$ is the identity matrix, ϵ is the strain tensor, and $\dot{\epsilon}$ is the strain rate. μ and λ are the Lamé parameters representing the elastic properties of the material. In the context of elasticity, μ is called the shear modulus, referred to as G in section 2.1. The Lamé constants are connected with the elasticity modulus E and the Poisson ratio ν by [51] [59]:

$$\lambda = \frac{E\nu}{(1+\nu)(1-2\nu)} \tag{4.9}$$

$$\mu = \frac{E}{2(1+\nu)} \tag{4.10}$$

The equation 4.8 is a constitutive equation expressing the stress-strain relationship. In order to express the σ tensor in the equation 4.1 in terms of the displacement $\mathbf{u}$, the compatibility equation is required [51].

$$\epsilon = \frac{1}{2}(\nabla \mathbf{u} + (\nabla \mathbf{u})^T) \tag{4.11}$$

The following four equations in the equation system refer to the boundary conditions and are illustrated in the figure 4.1. The equation 4.2 is the Dirichlet boundary condition imposed on the walls of the cannula (red color in figure 4.1). The x-component of the displacement is imposed to zero due to the constraints of the construct inside the cannula. The GAE-EngNT can progress inside the cannula so no displacement constraints are imposed in the y-direction. The equation 4.3, 4.4 and 4.5 are the Neumann boundary conditions and are represented in green in figure 4.1.

On one hand, there is the differential of pressure applied on the top and the bottom surface of the construct. Those aspiration pressures are oriented along the y-axis. Therefore, the traction force applied on the top and bottom surfaces of the construct defines 3 components of the stress tensor of all the points on those surfaces. The equation 4.12, shows the stress tensor definition due to the traction force applied on the top surface $\mathbf{p_2}$. The same results can be obtained for the bottom surface. However, the reference pressure is defined as zero below the construct. Therefore, the p2 value is the value of the aspiration pressure while p1 equals zero. The p2 value is chosen to be constant to focus on the research question formulated in section 3.1.4. However, future developments of this model could consider different applied aspiration stress profiles.

$$\sigma_{top} \cdot n_{top} = \mathbf{p2} = \begin{bmatrix} 0 \\ p2 \end{bmatrix} = \begin{bmatrix} \sigma_x * n_x + \tau * n_y \\ \tau * n_x + y * n_y \end{bmatrix}$$

$$n = \begin{bmatrix} 0 \\ 1 \end{bmatrix} \qquad \rightarrow \qquad \sigma_{top} = \begin{bmatrix} \sigma_x & 0 \\ 0 & p_2 \end{bmatrix} \tag{4.12}$$

On the other hand, the viscous stress $\mathbf{T_v}$ due to fluid friction on the cannula walls is considered. The origin of this stress is the choice of modelling friction between the cannula and EngNT assuming the existence of a lubrication layer between the solid construct and the wall boundaries [61]. As it can be seen in figure 4.1, this layer has a width of h and is composed of a fluid of viscosity η. Nevertheless, this lubrification width is not modelled in the geometry of the *in silico* representation. The model considered only the construct with the diameter of the cannula. The Dirichlet and Neumann conditions are applied to the wall boundaries of the construct. However, the effect of this lubrification layer and its interpretation is taken into consideration through the viscous stress $\mathbf{T_v}$. Indeed, the fluidic layer can be interpreted as an extremely thin liquid part of the collagen construct that interacts with the walls of the cannula [60] [61]. Due to the vertical aspiration pressure, the construct and the lubrification layer acquire a velocity profile. This one is rather flat for the construct which is considered in a solid phase. On the contrary, the velocity profile of the fluid increases with the distance to the boundary walls [50] [62]. Fluid can not support shearing stress but does resist shearing motions [60]. By analogy with the shear modulus in solid mechanics, the viscosity of the fluid is defined as its resistance to

shearing motion, and its formula is given by [60]:

$$\eta = \frac{shear\ stress}{rate\ of\ shear\ strain} = \frac{F/A}{du/dx} \quad [\frac{N.s}{m^2}] \tag{4.13}$$

Where u is the vertical velocity of the fluid of the lubrification layer. The fluid speed increases across the lubrification film, reaching a maximum (v) at the surface in contact with the GAE-EngNT solid construct [60]. The speed at which the construct moves is the maximum speed of the fluid (v) as figure 4.1 illustrates [60]. With a constant strain rate,

$$\frac{du}{dy} = \frac{v}{h} \tag{4.14}$$

The shear stress of the fluid is F/A. This stress is the viscous stress applied to the solid construct at the contact surface between the two, meaning when the velocity of the fluid is equal to v [60]. Consequently, the viscous force considered in the model of the construct is T_v and is defined as [60]

$$T_v = \frac{\eta}{h} * v \tag{4.15}$$

In the model, this viscous force is applied on the wall boundaries of the construct with a term that depends on the velocity of the construct $\dot{\mathbf{u}}$. Indeed, the viscous force T_v is the fluid analog of the sliding friction force between two solid surfaces and refers to fluid friction [60]. Like other frictional forces, viscous forces oppose the relative motion of adjacent fluid layers. Whereas solid frictional forces are approximately independent of velocity [60], viscous forces are proportional to the velocity of the construct with a viscous coefficient C_v [60].

$$\mathbf{T_v} = C_v * \dot{\mathbf{u}} \tag{4.16}$$

$$C_v = \frac{\eta}{h} \tag{4.17}$$

The model plays with this viscous coefficient instead of viscosity and width of the lubrification layer because the latter is not modelled in the *in silico* representation. Indeed, the fluid film can be considered as a thin layer of the liquid phase of collagen gel with more or less water content depending on the stabilisation process which is not modelled. Therefore, the viscosity of this fluid layer can vary a lot depending on the cannula size and applied aspiration stress. As a result, the interpretation of the viscous coefficient C_v will be given depending on the simulations. To give an order of magnitude, the viscosity of the hyper hydrated collagen gel is $6 * 10^4 N.s/m^2$ while the one of pure water is $10^{-3} N.s/m^2$. Similar to the aspiration differential of pressure, the viscous force applied on the wall boundaries imposes the three components of the stress tensor. The left and the right walls have different normal vector orientations, therefore, the imposed shear stress has the opposite sign.

$$\sigma_{walls} \cdot n_{walls} = \mathbf{T_v} = \begin{bmatrix} 0 \\ -T_v \end{bmatrix} = \begin{bmatrix} \sigma_x * n_x + \tau * n_y \\ \tau * n_x + y * n_y \end{bmatrix}$$

$$n_{wall\ left} = \begin{bmatrix} -1 \\ 0 \end{bmatrix} \qquad \rightarrow \qquad \sigma_{wall\ left} = \begin{bmatrix} 0 & T_v \\ T_v & \sigma_y \end{bmatrix} \tag{4.18}$$

$$n_{wall\ right} = \begin{bmatrix} 1 \\ 0 \end{bmatrix} \qquad \rightarrow \qquad \sigma_{wall\ right} = \begin{bmatrix} 0 & -T_v \\ -T_v & \sigma_y \end{bmatrix} \tag{4.19}$$

The two last equations, 4.6 and 4.7 are the initial conditions. The displacement and velocity fields of the construct are imposed to zeros at the initial time t=0.

4.1.2 Numerical resolution: Finite Element Method and Implicit solver

The formulation of the dynamic problem in the equation 4.1 is a continuum problem in space and in time. When expressing the stress tensor σ in terms of displacement u, the equation of the balance of linear momentum gives a Partial Differential Equation (PDE) in time (due to the time derivative of u) and in space (due to the nabla operator on the stress tensor).

Spacial discretisation

On one hand, to solve numerically the partial derivative in space, the Finite Element Method is used. FInite Element Method (FEM) is a general and efficient mathematical machinery for the numerical solution of PDEs [51]. The core principle is to discretise the model geometry into finite elements. The unknown function u for which the equations need to be solved, is called the trial function. The so-called function space (V) contains the trial function and specify its properties [51]. The values of the displacement are computed at the nodes. The distribution of the displacement inside each element is interpolated from those nodal displacements [54] [63]. The procedure to obtain this FEM resolution is to express the PDE in variational form. This weak form of the equation 4.1 is obtained by multiplying the PDE by a test function v and integrating the resulting equation over the domain Ω [51] [54] [63]. In addition, to reduce the second-order derivatives into first-order derivative term an integration by parts is performed. Therefore, the variational form can be written for all $v \in \hat{V}$ where $\hat{V}$ is a vector-valued test function space:

$$\int_\Omega \rho \ddot{\mathbf{u}} \cdot \mathbf{v} d\mathbf{x} + \int_\Omega \sigma : \nabla \mathbf{v} d\mathbf{x} - \int_{\delta\Omega_{top}} \mathbf{p2} \cdot \mathbf{v} ds - \int_{\delta\Omega_{bottom}} \mathbf{p1} \cdot \mathbf{v} ds - \int_{\delta\Omega_{walls}} \mathbf{T_v} \cdot \mathbf{v} ds - \int_\Omega \mathbf{b} \cdot \mathbf{v} d\mathbf{x} = 0 \tag{4.20}$$

The traction or stress vectors ($\mathbf{p2}, \mathbf{p2}, \mathbf{T_v}$) are prescribed on specific boundaries. They are the Neumann boundary conditions embedded inside the equation. On the remaining part of the boundary, the value of the displacement is given as a Dirichlet condition [51]. Instead of dealing with a long equation, a more convenient formulation can be introduced.

The canonical notation [51] [52] for variational problems finds $\mathbf{u} \in V$ such that

$$a(\mathbf{u},\mathbf{v}) = L(\mathbf{v}) \qquad \forall v \in \hat{V} \tag{4.21}$$

Where,

$$a(\mathbf{u},\mathbf{v}) = \int_\Omega \rho\ddot{\mathbf{u}} \cdot v d\mathbf{x} + \int_\Omega \sigma : \nabla v d\mathbf{x} - \int_{\delta\Omega_{walls}} \mathbf{T_v} \cdot v ds \tag{4.22}$$

$$L(\mathbf{v}) = \int_{\delta\Omega_{top}} \mathbf{p2} \cdot v ds + \int_{\delta\Omega_{bottom}} \mathbf{p1} \cdot v ds + \int_\Omega \mathbf{b} \cdot v d\mathbf{x} \tag{4.23}$$

a(**u**,**v**) is known as the bilinear form that gathers the terms which depend on the main variable **u**. L(**v**) is the linear form that gathers the terms which are independent of the main variable **u**. It can be noticed that $\mathbf{T_v}$ is dependent on the main variable **u** since it is proportional to the velocity distribution as shown in the equation 4.16.
The next step is to discretise the geometry into finite elements with a certain number of nodes, particularly at the corner of each element. The infinite-dimensional function spaces are replaced by discrete (finite-dimensional) trial and test function spaces for each finite element [51] [54] [63]. However, this element formulation problem does not change the continuity property of the displacement field **u** for each point inside each element. For this reason, the displacement field is computed from an interpolation of the values at the nodes following the formulation [54] [63] [66]:

$$\mathbf{u}(\mathbf{x}) = \sum_{i=1}^{n_{elm}} N_i(\mathbf{x})\mathbf{u_i} \tag{4.24}$$

Where $\mathbf{u_i}$ is the displacement at the node i, N_i is the interpolation function associated with the node i, and n_{elm} is the number of nodes for each element. The interpolation function depends on the type of element chosen for the method. The choice for this mathematical model is the standard P1 linear Lagrange element, which is a triangular element with nodes at the three vertices [51]. Thanks to the equation 4.24, the displacement field can be replaced by a finite number of unknowns which is the displacement at each node of each element. The vector of those nodal displacements can therefore be extracted from the integral over the element. Consequently, the weak form equation 4.20 can be expressed in terms of matrices. For each element, find the displacement at the nodes $\{u\} \in \mathbb{R}^n$ such that [53] [66]

$$\{v\}^T[M]\{\ddot{u}\} + \{v\}^T[C]\{\dot{u}\} + \{v\}^T[K]\{u\} = \{v\}^T\{F\} \qquad \forall\{v\} \in \mathbb{R}^n \tag{4.25}$$

With n the number of degrees of freedom of the problem which is the number of nodes in the FEM. In a dynamic problem, the matrices appearing in equation 4.25 are well-known [54] [63][64] [66].

- The [M] is the mass matrix: $\int_{\Omega_{elmt}} \rho\ N^T\ N d\mathbf{x}$
- The [C] is the damping matrix: $\int_{\delta\Omega_{walls\ elmt}} C_v\ N^T|_{walls}\ N|_{walls}\ ds$
- The [K] is the stiffness matrix: $\int_{\Omega_{elmt}} B^T\ C\ B\ d\mathbf{x}$
- {F} is the external applied load vector: $\int_{\delta\Omega_{top\ elmt}} \{p2\}\ N^T|_{top}\ ds + \int_{\delta\Omega_{bottom\ elmt}} \{p1\}\ N^T|_{bottom}\ ds + \int_{\Omega_{elmt}} \{b\}\ N^T\ d\mathbf{x}$

Where, N is the interpolation matrix, B is the space derivative of the interpolation matrix and C is the matrix considering the constitutive equation. It has to be noticed that the FEM solver is computing the [C] and {F} only for the nodes where the traction is applied which explained the notation $|_{applied\ nodes}$.

Temporal discretisation

On the other hand, dynamic problems require time-dependent analysis due to the effects of acceleration which are present and can not be neglected [65]. To solve the problem numerically, the time domain needs to be discretised. Therefore, the interval studied [0;T] is divided into N+1 time steps $t_0 = 0, t_1, ..., t_N, t_{N+1} = T$ with $\Delta t = T/N$ denoting the time step (supposed constant) [53]. The derivative in time presents in equation 4.1, needs also to be approximated. The state of the system at the next time step $(\mathbf{u}, \dot{\mathbf{u}}, \ddot{\mathbf{u}})$ has to be computed based on the old state. The way those two features are computed depends on the discrete-time dynamic resolution scheme chosen. In this research work, an implicit solver is used [65] [68] [69] [70]. Therefore, this algorithm searches for a solution for the next time step considering the current state of the system as well as its previous time state. The choice for an implicit method compared to an explicit solver can be explained by the unconditional stability and facility with larger time steps despite large computation cost [53] [70]. In addition, it allows for high frequency dissipation and offers a second-order accuracy, i.e. in $O(\Delta t^2)$ [53] [70]. As an implicit solver, the generalized-α method is used. It can be seen as an extension of the widely used Newmark-β method in structural dynamics [53] [71]. The method consists in solving the dynamic matrix form equation 4.25 at intermediate time between t_n and t_{n+1} as follows:

$$[M]\{\ddot{u}_{n+1-\alpha_m}\} + [C]\{\dot{u}_{n+1-\alpha_f}\} + [K]\{u_{n+1-\alpha_f}\} = \{F_{n+1-\alpha_f}\} \tag{4.26}$$

$$\{u_{n+1}\} = \{u_n\} + \Delta t\{\dot{u}_n\} + \frac{\Delta t^2}{2}((1-2\beta)\{\ddot{u}_n\} + 2\beta\{\ddot{u}_{n+1}\}) \tag{4.27}$$

$$\{\dot{u}_{n+1}\} = \{\dot{u}_n\} + \Delta t((1-\gamma)\{\ddot{u}_n\} + \gamma\{\ddot{u}_{n+1}\}) \tag{4.28}$$

$$\{\ddot{u}_{n+1}\} = \frac{1}{\beta\Delta t^2}(\{u_{n+1} - \{u_n\} - \{u_n\} - \Delta t\{\dot{u}_n\}) - \frac{1-2\beta}{2\beta}\{\ddot{u}_n\} \tag{4.29}$$

With $X_{n+1-\alpha} = (1-\alpha)X_{n+1} + \alpha X_n$.
Formulating the problem in terms of the unknown displacement ($\{u_{n+1}\}$) gives the equation solved in the *FEniCS* code in appendix F. Once the linear system has been solved for the displacement at the next time step, the new velocity and acceleration are computed using the equations 4.29 and 4.28.
The Generalised-α method has four parameters; α_m, α_f, γ, and β. The values of those parameters determine the stability and the accuracy of the numerical algorithm. An optimal choice for their values is therefore essential. The stability of the method means that the influence of a given disturbance in the solution for a certain moment should fade out [71]. For a second-order accuracy, the generalized-α method is unconditionally stable if the variables respect the following conditions [71]:

$$\alpha_m < \alpha_f < \frac{1}{2} \tag{4.30}$$

$$\beta > \frac{1}{4} + \frac{1}{2}(\alpha_f - \alpha_m) \tag{4.31}$$

Concerning the accuracy, the goal is to minimise the truncation error which is the difference between the true (analytical) displacement and its value obtained by numerical approximation [71]. For the generalised-α method, the second order accuracy is reached when [71]:

$$\gamma = \frac{1}{2} - \alpha_m + \alpha_f \tag{4.32}$$

In addition, a good algorithm should maintain low frequency modes and minimise the effect of high frequency modes. This feature is reached when defining β as [53] [71]:

$$\beta = \frac{1}{4}(\frac{1}{2} + \gamma)^2 \tag{4.33}$$

In conclusion, the values of the parameters which ensure unconditional stability, optimal dissipation and second-order accuracy are given as follow [53]:

- $\alpha_m = 0.2$
- $\alpha_f = 0.4$
- $\gamma = 0.7$
- $\beta = 0.36$

The choice of the Generalised-α method is based on its ability to control the damping and to keep the accuracy of second-order while damping in the high-frequency regime [68] [69] [72]. Indeed, high-frequency modes usually describe motions with no physical sense and also contain very large phase errors. This implicit solver also guarantees unconditional stability which makes easier the optimal definition of the parameters.

4.1.3 *FEniCS* project

FEniCS is the software chosen to solve numerically the dynamic problem of the GAE-EngNT construct inside the cannula using the FEM and Generalised-α solver. *FEniCS* Project is a collection of free and open-source software components for automated computational mathematical modelling [51]. It aims at creating an easy, intuitive, efficient, and flexible software for solving PDEs using FEM [51]. *FEniCS* solves each problem by transcribing, in a nearly one-to-one correspondence, the abstract mathematical exposition of the finite element basic theory. *FEniCS* software library by itself and all its scientific library source dependencies can be run on many different kinds of operating systems (Linux, Mac, Windows) [51]. The installation of the Project on the operating system of the computer can be challenging and long. Therefore, pre-built packages such as Docker containers and *Ubuntu* packages, are provided to make the installation easier and faster [51]. The programming language, which calls the use of *FEniCS* library functionalities, is *Python*. Some libraries in *FEniCS* allow certain results or desired values to be plotted. However, some open-source, multi-platform data analysis and visualisation applications such as *ParaView* provide a more detailed and complete analysis of the outcomes of the FEM [55]. *ParaView* is a dedicated application that facilitates building visualisations to analyse large dataset using qualitative and quantitative techniques [55].

The advantage of *FEniCS* is that the code stays compact and nice, very close to the mathematical formulation, even when the mathematical and algorithmic complexity increases [51]. It is also an open-source software with a lot of available tutorials and a dedicated forum. *FEniCS* enables solving partial differential equations coming from many different theories and considerations [51]. For all those reasons *FEniCS* was a quality choice of software to simulate the dynamic progress of the collagen construct in the GAE cannula. The *FEniCS* code implemented to solve the dynamic problem formulated in section 4.1.1 is presented in appendix F. This code is used to generate all the results presented in section 4.2 with parameter values explained in the following paragraph.

4.1.4 Parameter identification

The parameters of this model are listed below:

1. The geometry: The diameter and the length of the construct depend on the needle gauge number. In this research work, five needle gauge numbers are considered. Depending on the simulated case, the values of these two parameters are taken from table 4.1. The data of this table were computed previously and already reported in table 2.6 and 2.9.

Needle gauge number	Inner diameter [m]	Length [m]
8G	$3.429*10^{-3}$	$8*10^{-3}$
10G	$2.692*10^{-3}$	$8.75*10^{-3}$
12G	$2.159*10^{-3}$	$9.58*10^{-3}$
14G	$1.6*10^{-3}$	$10.33*10^{-3}$
16G	$1.194*10^{-3}$	$12*10^{-3}$

Table 4.1: Length and inner diameter parameter values for each needle gauge number (based on [24] and [42])

2. The density (ρ): This parameter has not been measured directly by the different research teams. Therefore, it is necessary to compute the density for each needle gauge number. Thanks to the length of the construct (reported in the table 2.9) and the cross-section area (reported in the table 2.6), the final volume of the GAE-EngNT construct could be estimated. The ratio between the final and the initial volume of HHC gel gives the volume fold. The value for each needle gauge number is reported in the table 4.2. Thanks to this parameter the collagen concentration in the final construct could be evaluated using the initial collagen concentration in the HHC gel total volume:

$$Final\ collagen\ concentration = Co\ parameter\ in\ the\ table\ 2.1 \ * \ \%\ volume\ of\ the\ final\ volume \quad (4.34)$$

In order to derive the final construct density, the collagen concentrations calculated at the previous step is multiplied by the CFD which is reported in table 2.9.

$$density\ of\ the\ final\ construct = \frac{mass\ collagen}{Final\ volume} * \frac{mass\ construct}{mass\ collagen} \quad (4.35)$$

The initial gel density is found using the initial collagen concentration and the initial CFD value. Its value is evaluated at 0.375 g/mL. The final construct density is calculated for each cannula size except for the 16G due to a lack of CFD data. The values are reported in table 4.2. The *Matlab* code in appendix C is used to compute the simple calculations explained here above.

Team	Needle gauge number	Volume fold	GAE-EngNT construct density (g/mL)
Neysan O. Kamranpour et al. [24]	8G	20	1.01
Initial volume: 1.5mL	10G	30	1.13
Initial collagen concentration: 3mg/mL	12G	43	1.02
CFD: 0.8 wt%	14G	72	1.2
UCL Centre for Nerve Engineering Initial volume: 1mL Initial collagen concentration: 1.6mg/mL	16G	74	Missing CFD data

Table 4.2: Volume fold of the GAE process and GAE-EngNT construct density for each needle gauge number (based on [16] [21] [24] and interviews)

It can be observed that the value of the final density for each needle gauge number is always close to 1.1 kg/m^3. This value seems reasonable since the construct is expected to have a density close to the one of water. Therefore, the unique and constant value of 1.1 kg/m^3 is given for all the simulations.

3. The damping or loss coefficient (η_{GAE}): The GAE-EngNT has a viscoelastic behaviour described in the model through the equation 4.8. The first two terms refer to the Hook law of an homogeneous linear elastic material. The last term depending on η_{GAE} introduces the dissipative properties of the material that can not be neglected as explained in section 2.2.5. The value of this damping was measured by Papon Muangsanit [16] and estimated at the constant value of 0.2 below 10 Hz.

4. The Young's modulus (E): Capturing the linear elastic behaviour, Young's modulus defines the linear coefficient between the stress and the strain. Therefore, it can be found by taking the slope of the stress-strain curve of the GAE-EngNT in the approximated linear part. All the stress-strain curves acquired by quasi-static tensile tests for the different cannula sizes are given by Neysan O. Kamranpour et al [24] in figure D.1. The data of those curves are extracted using the *Matlab* code of Marco Stevanella from Politecnico di Milano in appendix D.2. Afterwards, using the *Matlab* code in appendix D.3, the linear part is isolated and a linear interpolation enabled to extract the slope which defines Young's modulus. The team of Neysan O. Kamranpour does not provide any data for the 16G cannula. Despite the mechanical analysis provided by the Papon Muangsanit publication [16], it is better to interpolate the modulus values of the lower needle gauge numbers to obtain an approximation of the 16G construct. This interpolation is shown in appendix D.4 and the *Matlab* code can be found in the second part of the appendix D.3. The Young's modulus value for each needle gauge number is reported in table 4.3. Depending on the simulation cases, the corresponding Young's modulus value is picked up similarly as for the table 4.1.

Needle gauge number	Young's modulus [Pa]
8G	$0.14 * 10^3$
10G	$2.06 * 10^3$
12G	$3.6 * 10^3$
14G	10^4
16G	$3.26 * 10^4$

Table 4.3: Computed Young's modulus for each needle gauge number

5. The Poisson's ratio (ν): It is a dimensionless number that measures the deformation in the material in a direction perpendicular to the direction of the applied force [73]. It ranges between 0.1 and 0.45. As explained in section 2.2.5, A. P. G. Castro et al [37] reported that the solid part of collagen hydrogels tends to adopt a Poisson's ratio between 0.20 and 0.30. Therefore, the GAE model used 0.3 as the value for this parameter.

6. Duration of the aspiration (T): As explained in the section 2.4.2, the timing of the GAE process varies sensibly depending on the aspiration pressure values and the needle gauge numbers. Neysan O. Kamranpour et al [24] reported the aspiration timing process to 100 s using a 14G cannula size. On the contrary, the UCL Centre for Nerve Engineering reported approximately 270 s to fully aspirate the collagen gel into the 16G cannula. Therefore, all the simulations dealing with the 14G cannula size run on 100 s as maximal process time. On the contrary, the simulations, computing the 16G cannula run on 270 s as process duration. The value of 270 s is also used in the simulations when the different cannula sizes are compared. This choice is justified by the aim of the automation of the GAE process. The longer process time is chosen for all the cannula size experiments to have a feasible common value.

7. Generalized-α parameters (α_m, α_f, γ, and β): As explained in the previous section, those parameters are the coefficients of the discrete-time resolution scheme of the dynamic problem. The optimised values were discussed and exposed in section 4.1.2.

8. Time step ($dt = T/Number\ of\ time\ steps$): The Generalized-$\alpha$ method is used for solving the dynamic problem with discretised time. The time step for the discretisation is an important feature that influences the precision of the results. The optimal value for a good balance between the convergence and the computational time is obtained using 100 time steps as it will be reported in section 4.2.1.

9. Space convergence parameters (N_x *and* N_y): The resolution of the GAE process using FEM requires the discretisation of the material geometry into finite elements. The resolution in the x- and y-direction are two parameters defining the number of elements in those directions. These values are set to 150 to ensure the convergence of the model as it will be reported in the section 4.2.1.

10. Aspiration differential pressure ($p_2 - p_1$): As a reference, the pressure at the bottom of the construct in the cannula is considered equal to zero. Therefore, p_1 parameter is fixed and p_2 becomes the unique constant aspiration pressure parameter considered for this model. No precise values have been reported in the literature. Due to a defective pressure gauge, the UCL Centre for Nerve Engineering could not measure any aspiration pressure values. Neysan O. Kamranpour et al [24] provide an approximated value of $1 * 10^5$ Pa and $5 * 10^3$ Pa using respectively a 14G and 8G cannula size. It is interesting to play with this parameter in the model to have a better understanding of the process and find a range of aspiration pressure values that would allow a successful GAE process.

11. Viscous coefficient (C_v): This parameter is introduced in the model to represent the dissipation due to fluid interaction of the collagen gel with the cannula walls. Therefore, no similar values can be found in the literature. However, it is interesting to investigate the effect of this parameter on the GAE process, to interpret the values and the nature of the lubrification layer using the equation 4.17.

4.1.5 Useful tools to analyse the different interactions in the system

Different quantities are interesting to compute during the simulation to highlight specific features to answer the model focus expressed in section 3.1.4. Firstly, an energy balance is useful to see the time evolution of the different energies in the system, checking the total energy conservation and the transfer of energies inside the system. This study enables to understand the physics of the aspiration process and the phenomena that is modelled. The energy balance is written as:

$$E_{total} = E_{el} + E_{damp} + E_{kinetic} - E_{ext} \tag{4.36}$$

Where [53],

- E_{total} is the total energy in the system which is conserved and constant in a real-world process

- E_{el} is the elastic potential energy of the system. This energy is linked to the energy stored when applying a force on an elastic material. When the force is not applied anymore, this energy can be restored entirely by definition of the elastic property of the material. The elastic energy is therefore linked to the material properties of the GAE-EngNT construct:

$$E_{el} = \int_\Omega \frac{1}{2}\sigma(\mathbf{u}) : \epsilon(\mathbf{u}) d\mathbf{u} \tag{4.37}$$

- E_{damp} is the damping energy of the system. It is the energy lost by the dissipation mode. Therefore, it is defined as the integral over time of the dissipation term D:

$$E_{damp} = \int_0^T D \ dt \tag{4.38}$$

- $E_{kinetic}$ is the kinetic energy of the system. It is the form of energy due to the motion of the construct inside the cannula. It is defined as:

$$E_{kinetic} = \int_\Omega \frac{1}{2}\rho \dot{\mathbf{u}} \cdot \dot{\mathbf{u}} \ d\mathbf{x} \tag{4.39}$$

- E_{ext} is the work developed by the external forces. In this case, the external forces are the independent stresses applied as Neumann conditions on the boundaries of the construct. Gathering all the external forces together in a quantity called F, the external work is given by:

$$E_{ext} = \int_0^T F * (\mathbf{u} - \mathbf{u_{old}})\ dt \tag{4.40}$$

Secondly, the GAE-EngNT material inside the cannula has an elasticity which can impact the behaviour of the construct when it is aspirated. The effect of the elastic property of the material on the dynamic progression of the construct inside the cannula is evaluated thanks to the u_{diff} quantity. The outcome of the simulation to observe this feature is the difference between the vertical displacement of the middle point on the top surface and the corresponding point at the bottom surface of the construct over time. This quantity allows evaluating the mismatch between the vertical displacement of the top and the bottom part of the construct due to the elastic property of the material.

$$u_{diff}(t) = u_{top} - u_{bottom} \tag{4.41}$$

The energy balance and the vertical displacement data are post-processed using the *Matlab* code in appendix H.1.

Thirdly, the shear stress is the non-diagonal terms in the 2D stress tensor. The distribution of shear stress inside the material during the aspiration can give some cues about the cell viability. The relationship between shear stress and cell viability is not yet quantified but a clear influence is already reported in the literature and discussed in section 2.2.6. As a first step, evaluating the shear stress distribution can give a qualitative analysis of the cell viability. As a second step, future studies can quantify this link between cell death and shear stress level which would be extremely useful for understanding, predict and control the seeded cells behaviour processed by the GAE method.

Another interesting quantity is the major principal stress which gives some cues on the seeded cell alignment. Indeed, this stress is important to provide the maximum normal stress and its orientation acting inside the material [74]. Since the GAE-EngNT is the substrate of the seeded cells, the maximal normal stress and its orientation act on those cells providing them, to some extend, an alignment. The principal stresses are the corresponding normal stresses at an angle θ at which the shear stress τ is zero [74]. The maximum value of normal stress is known as major principal stress and is computed as follows [74]:

$$\sigma_{max} = \frac{\sigma_x + \sigma_y}{2} + \sqrt{(\frac{\sigma_x - \sigma_y}{2})^2 + \tau^2} \tag{4.42}$$

The orientation of this major principal stress is obtained as follows:

$$tan(2\theta) = \frac{2\tau}{\sigma_x - \sigma_y} \tag{4.43}$$

To form the field of major principal stress, its amplitude and orientation are combined into a vectorial field using post-processing tools by *Paraview*. Lastly, the sensitivity of the model to variations in the parameter space is tested with the two following parameters, p_2 and C_v. They are respectively the aspiration pressure on the top surface of the construct and the viscous coefficient measuring the amplitude of the fluid friction dissipation.

4.1.6 Simulation strategy

To answer the research question formulated in section 3.1.4, a strategy in the model simulation has been implemented.

Spacial and temporal convergence

Firstly, it is necessary to assess the convergence of the numerical model in order to identify the space convergence and time convergence parameters. This step is crucial to ensure the validity of the numerical model. Due to a spacial and temporal dependency of the dynamic problem, spatial and temporal convergence are assessed. The *Matlab* code in appendix G is used to generate the results. Spacial convergence is computed using the parameter defined for the 14G cannula size. Since the time convergence is not yet assessed, an adequate number of time steps is given to allow a reasonable computation time and coherent results. This parameter is chosen to be 50. Relevant starting values are given to the viscous coefficient and the aspiration pressure providing an average displacement outcome that is reasonable. Therefore, C_v is fixed to $6.66 * 10^6$ $N.s/m^3$ and p_2 is given at 10^4 Pa. The number of elements in the x- and y- direction is increased by 20 for 10 times starting from 10 elements for each dimension.
Two important quantities (maximal major principal stress at the last time step and the total energy in the system at the last time step) are computed with an increasing number of elements. In addition, the CPU time is also computed over the number of elements. It can be defined as the exact amount of time that the Central Processing Unit of the computer has spent processing data for one simulation.

Temporal convergence is computed using the same set of parameter values. The optimal computed number of elements in the x- and y-direction is used and set to 150. The number of time steps is increased by 20 for 10 times starting from 5 initial number of time steps. The same two quantities and the CPU time are computed over the number of time steps.

Impact of wall friction on dissipation

Secondly, the need for a dissipation mode is shown. The impact of introducing viscous stress on the wall boundaries as the dissipation mode is also evaluated. To do so, a first simulation is run without viscous stress at the wall boundaries, i.e. $\mathbf{T_v} = \mathbf{0}$. This stress does not depend on the velocity anymore. Therefore, the applied stress at this boundary need to be included in the $L(\mathbf{v})$ term similarly to $\mathbf{p_1}$ and $\mathbf{p_2}$ in equation 4.23. The optimised values for the space and time convergence are given following the conclusion of the previous section with $N_x = N_y = 150$ and $Number\ of\ time\ steps = 100$. Concerning process parameters, the Canadian team of Neysan O. Kamranpour et al. [24] provided an estimation of parameter values for the GAE process using the 14G cannula. Therefore, this cannula size is a good reference to perform the first set of simulations. In sum, the parameter values for the geometry and Young's modulus are given for the 14G cannula. Using this cannula shape, Neysan O. Kamranpour et al. [24] stated to perform the aspiration process in 100 s using applied suction stress of approximately 10^5 Pa. Those two values enable to define the T and p_2 parameter values.

A second simulation is run using the same cannula and the same convergence parameters. However, the fluid friction dissipation mode is introduced with the $\mathbf{T_v}$ term as explained in section 4.1.1. The goal of the simulation is to find the correct value for the viscous coefficient parameter C_v to obtain a reasonable displacement of the GAE-EngNT construct inside the cannula. To simulate the aspiration stage, the desired displacement of the construct inside the cannula is the length of the construct.

Different features are targeted as results of the two simulations. Firstly, the value of the viscous coefficient chosen as a parameter for the model is found. Secondly, the resulting average vertical displacement at the last time step, i.e. when t=100 s, is computed by the simulation with the corresponding C_v value. Afterwards, an energy balance is presented to present the main driver of the dynamic aspiration of the construct inside the tube, as explained in section 4.1.5. Finally, the effect of the elastic property of the material on the dynamic progression of the construct inside the cannula is evaluated through the u_{diff} quantity exposed in section 4.1.5.

Adaptation of the applied stresses

Thirdly, adaptations of the applied stress values show different behaviour occurring in the cannula. Two different balances between the applied suction stress (p_2) and the viscous effect (C_v) are compared. The aim is to understand failure situation during the aspiration and the importance of this balance for the properties of the GAE-EngNT construct. For this purpose, two simulations are computed. The first simulation is the same than previously, i.e. a system with fluid friction dissipation. The parameters are the ones of the 14G cannula, with the spacial and temporal convergence. The aspiration is performed by applying a suction stress of 10^5 Pa for 100 s. The viscous coefficient used is the one obtained in the previous simulation to compute a vertical displacement of the length of the construct. Therefore, $C_v = 3.5 * 10^8 N.s/m^3$.

The second simulation uses the same cannula size and the same process time, i.e. 14G cannula for 100 s process time. However, the applied pressure and the viscous coefficient values are adapted to obtain a successful aspiration of the entire construct. These two parameter values are the maximum ones to create a displacement of the length of the construct with a limited elastic effect. This last requirement is represented by relatively small displacement differences between the top and the bottom of the construct following the definition in equation 4.41 The distribution of the vertical displacement and shear stress over time in both situations are compared. The energy balance and the displacement difference between the top and the bottom of the construct are also evaluated in parallel.

Successful parameter identification for the different cannula sizes

Afterwards, the strategy of the previous simulation to ensure the success of the process is adopted for the different needle gauge numbers. The maximum aspiration pressure (p_2) with the corresponding viscous coefficient values (C_v) are found to guarantee the minimum success of the aspiration process without elastic rupture. A reverse engineering strategy is applied. Indeed, the value of these two parameters is searched to obtain as a result of the simulation the desired displacement. The latter is a displacement equal to the length of the construct after the 270 s of the aspiration process. This strategy is applied for five

cannula sizes (8G, 10G, 12G, 14G, and 16G). The values of the parameters corresponding to the five needle gauge numbers are provided in the code. The maximum process time is 270 s because it's the larger time reported for the aspiration. A double Y-axis graph is obtained as a result showing the evolution of the two computed parameters over the needle gauge number. This diagram is obtained by post-processing the simulation outcomes with the *Matlab* code in appendix H.2.

Biomechanical impact of the aspiration stage

Finally, the impact of the aspiration stage on the biomechanical properties of the construct is evaluated. On one hand, a first complete analysis is conducted for the 16G cannula with the successful parameter values computed in the previous section. Therefore, the aspiration is performed by applying an aspiration pressure of $5 * 10^3$ Pa during 270 s. The viscous coefficient is fixed to $5.5 * 10^6$ $N.s/m^3$. The other parameters are the ones of the 16G cannula size and the parameter values that lead to convergence. The 16G cannula is selected because it's the one used at the UCL Centre for Nerve Engineering. A first analysis of the model considerations is conducted to evaluate the validity of the model. In addition, the stress-strain curve is verified. The vertical normal stress and strain values at the specific node 437 of the mesh are put in parallel and the curve is obtained using the *Matlab* code I.1.

After that, the stress and strain tensors at different points of the construct over time enable to observe the stress level subjected to the seeded cells. The time evolution is evaluated with the normal vertical stress. The shear stress distribution and the major principal stress field are shown to give some cues about respectively the cell viability and the alignment of the cells or the fibrils. On the other hand, the maximum shear stress value and the maximum major principal stress at the last time step (t=270 s) are compared for the different needle gauge numbers. The graph is obtained by using the *Matlab* code in appendix H.3. The parameter values corresponding to the different needle gauge numbers are given in the following table 4.4:

Needle gauge number	Constant parameters	Length [m]	Diameter [m]	Young's modulus [Pa]	Aspiratio pressure [Pa]	Viscous coefficient $[N.s/m^3]$
8G	$N_x = N_y = 150$	$8 * 10^{-3}$	$3.429{*}10^{-3}$	$0.14 * 10^3$	10	$7 * 10^4$
10G	Nb = 100	$8.75 * 10^{-3}$	$2.692{*}10^{-3}$	$2.06 * 10^3$	$2 * 10^2$	10^6
12G	$\rho = 1.1$ $[kg/m^3]$	$9.58 * 10^{-3}$	$2.159{*}10^{-3}$	$3.6 * 10^3$	$3 * 10^2$	10^6
14G	T = 270 s	$10.33 * 10^{-3}$	$1.6 * 10^{-3}$	$2 * 10^4$	$2 * 10^3$	$4 * 10^6$
16G	$\nu = 0.3$ $\eta_{GAE} = 0.2$	$12 * 10^{-3}$	$1.6 * 10^{-3}$	$3.26 * 10^4$	$5 * 10^3$	$5.5 * 10^6$

Table 4.4: Parameters for the simulation of the comparison of the biomechanical properties of the construct between the different needle gauge numbers

4.2 Results

4.2.1 Convergence

Spacial convergence

The evolution of the maximum major principal stress at the last time step, the total energy in the system at the last time step, and the CPU is presented over the total number of elements in figure 4.2. Concerning the major principal stress, its value increases with the number of elements before stabilising rapidly. The total energy is also decreasing rapidly before converging. The convergence of the model is therefore proved. However, the CPU time is increasing nearly linearly with the number of elements. That is why, a good balance needs to be found between accuracy and computational time. A total number of elements of 22500 seems enough to ensure stable values of the important measured quantities with an average computational time of 25 s. The values of the N_x and N_y parameters can be deduced since

$$Total\ number\ of\ element = N_x * N_y \tag{4.44}$$

The choice for this research work is 150 elements on each direction.

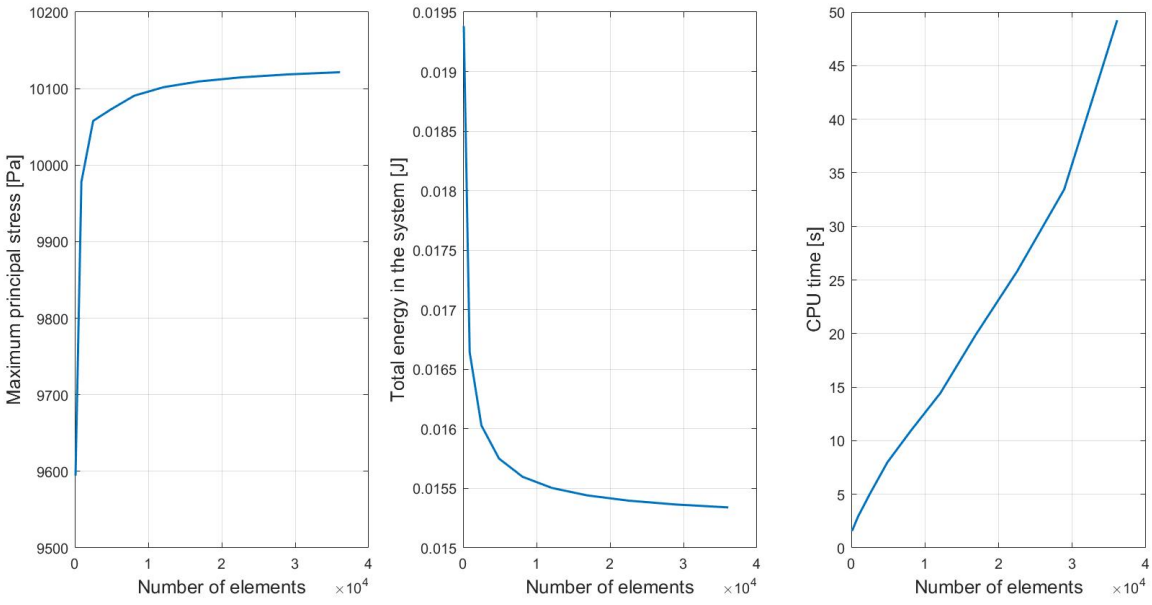

Figure 4.2: Spacial convergence

Temporal convergence

The evolution of the CPU, the maximum major principal stress, and the total energy in the system at the last time step are presented over the total number of time steps in figure 4.3. The major principal stress decreases rapidly before acquiring a constant value. The total energy is also decreasing with the number of time steps but slowlier. However, convergence is visible. Similar to spatial convergence, a good balance between accuracy and computational time have to be found. The choice is made for 100 time steps allowing to stay below the minute in terms of computational time. With a total process time of 100 s and 270 s, the time step value is respectively sets to 1 s and 2.7 s.

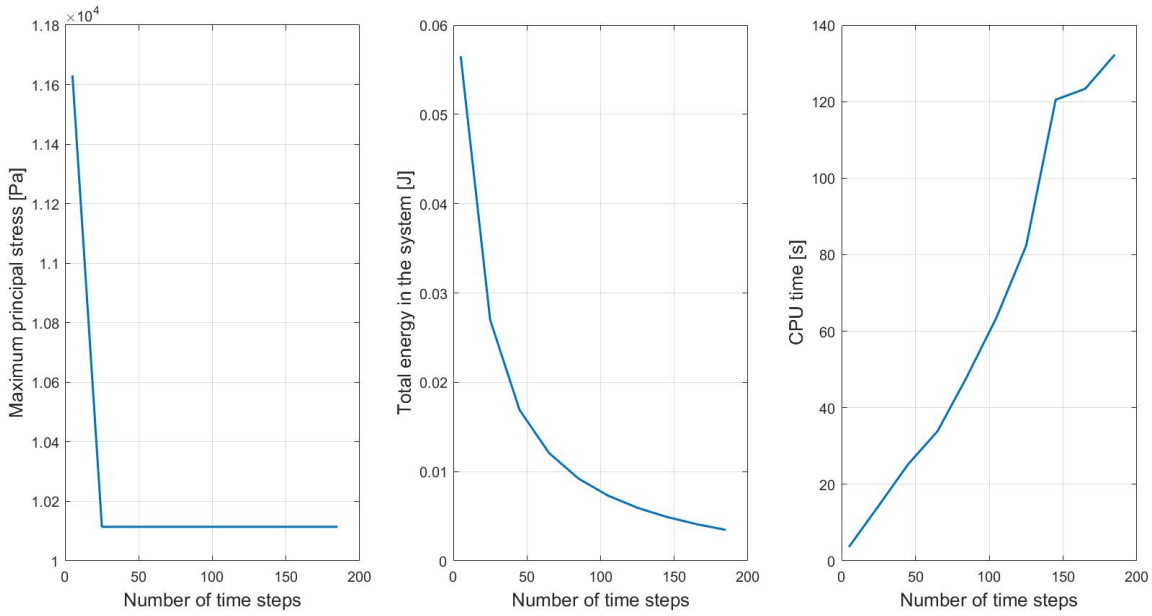

Figure 4.3: Temporal convergence

4.2.2 Impact of wall friction on dissipation

Without dissipation mode

The average vertical displacement at the last time step is $u_y = 43844329.9059\ m$.
The energy balance evolution over time is shown in figure 4.4. Finally, the difference between the top surface displacement and the bottom surface displacement over time is presented in figure 4.5.

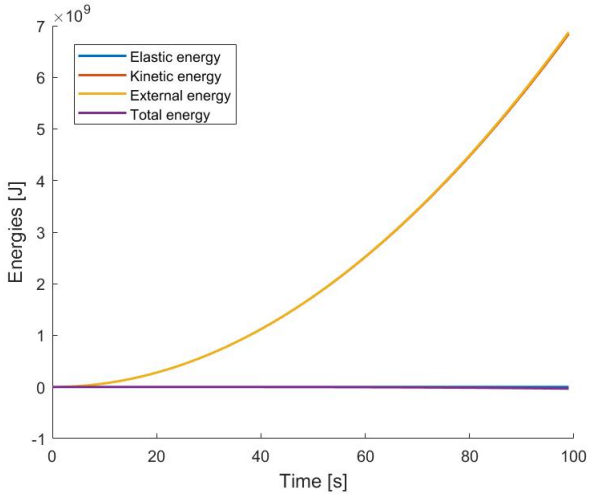

Figure 4.4: Energy balance in the system without dissipation mode

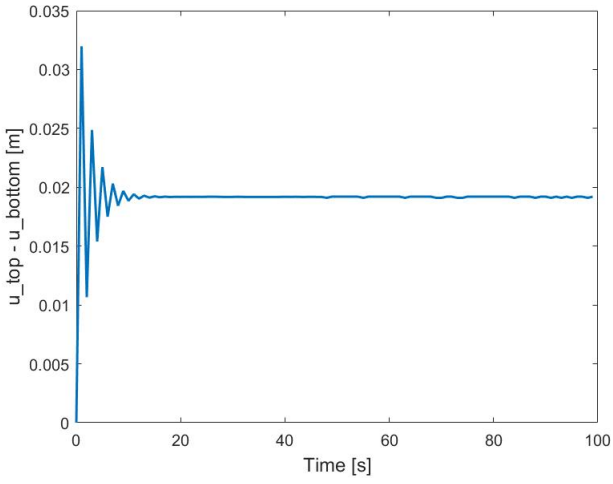

Figure 4.5: Displacement difference between the top and the bottom of the construct in a system without dissipation mode

With a fluid friction mode of dissipation

A dissipation mode is introduced. A fluid friction dissipation is added through the introduction of the term T_v. As explained in section 4.1.1, this applied stress is proportional to the velocity field. The coefficient of proportionality is C_v. This simulation aims at finding the value of this viscous coefficient to obtain, as a simulation output, an average vertical displacement at the last time step equal to the length of the construct. With a value of $C_v = 3.5 * 10^8\ N.s/m^3$, the average vertical displacement at the last time step is $u_y = 0.009981$ m. The energy balance evolution over time is shown in figure 4.6. Finally, the difference between the top surface displacement and the bottom surface displacement over time is presented in figure 4.7.

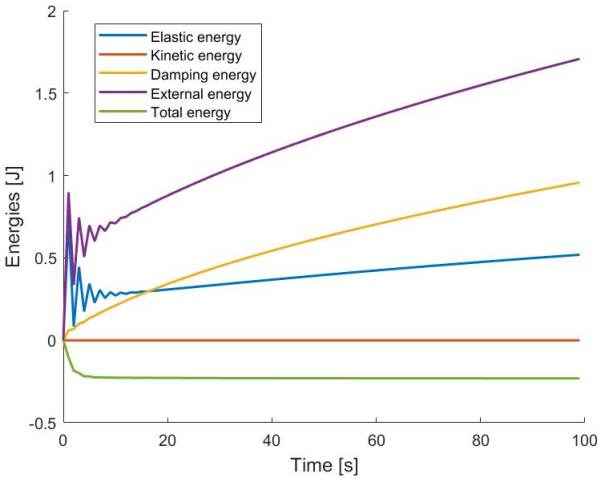

Figure 4.6: Energy balance in the system with fluid friction dissipation mode

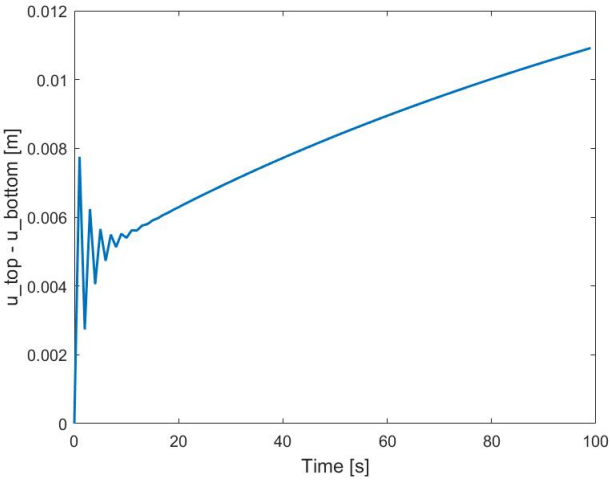

Figure 4.7: Displacement difference between the top and the bottom of the construct in a system with fluid friction dissipation mode

4.2.3 Adaptation of the applied stresses

Without adaptation

Vertical displacement over time

As computed just above, the parameter values of the applied suction pressure $p_2 = 10^5$ Pa and the viscous coefficient $C_v = 3.5 * 10^8\ N.s/m^3$ give an average vertical displacement at the last time step of 9.9 mm. Considering the lubrification layer as the HHC gel, the interpretation of the viscous coefficient value can give a width of $1.714 * 10^{-4}$ m of fluid friction film. To add information on the propagation of the construct inside the cannula, the distribution of the vertical displacement over time (screenshot at 10 s, 60 s, and 99 s) is shown in the figure 4.8. This figure comes in complementary to figure 4.7 and the average displacement value.

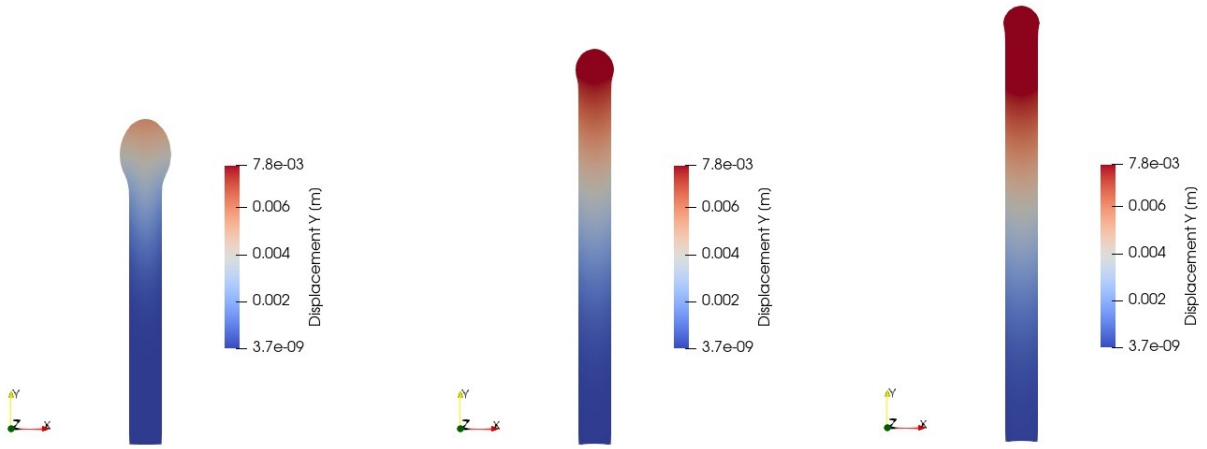

t = 10 s t = 60 s t = 99 s

Figure 4.8: Vertical displacement distribution over time of the system without adaptation

Shear stress distribution over time

The effect the values of the aspiration pressure and the viscous coefficient have on the properties of the construct is evaluated in figure 4.9. The shear stress distribution over time (10 s, 60 s and 99 s) is particularly interesting to link to the cell viability.

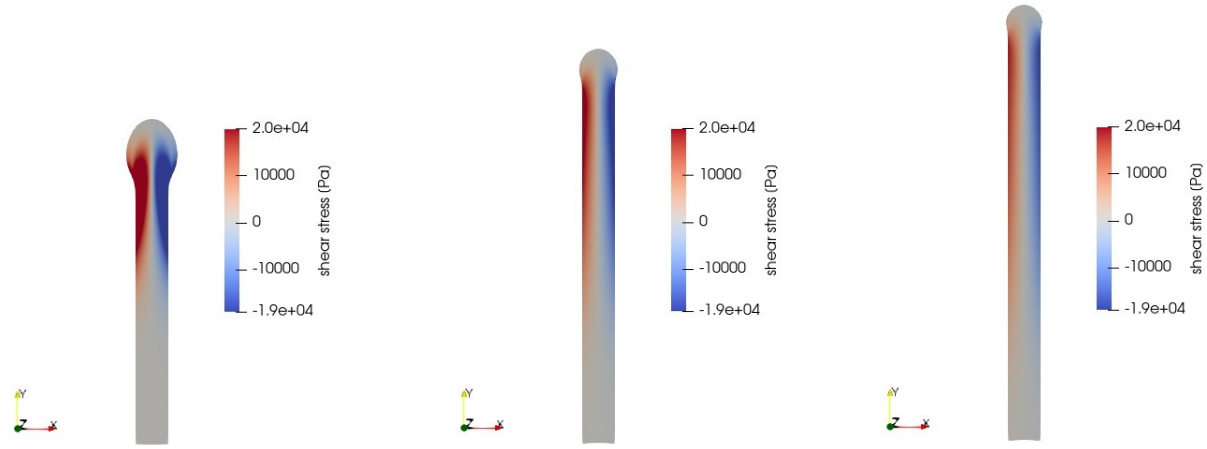

t = 10 s t = 60 s t = 99 s

Figure 4.9: Shear stress distribution over time of the system without adaptation

With adaptation of the p_2 and C_v values

Vertical displacement over time

The values of the aspiration pressure and the viscous coefficient are adapted to remove the elastic rupture effect observed in the previous non-adapted situation. The maximum parameter values are $p_2 = 8 * 10^3$ Pa and $C_v = 7 * 10^6$ $N.s/m^3$ to obtain the average vertical displacement at the last time step of 0.0098 m. If the lubrification layer is interpreted as the HHC gel, the width parameter of this friction layer is 0.0085 m. However, the average displacement value is not sufficient, the change in vertical displacement distribution over time is shown in figure 4.10.

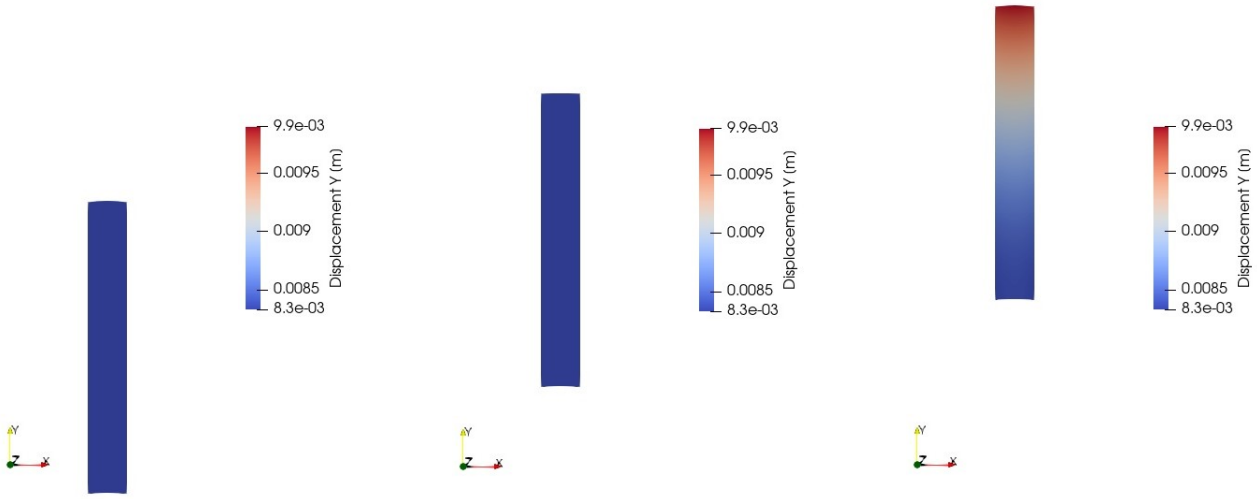

t = 10 s t = 60 s t = 99 s

Figure 4.10: Vertical displacement distribution over time of the system with adapted parameters

Elastic effect

The cancellation of the elastic rupture event that occurred in the non-adapted case is also presented in figure 4.10 in complementary of figure 4.12. The change in the energy balance is also computed in figure 4.11. Those two figures need to be seen in parallel with figures 4.7 and 4.6.

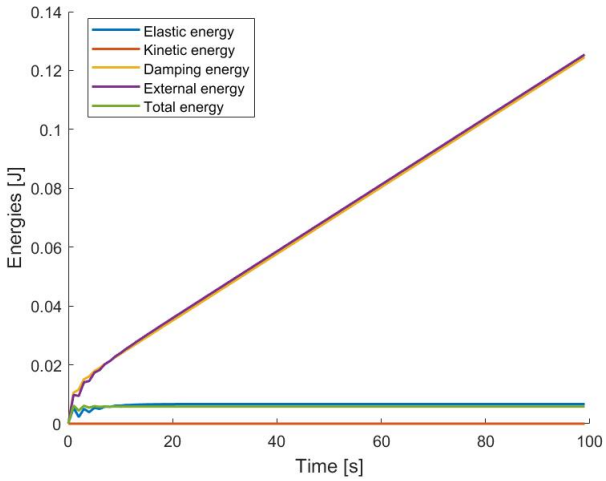

Figure 4.11: Energy balance in the system with adapted parameters

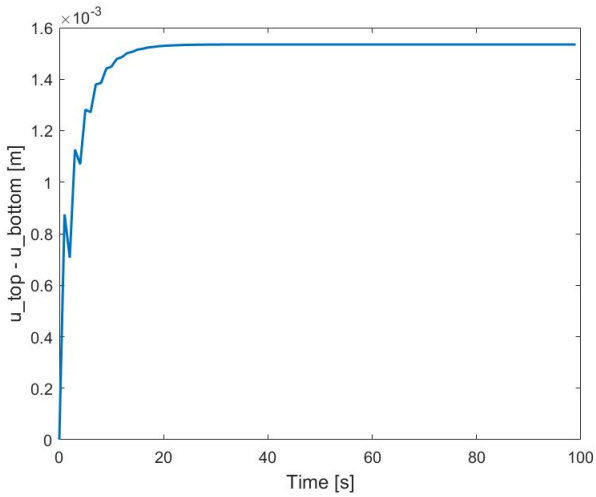

Figure 4.12: Displacement difference between the top and the bottom of the construct in a system with adapted parameters

Shear stress distribution over time

The adaptation of the two parameter values has some effect on the shear distribution over time as it is shown in figure 4.13. This figure has to be put in parallel with figure 4.9.

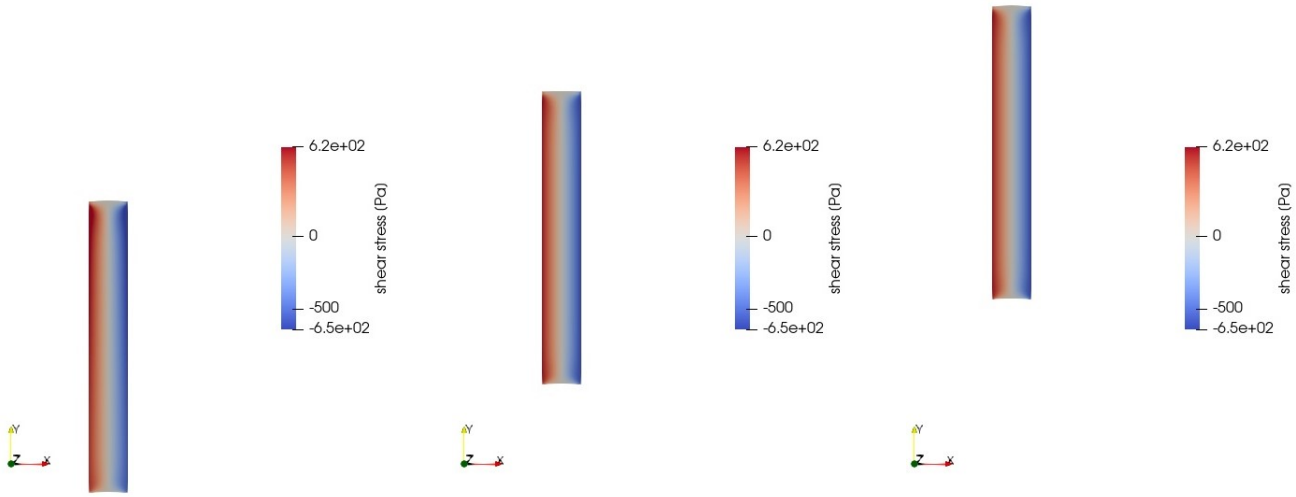

t = 10 s t = 60 s t = 99 s

Figure 4.13: Shear stress distribution over time of the system with adapted parameters

4.2.4 Successful parameter identification for the different cannula sizes

With the same strategy as the previous simulation, the values of the two parameters are investigated to obtain the desired displacement of the construct in the cannula. The results are presented in figure 4.14. Additionally, table 4.5, presents the outcomes of the simulations in terms of displacement for each needle gauge number. The value of the width of the lubrification layer interpreted as the HHC gel is also computed and given in the table.

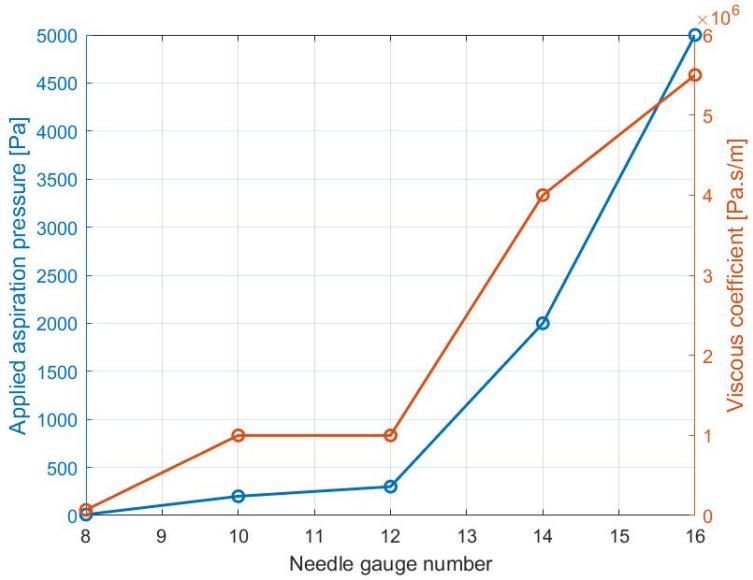

Figure 4.14: Applied aspiration pressure and viscous coefficient values to obtain a successful aspiration of the construct in the cannula for different needle gauge numbers

Needle gauge number	Average displacement at the last time step [m]	$\mathrm{Max}(u_{top} - u_{bottom})[m]$	Width of the lubrification layer of HHC gel [m]
8G	0.0084	$2.7 * 10^{-4}$	0.8
10G	0.0085	$3.5 * 10^{-4}$	0.06
12G	0.0093	$3.2 * 10^{-4}$	0.06
14G	0.0107	$4 * 10^{-4}$	0.015
16G	0.01265	$6.8 * 10^{-4}$	0.011

Table 4.5: Displacement outcomes for the simulations of the successful parameter identification for the different needle guauge numbers

4.2.5 Biomechanical impact of the aspiration stage

16G cannula

Validation

The dynamic model of the aspiration of the gel inside the cannula can be validated by a few result observations. Firstly, the 2D consideration is proved by the fact that all the components of the third dimension are equal to zero. Indeed, the distribution of the z-component of the displacement is equal to zero everywhere and for any time step. The stress and strain tensors are shown as a 3x3 matrices:

$$\sigma = \begin{bmatrix} \sigma_{xx} & \sigma_{xy} & \sigma_{xz} \\ \sigma_{yx} & \sigma_{yy} & \sigma_{yz} \\ \sigma_{zx} & \sigma_{zy} & \sigma_{zz} \end{bmatrix} \tag{4.45}$$

All the components that depend on the third dimension are equal to zero. The stress and strain tensors come back to 2x2 matrices:

$$\sigma = \begin{bmatrix} \sigma_x & \tau \\ \tau & \sigma_y \end{bmatrix} \tag{4.46}$$

In the equation 4.46, the two shear stress (and strain) components are equal. Indeed, in continuum mechanics, the stress (and strain) tensor is symmetric due to the moment of equilibrium equation. This feature is verified in the results of the simulations by the observation of the equalities $\sigma_{xy} = \sigma_{yx}$ and $\epsilon_{xy} = \epsilon_{yx}$ for any kind of simulation. Concerning the shear stress, the distribution over the construct shows positive values on the left and negative values on the right. An example of this distribution can be seen in figure 4.13. This is due to the normal vectors of the wall boundary surfaces which are of opposite signs. This result is in agreement with equation 4.18 and 4.19

The model can also be verified by checking the values of displacements and/or stresses at the boundaries. For instance, for any points on the wall boundaries, the x-component of the displacement is equal to zero. This result is coherent with the Dirichlet boundary condition imposed at this boundary. Lastly, the stress-strain curve is shown in figure 4.15. It is evaluated at node 437 of the mesh that can be seen in figure 4.16.

Stress level distributed in the construct

Some interesting properties of the construct can be analysed at each node of the mesh. Examples of properties that can be observed are the different components of the strain and the stress tensors (normal along with x-axis, normal along with y-axis and shear components). An analysis of the time evolution of the stress or the strain properties at different particular nodes of the constructs is conducted. It can be observed that the property values stabilise quickly after a few seconds at constant values. This result is illustrated in figure 4.16. The position of node 437 in the mesh is shown and the vertical normal stress level at this node is plotted over time.

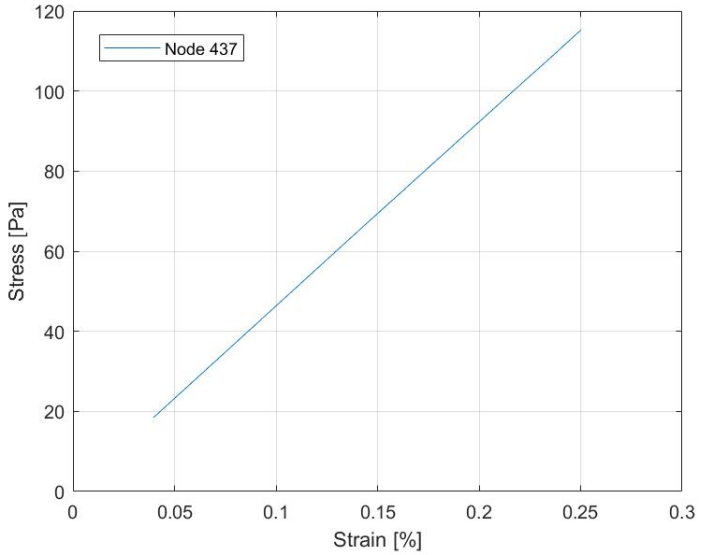

Figure 4.15: Stress-strain curve of node 437

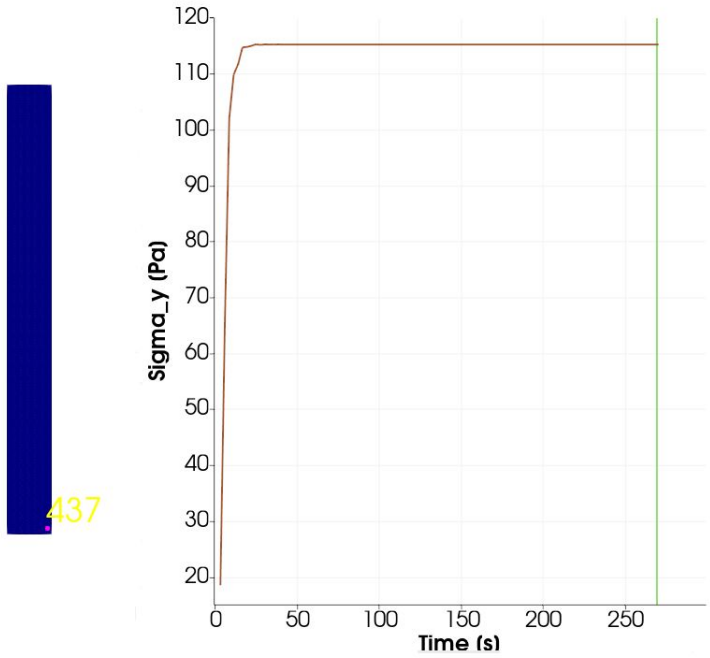

Figure 4.16: Position of node 437 in the mesh and normal vertical stress amplitude over time at node 437

Afterwards, the most interesting properties of the cell viability and alignment are analysed at the last time step, i.e. after 270 s. On the left-hand side of figure 4.17, the distribution of the shear stress level is shown. On the right-hand side of figure 4.17, the major principal stress vectorial distribution is presented. The orientation of the vector corresponds to the orientation of the major principal stress at this node. The amplitude of the vector and the color bar expose the level of the major principal stress at this node.

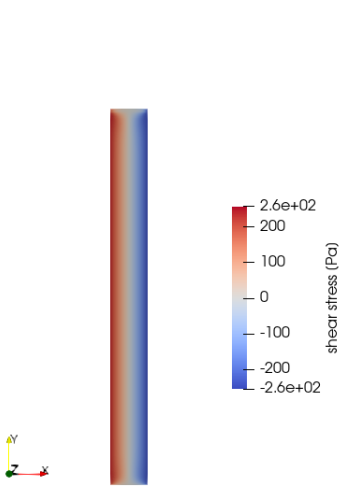

Shear stress distribution

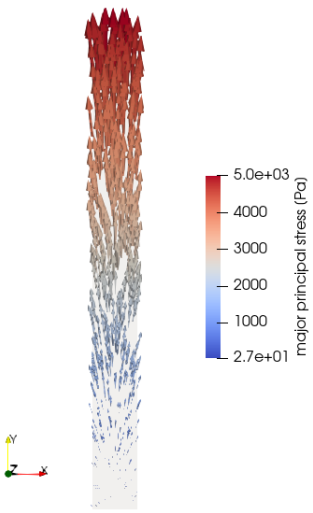

Major principal stress field

Figure 4.17: Shear stress distribution and maximum major principal stress field over the 16G construct after 270 s of aspiration process

Comparison with different needle gauge numbers

The two interesting features of the previous figure 4.17 can be analysed for the different needle gauge numbers. Therefore, the maximum stress levels of both distributions are taken at the last time step (t=270 s). An evolution of the shear stress and the major principal stress for different needle gauge numbers are presented in figure 4.18.

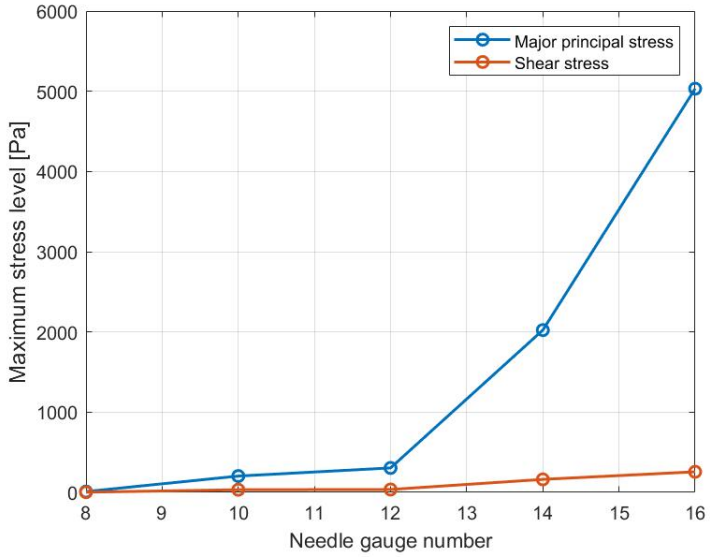

Figure 4.18: Maximum shear stress level and maximum major principal stress level at the last time step (t=270 s) for different needle gauge numbers

4.3 Discussion

Convergence

Firstly, the convergence of the model was assessed. A clear spatial and temporal convergence is observed for two important quantities for the GAE-EngNT construct. The proof of a convergent model is important to validate the model [54] [63] [76]. In addition, the values of the FEM parameters (N_x, N_y and the number of time steps) are determined to guarantee the independence of the results regarding the time and space discretisation. These parameter values complete the list of parameters that have constant values for all the simulations.

Impact of wall friction on dissipation

Secondly, a first simulation of the model was performed without any dissipation mode. The situation was similar to the aspiration process performed by the Canadian team of Neysan O. Kamranpour [24]. A construct of the 14G cannula dimension is constrained by the cannula walls and subjected to an aspiration pressure on the top surface. The EngNT viscoelastic material properties are considered but no interactions with the wall boundaries are present. The 10^5 Pa of aspiration pressure gives particularly high energy to the system. Most of this energy is converted into kinetic energy as shown by the yellow and red curves in figure 4.4. These energies increase exponentially with time and reach an order of magnitude extremely high ($7 * 10^9$ J). This energy balance analysis explains the excessively high average vertical displacement of the construct in the cannula, which is in the order of $5 * 10^4$ km. Furthermore, the total energy of a real physical system should always stay constant over time. The energy is simply transformed into different forms in the system. The energy balance of the model in figure 4.4 shows a nearly constant total energy component which validates the model. The slight decrease over time is due to numerical damping. However, it is limited. As mentioned earlier, the external energy of the applied aspiration pressure is nearly entirely converted into kinetic energy. Indeed, the elastic energy form stays extremely small. This observation explains figure 4.5 which shows a particularly small displacement difference between the top and the bottom of the construct ($u_{diff} <<<< u_y$). The early oscillations are certainly due to the numerical method that needs to stabilise. Increasing the amplitude of the damping could improve those early oscillations though introducing a leak of total energy in the system due to a numerical effect and not a physical event. Reducing the time step could improve the accuracy of the solver but with a high cost of computation time. A proper study of the parameter values of the time integration scheme as well as the comparison between different discretised time solvers can be useful to identify the best choice to avoid those oscillations. In conclusion, the construct is progressing in the cannula extremely high as one entire solid material that is pulled upwards without any dissipation in the system. This simulation shows that the model without dissipation is not realistic. The introduction of a dissipation mode is needed to compensate the external energy and keep the kinetic energy low. The viscosity properties of the material are already modelled and do not provide sufficient dissipation. Intuitively, most of the dissipation could be due to the interaction of the construct with the wall boundaries of the cannula. This shows the importance of the interaction of the construct with the boundary walls during the aspiration process.

Therefore, the second simulation introduces the T_v term. It adds the consideration of a fluid layer between the construct and the wall boundaries which highly dissipates energy in the form of fluid frictions. This lubrification layer can be considered as part of the liquid phase of the GAE-EngNT. Indeed, the mathematical model represents the construct as a solid monophasic material while in reality, the construct is a biphasic material with a fluid phase interacting with the boundaries. The *in silico* representation does not model the fluid phase but models its interaction with the boundary through the viscous coefficient C_v as explained in section 4.1.1. Considering that the fluid phase is the initial collagen gel that did not stabilised, the width of the lubrification layer is 0.17 mm. Due to the extremely high order of magnitude of the kinetic energy, the dissipation needs also to be high to compensate. Therefore, the viscous coefficient requires large values which implies a narrow film of a highly viscous fluid. The energy balance of figure 4.6 shows the desired effect. The kinetic energy is almost zero. The external energy from the aspiration is converted into elastic and damping energies due to fluid friction dissipation. The order of magnitude is radically decreased compared to the system without dissipation. However, elastic energy is, by now, much more important in the energy balance. This result leads to the creation of an elastic effect in the construct during the aspiration. As it can be seen in figure 4.7, the difference between the displacement at the top surface and the one at the bottom surface is high and increases with time. A deeper study of this elastic effect is therefore necessary.

Adaptation of the applied stresses

Thirdly, the previous simulation is analysed in detail. The presentation of the vertical displacement distribution over time in figure 4.8 shows explicitly the elastic effect discovered in figure 4.7 in the previous paragraph. The elastic energy is too high compared to the order of magnitude of the other forms of energy. Consequently, the construct is not rigid enough to support this high-pressure level and viscous effect. The material behaves like an elastic that is stretched on one side. The top surface of the construct reaches 8 mm in height but the bottom surface is barely moving. The aspiration process is failing. This situation might model the failure of the construct during the aspiration, as reported in section 2.4.2. The top of the construct can propagate in the cannula and be aspirated. However, the construct stops during the aspiration because its bottom part can not follow. The failure is explained by an inappropriate aspiration pressure and viscous coefficient. Indeed, the viscous coefficient is too high and blocks the bottom part of the construct. To release the effect of the fluid friction while keeping a desired displacement in the cannula, the applied aspiration pressure needs to be decreased.

The third simulation with the adapted parameter values finds a lower aspiration pressure and a lower viscous coefficient for a similar 10 mm displacement in the cannula. The vertical displacement distribution overtime in figure 4.10 shows the cancellation of the elastic effect. The entire construct is aspirated and moves vertically as a solid unit. The elastic property of the material is still present but constant and relatively low compared to the order of magnitude of the entire construct displacement. Indeed, figure 4.12 shows a difference between the top and the bottom displacement which stabilises quickly around 1.5 mm while the construct is moving to 10 mm upwards. The energy balance in figure 4.11 provides a good understanding of the phenomena during the aspiration in the can-

nula. The kinetic energy is kept extremely low to allow a displacement in the order of magnitude of a tenth of millimeters. The external energy provided to the system by the application of the aspiration force is mostly converted into damping energy that is dissipated due to the interaction with the wall boundaries. This quasi-complete compensation enables to keep the elastic energy at a low order of magnitude compared to the external energy. In this way, the elasticity of the material does not impact the aspiration of the entire construct and guarantees a successful process.

In addition, those two simulations enable the analysis of this elastic effect on the stress levels applied to the seeded cells inside the construct. Indeed, the comparison of the shear stress distributions over time in figure 4.9 and 4.13 shows clear differences. In the model without the adapted parameter values (figure 4.9), the peak of shear stresses is present at the top of the construct. This firstly aspirated region is subjected to a shear stress level of $2 * 10^4$ Pa. This shear stress peak is then spreading along the construct with time. However, a clear in-homogeneity of the shear stress distribution along the construct is observed. On the contrary, for the model with the adapted parameter values (figure 4.13), the shear stress level is lower (around $6.2 * 10^2$ Pa). In addition, this shear stress distribution is evenly distributed along the construct. As explained in section 2.2.6, the shear stress might affect the cell viability. In a case where the elastic effect appears and is not negligible, the cells in the first aspirated area would be subjected to the higher shear stress level. This could induce a higher cell death level in the top area of the construct. This is not the observation of the UCL Centre for Nerve Engineering as reported in section 2.4.3. Therefore, the disparity in cell viability might not come from the elastic failure during the aspiration. Besides, a perfectly aspirated construct has homogeneous shear stress distribution. Therefore, the GAE-EngNT construct does not have any in-homogeneity in the cell viability coming from the aspiration process. Additionally, the aspiration stage of the entire GAE process might not be the cause of cell death in the entire construct in general. Indeed, the order of magnitude of the shear stress is relatively low. The stress level in the construct has generally two orders of magnitude lower when the construct is successfully aspirated. This proved the potential of the GAE method to produce EngNT when the process is successful. This potential is already observed experimentally thanks to a good quality of GAE-EngNT explained in section 2.4.4 [16] [21] [24].

Successful parameter identification for the different cannula sizes

Afterwards, it is interesting to give the parameter values to guarantee a successful aspiration process with different needle gauge numbers. The third column of table 4.4 guarantees the success of the aspiration. The elastic effect stays around $5 * 10^{-4}$ m. Furthermore, figure 4.14 shows that with an increasing needle gauge number, higher aspiration pressure can be used. This makes the method suitable to use with pressure values not extremely low. This is the case of the 8G cannula where the construct is particularly elastic and required therefore a low aspiration pressure and a low viscous coefficient. This is due to a less efficient stabilisation process which causes a less rigid construct. Concerning the viscous coefficient, it must increases with the applied pressure in order to keep a desired low displacement which models the reality.

In addition, the interpretation of the lubrification layer is coherent with the order of magnitude of this C_v parameter. Indeed, when the inner diameter of the cannula is larger, the

construct is less rigid due to a lower dehydration level. This situation leads to a construct with a higher liquid phase percentage. Therefore, the liquid part which interacts with the boundary walls is more liquid. Consequently, the viscosity of this lubrification layer is lower than the one of the HHC gel. Following equation 4.17, decreasing the viscosity decreases the width of the film for the same viscous coefficient value. Therefore, the high values of the film width for low needle gauge numbers are not realistic. However, these values have an interpretation and can find a reasonable order of magnitude with a correct consideration of the viscosity of this lubrification layer.

Biomechanical impact of the aspiration stage

Lastly, the successful aspirated condition using the 16G cannula is considered. The goal is to imitate the process performed by the UCL Centre for Nerve Engineering. A first analysis is performed to partially validate the model. Coherent outcomes with the model definition partially proves the validity of the numerical resolution. The stress-strain curve in figure 4.15 seems linear. However, the viscosity of the collagen gel material is considered and induces a slight non-linearity. The presence of this non-linearity is proved with linear interpolation in appendix I.2. The particularly small non-linearity proves the elastic dominance of the viscoelastic construct. This result is confirmed by the experimental analysis reported in section 2.2.5 and in the publications [8] [16].

In addition, to analyse the cell viability and alignment in the GAE-EngNT construct produced by the UCL Centre for Nerve Engineering, a stress level analysis is performed. First of all, the focus is on time evolution. At a specific node of the mesh, different stress components are observed over time. The amplitude of the stress increases and needs to stabilised during the first seconds before finding a constant value for the majority of the time interval. An example of such analysis is shown in figure 4.16. Therefore, for a successful aspiration process, the stress properties can be observed at the last time step and considered at a steady state during the entire aspiration. The two interesting types of stress to analyse are the shear stress and the major principal stress.

As explained in section 4.1.5, the shear stress distribution in the construct provides some cues about the stress level to which the seeded cells are subjected. This specific stress is studied to be one of the causes of cell death or cell damage in bioprinting [56] [57] [58]. The shear stress level appearing due to the aspiration process is relatively small with a maximum shear stress value of 260 Pa. In the literature, no range of shear stress values was determined to define the risk of cell damage or cell death [56] [57] [58]. Moreover, it seems to depend on the type of cells used as discussed in section 2.2.6 [56]. However, the range of shear stress value observed on the left part of figure 4.17 is particularly small. This might indicate that the aspiration stage of the GAE process is not impactful on the cell viability. Nevertheless, it is interesting to look at the distribution of the shear stress. It can be observed a perfect symmetry along the construct. Heterogeneity in the cell viability along the construct reported in section 2.4.3 and in the publication [21] does not have its origin in the success of the aspiration process. On the contrary, a gradient can be observed in the radial direction. Indeed, the shear stress is maximum at the wall boundaries and decreases until being nearly zero at the centre of the construct. It could be interesting to put this result in parallel with experimental observations of cell viability in a transverse section of the GAE-EngNT construct.

The second type of interesting stress is the major principal stress. Its amplitude and orientation can give cues on the normal stress and the direction of this maximal normal field appearing in the matrix during the aspiration. The collagen matrix is the substrate of the seeded cells. Therefore, looking at the maximum normal stress and its orientation could be an indication of the force field to which the seeded cells are subjected. The right part of figure 4.17 shows clearly the more the stress aligned with the vertical axis, the higher is the amplitude of the stress. Low amplitude stresses hold on the bottom of the construct with a divergent orientation, directing the stress vector outside the construct. On the contrary, at the top of the construct, the major principal stress amplitude is much higher, between 4000 to 5000 Pa. In addition, those high amplitude stress vectors have a quasi-vertical orientation. This observation could force the seeded cells at the top of the construct to align along the longitudinal axis. This clear heterogeneity along the construct in terms of cell alignment is also reported by Papon Muangsanit [16] [21]. A higher cell alignment is observed in the first aspirated area of the construct. This matches exactly the major principal stress field analysis. However, other researchers from the UCL Centre for Nerve Engineering found different results concerning this inhomogeneity in cell alignment as explained in section 2.4.3. No clear explanation of the inter-user variability is found with this model. Nevertheless, the maximum major principal stress values stay relatively low. Therefore, other stages of the process could generate higher stress levels. This feature would need to depend on the variability parameters identified in table 2.8 to explain the variability. In some cases, other stages of the process generate a higher major principal stress field which overtakes the aspiration stage. In other situations, the aspiration stage modelled in this research is the most impactful, and the alignment at the top of the construct finds an explanation. Comparing the order of magnitude of both stresses, the major principal stress has one order of magnitude higher than the shear stress. This confirms the correspondence with experimental data explained in section 2.4.3 in terms of cell alignment. On the contrary, the shear stress amplitude during the aspiration stage is too low to explain the experimental data on cell viability.

Furthermore, it is interesting to look at the amplitude of those two stresses (maximum shear stress and maximum major principal stress) for different needle gauge numbers. Figure 4.18 shows that both stress levels increase with the use of higher needle gauge numbers. However, the shear stress values stay relatively low. This result confirm the previous analysis. The aspiration stage seems to not influence the cell viability thanks to low level of shear stress whatever the cannula size used. Oppositely, the major principal stress increases of one order of magnitude with the 14G and 16G. Those cannula sizes where determined to be the best ones to produce GAE-EngNTs which promote nerve regeneration [16] [24]. This experimental observation can be confirm with the mathematical model. Higher needle gauge numbers increase radically the amplitude of the normal stress which acts on the seeded cells to promote their alignment. The GAE process using the 14G and 16G cannula produces highly aligned GAE-EngNT construct thanks to higher amplitude of the major principal stress. Moreover, the cell viability is not altered thanks to a low level of shear stress.

4.4 Limitations and future developments

The limitations of the model lie in two major features. On one hand, by definition of the focus of the mathematical model, a lot of assumptions and simplifications are done. Therefore, the model is not targeting the entire GAE process but only a specific stage with additional simplifications. Those drawbacks are internal limitations due to the definition of the *in silico* representation. Firstly, the model is in 2D while the reality of the process is in 3D. The wall interaction with the cylindrical cannula and the definition of the concentration in terms of quantities per unit volume are 3D consideration. They are neglected in the current model. The second limitation is the linear elastic behaviour assumption. Indeed, the material is considered viscoelastic in the model but the elastic properties are only considered linear. The experimental non-linear stress-strain curves presented in section 2.4.3 from the publication [24] are impossible to reproduced. Moreover, the material is modelled as a monophasic material while the reality of the collagen gel construct is a biphasic material as concluded from section 2.2.5. Furthermore, the model focus only on the propagation of the GAE-EngNT construct inside the cannula. The previous stages of stabilisation and first aspiration steps are not considered. This implies the impossibility of the model to answer most of the experimental challenges formulated in section 3.1.1. In addition, the nature of the lubrifiaction layer is difficult to identify due to the non-consideration of the stabilisation process. This limits the interpretation and understanding of the model results. Another limitation is the choice of the propagation of the construct when it is already in the cannula. Consequently, the model is not representing the progressive entry of collagen gel inside the cannula. This focus is not representative of the exact reality of the GAE process.
On the other hand, the lack of experimental data to feed the model to best suits the mathematical model with the real *in vitro* process is a limitation of this research work. Firstly, some experimental data are missing to identify parameters for the dynamic GAE model. Indeed, the exact density of the construct for each cannula size is not directly measured. For the 16G cannula, data about the mechanical properties of the construct are missing. The value used in this research is an interpolated value from another research group than the UCL Centre for Nerve Engineering. Moreover, the initial concentration of collagen fibrils in the HHC gel is slightly different in the two research teams as explained in section 2.2.2. The viscoelastic properties of the final construct are, therefore, impacted. The Young's modulus used in the current model is the one obtained using the data of only one team which did not use the 16G cannula size. The results for this needle gauge number can be affected by an error when compared with the experimental outcomes of the UCL Centre for Nerve Engineering. In sum, the data for the identification comes from different studies and different research groups or computed from measurements made on reported pictures. This in-homogeneity in the source of data is a real limitation that can significantly affect the results. Secondly, a lack of experiments, specially dedicated to the validation of the model, weakened the current approach. Poor evaluation of the applied aspiration pressure and the process timing makes difficult the validation of the model results on the values of the two parameters (p_2 and C_v) to guarantee the success of the aspiration process. Experiments specifically oriented are missing to refine, validate, and improve further the mathematical model of the GAE process into the integrated approach strategy.

The primary mathematical model of this research work is only a first trial to initiate a larger strategy for the control of the GAE process. Considering only the model focus selected for this research, plenty of future developments are still to be made. The 2D model can be improved by considering a 2D axisymmetric problem or a 3D model. Another development to improve the model is considering the progressive entry of the stabilised collagen gel in the cannula. The zero reference pressure at the bottom of the construct should also be modified to model the link with the hyper-hydrated gel not yet aspirated. A change in the boundary conditions could allow the modelling of this situation. Another idea is to use two different domains and model a mass transfer from one subset to the other. Furthermore, future developments can be made in terms of material properties. The model can be adapted to a hyperelastic material trying to reproduce the experimental stress-strain curves. Another adaptation is to consider a biphasic material. It would also be easy to adapt this dynamic model approach to analyse the ejection stage as well as both aspiration and ejection process with different application profiles. This study could gives ideas on the impact of one or the other stage on construct properties and the required stress application profile to guarantee successful aspiration and ejection stages. In addition, the comparison between the different needle gauge numbers could be further developed. The aim is to find the physical explanation for the choice of the 16G cannula as the optimal cannula for the GAE process in terms of nerve regeneration. Another interesting future consideration is the presence of seeded cells inside the construct. The idea would be to introduce the cells as inert loads and look at where they are moving inside the construct during the aspiration process. Looking at the stress history applied to those particles in the construct would also allow the consideration of the level but also how long the cells are subjected to shear stress. This could give more cues about the distribution of cell viability along the construct. Different pressure profiles could also be tested to see the effect of discontinuous aspiration pressure application. Some variability parameters presented in table 2.8 could also be integrated into the model and a sensitivity analysis could be performed. The goal would be to identify the variability origin which affects the most the aspiration process. The result would bring some suggestions for the UCL Centre for Nerve Engineering to reduce this variability by controlling the important parameter.

The last suggestion for further studies is the implementation of the integrated approach loop as presented in figure 3.1. Firstly, some experiments should be conducted to allow better parameter identification. Indeed, quasi-static tensile tests should be performed with the five cannula sizes (especially the 16G). The aim is to obtain stress-strain curves to extract the data for the material properties parametrisation. Other mechanical tests could also be performed to determine the Poisson's ratio. The mass and the volume of the construct could also be measured accurately to determine the density of the construct for each needle gauge number. Exact timing and applied pressure measurements should be performed in order to obtain the exact data for the model simulations. Afterwards, isolated experiments of a construct inside the cannula being aspirated on the top surface, is a good way to validate the model experimentally. Mismatches between the experiments and the model could allow to refine the model and find other features to explain experimental results.

Chapter 5

Conclusion

In conclusion, this research work focuses on building a primary mathematical model to control the production methods of the Engineered Neural Tissue. Indeed, most of the literature deals with the optimum design of EngNT to promote nerve regeneration. Therefore, there is a large gap to study and explore the potential of the two promising manufacturing methods of the desired construct. Consequently, this work aims at rising the interest in this field, at initiating the strategy to answer the scientific gap and proposing future perspectives. For this purpose, this research builds a primary mathematical model to initiate the control of the stabilisation methods of the EngNTs in three steps.

Firstly, a study of the experimental context is essential to define the framework of the mathematical model. It is important to fully define and analyse beforehand what needs to be represented *in silico*. Since the collagen gel is the material processed by the stabilisation methods, it is important to study it entirely. The most important characteristics of the collagen gel are its initial concentration in collagen fibrils which radically influences the mechanical properties of the matrix, its initial volume, and the seeded cells used. The preparation of the gel creates a hyper-hydrated collagen gel after being set. The mechanical characteristics of the gel are much different when it is an HHC gel compared to the stabilised gel. On the one hand, the HHC gel has a viscoelastic behaviour mostly with an elastic dominance. The gel is closer to a solid than to a liquid and mathematical models use rheological power-laws or hyperelasticity theories to simulate further mechanical test behaviours. On the contrary, the stabilised gel is more rigid and has a linear viscoelastic behaviour. The elastic component dominates in tension while the viscous behaviour is higher in compression. On the other hand, the stabilisation methods need to be defined with all their variability in uses and specificity. It appears that both techniques have large potential though neither standardised nor automatised. This leads to a clear lack of control. Consequently, outcomes of the stabilisation methods are affected and this leads to sub-optimal manufacturing of EngNTs. Additionally, interesting outcomes do not find any justification. Consequently, the need for mathematical models appears.

Secondly, the model focus is the following step to answer the question of how to build a primary mathematical model of the production methods of EngNTs. The priority of this research work is given to the GAE method as it is the most recent and promising one. It is also the one used at the UCL Centre for Nerve Engineering. The sub-optimalities and experimental challenges identified previously can be solved using mathematical modelling. However, *in silico* models have some drawbacks. Therefore, the best strategy would be to

opt for an integrated approach combining experiments and *in silico* simulations to answer the need of controlling the GAE process. The current stage is only the initiation of this multi-disciplinary workflow. The first step is, therefore, to propose a primary mathematical model. One of the main limitations of mathematical models is the impossibility to model the entire process. Indeed, a model is always dependent on the assumptions made and on the selected focus. Different approaches to the GAE model are explored such as the consolidation theory focusing on the stabilisation process. This perspective would be interesting to develop in a future study, especially with the parallel modelling of the GAE and PC stabilisation method. However, the model chosen for this research work is more restrictive and focuses on the propagation of the GAE-EngNT construct inside the cannula after the stabilisation. The model aims at studying the impacts of this stage on the properties of the final GAE-EngNT and the phenomena for successful aspiration.

Thirdly, the primary model is implemented following the materials studied in the first step, and the model focus defined in the second stage. A dynamic analysis is used to simulate the progression of the GAE-EngNT construct inside the cannula due to the aspiration pressure applied on the top surface. Finite Element Methods implemented in $FEniCS$ combined with a Generalised-α time discretisation solver are used to solve the problem set as partial differential equations in space and in time. It appears in the results that a dissipation mode is required in the model to fit the real displacement observed in the cannula. This dissipation has an important order of magnitude and proves that the viscosity of the collagen gel itself is not sufficient. Indeed, the interaction of the GAE-EngNT construct with the walls of the boundaries provides the desired dissipation. Because the collagen gel is a biphasic material, it has a solid phase being aspirated upwards and a fluidic phase interacting with the boundaries creating fluid friction dissipation. However, in the case of high applied suction pressure, this fluid friction dissipation needs to be high. This feature is interpreted as a thin lubrification layer of an extremely viscous fluid such as HHC gel just in the contact area with the walls. This non-adapted situation leads to an elastic rupture of the construct inside the cannula. The top of the gel is moving while the bottom can not follow. This situation might simulate one of the failure processes of the aspiration stage. To guarantee the success of this stage, the adapted value of applied aspiration pressure allows the decrease of the amplitude of the dissipation at the wall. However, the aspiration failure situation does not seem to explain the in-homogeneity in the cell viability and cell alignment along the cannula. That is why, it is interesting to analyse those two interesting features in the successful aspiration situation. The shear stress level appears to be always relatively low. Consequently, it can be concluded that the aspiration stage is not the cause of cell death or the disparity in cell viability inside the GAE-EngNT construct. On the contrary, high major principal stress directed in the longitudinal axis of the construct seems to indicate higher cells' or fibrils' alignment in the first aspirated area. This positive feature is particularly important for high gauge numbers which confirms that the 16G is the best choice for manufacturing optimal GAE-EngNT construct. By definition of the model focus, this dynamic approach has several important limitations which are also linked to the challenges of this research work.

Furthermore, the choice of the approach, implementation, and simulation strategy for the model has been done according to the framework of this research project. Indeed, different limitations for the explanation of how to build the primary model of the stabilisation methods can be highlighted. First of all, the answer to the research question

tightens up to a primary mathematical of the GAE process throughout the three steps. Indeed, the model implemented only focuses on a particular stage of the GAE process. This model explores only a small part of the entire understanding and control of the stabilisation methods. Additionally, the research work explains both stabilisation methods but limits the mathematical model focus and implementation to the GAE method. However, the PC method has also been used by the UCL Centre for Nerve Engineering and has a lot of potential for EngNT manufacturing. Both techniques should be studied in parallel and compared to use both in dedicated situations in an optimal way. The challenge of this research work is also the short amount of time allocated which limited a complete study of the collagen gel, the PC methods, and the model focus of the GAE technique. Another challenge of this research is the poor physical framework and literature studies on the EngNT manufacturing techniques. In addition, no modellers are yet focusing on those methods in Professor Shipley's research team. Consequently, the exploration for the control of the stabilisation processes started from scratch. Moreover, no experiments dedicated to such research questions have been conducted so far. Consequently, statistical studies and model parameter identification are more difficult. Therefore, the choice for the model focus is dictated by all those challenges which can be reduced in a longer and deeper study focusing on this potential topic.

Future perspectives are provided throughout the research work since the inner limitation of this project is to provide only primary stages in this research field. Furthermore, improvements for the GAE aspiration model implemented in this work are also presented. For instance, the 3D model, progressive entry in the cannula, hyperelastic material behaviour, and the presence of seeded cells can be considered. A sensitivity analysis of different variability parameters previously identified could be especially useful to improve the standardisation and the automation of the model. More generally, to improve the control of the stabilisation methods, dedicated experiments should be conducted firstly to collect statistical data on the failure cases, on the different application profiles of the aspiration pressure, on the use of some supports, and on the different types of geometries (well-plates, volumes, and needle gauge numbers). Those data could be used to target specific model focus to initiate integrated approach studies. Secondly, dedicated experiments need to be conducted to allow parameter identification. For instance, the weight and the final volume of the construct could be measured to allow a proper computation of the density of the construct. Proper mechanical tests should also be conducted to look at the stress-strain curves with different needle gauge numbers and different initial concentrations of collagen fibrils. If possible, rheological studies can be conducted on the HHC gel as well as on the stabilised gel to obtain the viscosity and the fluidic behaviour of the material. Thirdly, during the integrated approach study, isolated experiments on the targeted GAE stage should be conducted to put in parallel the experimental and the *in silico* outcomes. This would allow to refine or validate the model.

In conclusion, this research project aims to raise the interest in the control of the stabilisation methods of EngNTs using mathematical modelling. Despite its numerous limitations, this research work initiates the strategy to answer the scientific gap, exploring future perspectives and proposing a primary model to increase our understanding, particularly of the GAE process. A little step has been done but a great future is expected for the mathematical modelling and the use of the automated PC and GAE stabilisation methods.

References

[1] Ming-Shaung JU, Chou-Ching K. LIN and Cheng-Tao CHANG. (2017). Researches on biomechanical properties and models of peripheral nerves - a review. *Journal of Biomechanical Science and Engineering*. Vol.12, No.1

[2] Susan Standring. (2019). The History of Nerve Repair. *Peripheral Nerve Tissue Engineering and Regeneration. springer* pp 1-32

[3] Rachel Hannah Coy. (2019). Modelling the Impact of Cell Seeding Strategies on Cell Survival and Vascularisation in Engineered Tissue. *Thesis submitted to UCL*

[4] Smaranda Badea, Wutian Wu. (2019). Nanoengineered biomaterials for bridging gaps in damaged nerve tissue. *Nanoengineered Biomaterials for Regenerative Medicine*. chap 2.2

[5] Cristiana R. Carvalho, Joaquim M. Oliveira and Rui L. Reis. (2019). Modern Trends for Peripheral Nerve Repair and Regeneration: Beyond the Hollow Nerve Guidance Conduit. *Front. Bioeng. Biotechnol.. review article*

[6] Beatrice Yue. (2015). Biology of the Extracellular Matrix: An Overview. *J Glaucoma. 2014 Oct-Nov : S20–S23.*

[7] M.F. Griffin, M. Malahias, S. Hindocha and Wasim S. Khan. (2014). Peripheral Nerve Injury: Principles for Repair and Regeneration. *The Open Orthopaedics Journal, 2014, 8, (Suppl 1: M10)*. pp199-203

[8] Celine Kayal. (2019). Spatial Control of Mechanical Factors: a New Design Rationale for Nerve Tissue Engineering. *Thesis submitted for UCL, Mechanical Engineering*

[9] Taylor, Christopher A. MD, Braza, Diane MD, Rice, J Bradford MA, Dillingham, Timothy MD. (2018). The Incidence of Peripheral Nerve Injury in Extremity Trauma. *American Journal of Physical Medicine Rehabilitation: Volume 87 - Issue 5*. p 381-385

[10] Tyler Wheeler. (2021). Neuropathic Pain Management. *WebMD.com*. URL: https://www.webmd.com/pain-management/guide/neuropathic-pain

[11] Bridin P Murnion. (2018). Neuropathic pain: current definition and review of drug treatment. *Aust Prescr 2018;41:60–3. npsmedicinewise*. URL: https://www.nps.org.au/australian-prescriber/articles/neuropathic-pain-current-definition-and-review-of-drug-treatment

[12] Tomer Yona. Classification of Peripheral Nerve Injury. *Physiopedia.com*. URL: https://www.physio-pedia.com/Classification_of_Peripheral_Nerve_Injury

[13] S.L. Carroll, S.H. Worley.(2017).Wallerian Degeneration. *Reference Module in Neuroscience and Biobehavioral Psychology.* pp 485-491

[14] Cristiana R. Carvalho1, Joaquim M. Oliveira and Rui L. Reis. (2019). Modern Trends for Peripheral Nerve Repair and Regeneration: Beyond the Hollow Nerve Guidance Conduit. *Front. Bioeng. Biotechnol.*

[15] Di Wu and Alexander K. Murashov. (2013). Molecular mechanisms of peripheral nerve regeneration: emerging roles of microRNAs. *Front. Physiol.*

[16] Papon Muangsanit.(2020).Aligned endothelial cell and Schwann cell structures in 3D hydrogels for peripheral nerve tissue engineering. *Thesis submitted to UCL*

[17] Introduction to Cell Culture. *thermofisher.com.* URL: https://www.thermofisher.com/uk/en/home/references/gibco-cell-culture-basics/introduction-to-cell-culture.html: :text=Cell%20culture%20refers%20to%20the, in%20a%20favorable%20artificial%20environment.text=A%20cell%20strain%20often %20acquires,initiation%20of%20the%20parent%20line

[18] R. Coy, G. Al-Badri, C.Kayal, C.O'Rourke, P. J. Kingham,J. B. Phillips and R. J. Shipley. (2020). Combining in silico and in vitro models to inform cell seeding strategies in tissue engineering.*J. R. Soc. Interface17: 20190801.*

[19] James B. Phillips. (2021). 'EngNT' — Engineering live neural tissue for nerve replacement. *Emerging Topics in Life Sciences 5 699–703*

[20] Melanie Georgiou, Stephen C.J. Bunting, Heather A. Davies, Alison J. Loughlin, Jonathan P. Golding, James B. Phillips. (2013). Engineered neural tissue for peripheral nerve repair. *Biomaterials 34 7335-7343*

[21] Papon Muangsanit, Adam Day, Savvas Dimiou, Altay Frederick Ataç, Céline Kayal, Hyeree Park, Showan N Nazhat and James B Phillips. (2020). Rapidly formed stable and aligned dense collagen gels seeded with Schwann cells support peripheral nerve regeneration. *J. Neural Eng. 17 046036*

[22] Umber Cheema and Robert A. Brown. (2012). Rapid Fabrication of Living Tissue Models by Collagen Plastic Compression: Understanding Three-Dimensional Cell Matrix Repair In Vitro. *ADVANCES IN WOUND CARE, VOLUME 2, NUMBER 4*

[23] Robert A Brown, M. Wiseman, Cher Bing Chuo, Umber Cheema, S.N. Nazhat. (2005). Ultrarapid Engineering of Biomimetic Materials and Tissues: Fabrication of Nano- and Microstructures by Plastic Compression. *Advanced Functional Materials 15(11)*

[24] Neysan O. Kamranpour, Amir K Miri, Mark James-Bhasin and Showan N Nazhat. (2016). A gel aspiration-ejection system for the controlled production and delivery of injectable dense collagen scaffolds. *Biofabrication 8 015018*

[25] Hyperelastic Materials. *SIMSCALE DOCUMENTATION.* URL: https://www.simscale.com/docs/simulation-setup/materials/hyperelastic-materials/: :text=Hyperelastic%20materials%20are%20the%20special,well%20as%20large %20shape%20changes.

[26] Rosso, G., Young, P., and Shahin, V. (2017). Implications of Schwann Cells Biomechanics and Mechanosensitivity for Peripheral Nervous System Physiology and Pathophysiology. *Front. Mol. Neurosci., 10:345*

[27] D I Wilson.(2017). What is rheology?.*Eye (Lond). 2018 Feb; 32(2): 179–183.*

[28] Suzette T. Lust, Catherine M. Shanahan, Rebecca J. Shipley, Pablo Lamata, Eileen Gentleman. (2021). Design considerations for engineering 3D models to study vascular pathologies in vitro. *ACTBIO 7210*

[29] Tanaya Walimbe and Alyssa Panitch.(2020). Best of Both Hydrogel Worlds: Harnessing Bioactivity and Tunability by Incorporating Glycosaminoglycans in Collagen Hydrogels. *Bioengineering 2020, 7(4), 156*

[30] Davide Ruffoni. (2020). Soft Tissues, Tendons and Ligaments. *'Biomechanics' at Liège University - Department of Aerospace and Mechanical engineering.* Chap2, slides 5-7

[31] Mesenchymal stem cell. *Wikipedia.com.* URL: https://en.wikipedia.org/wiki/Mesenchymal_stem_cell

[32] A. P. G. Castro, P. Laity, M. Shariatzadeh, C. Wittkowske, C. Holland, D. Lacroix. (2016). Combined numerical and experimental biomechanical characterization of soft collagen hydrogel substrate. *J Mater Sci: Mater Med (2016) 27:79*

[33] Grahame A. Busby, M. Helen Grant, Simon P. MacKay, Philip E. Riches. (2012). Confined compression of collagen hydrogels. *Journal of Biomechanics 46 (2013) 837–840*

[34] David M. Knapp, Victor H. Barocas, and Alice G. Moona, Kyeongah Yoo and Linda R. Petzold, Robert T. Tranquillob. (1997). Rheology of reconstituted type I collagen gel in confined compression. *The Society of Rheology, Inc. J. Rheol. 41[5], September/October 1997 0148-6055/97/41 5!/971/23/$10.00*

[35] Darrell Velegol and Frederick Lanni.(2001). Cell Traction Forces on Soft Biomaterials. I. Microrheology of Type I Collagen Gels. *Biophysical Journal Volume 81 September 2001 1786 –1792*

[36] Brooks A.Lane, Katrin A.Harmon, Richard L.Goodwin, Michael J.Yost, TarekShazly, John F.Eberth. (2018). Constitutive modeling of compressible type-I collagen hydrogels. *Medical Engineering Physics Volume 53, March 2018.* pp 39-48

[37] André P. G. Castro, Jiang Yao, Tom Battisti and Damien Lacroix. (2018). Poroelastic Modeling of Highly Hydrated Collagen Hydrogels: Experimental Results vs. Numerical Simulation With Custom and Commercial Finite Element Solvers. *Front. Bioeng. Biotechnol. 6:142.*

[38] Knapp DM, Barocas VH, Moon A, Yoo K, Petzold L, Tranquillo R.(1997). Rheology of reconstituted type I collagen gel in confined compression. *J Rheol (NY). 1997;41:971–93.*

[39] Hannah J. Levis, Alvena K. Kureshi, Isobel Massie, Louise Morgan, Amanda J. Vernon and Julie T. Daniels. (2015). Tissue Engineering the Cornea: The Evolution of RAFT. *J. Funct. Biomater. 2015, 6, 50-65*

[40] Frank Sauer, Linda Oswald, Angela Ariza de Schellenberger, Heiko Tzschätzsch, Felix Schrank, Tony Fischer, Jürgen Braun, Claudia T. Mierke, Rustem Valiullin, Ingolf Sack and Josef A. Käs. (2019). Collagen networks determine viscoelastic properties of connective tissues yet do not hinder diffusion of the aqueous solvent. *Soft Matter*

[41] Ensanya A. Abou Neel, Umber Cheema, Jonathan C. Knowles, Robert A. Brown and Showan N. Nazhat. (2006). Use of multiple unconfined compression for control of collagen gel scaffold density and mechanical properties. *Soft Matter*

[42] Vincent Rocher. (2019). Needle gauge table. *darwin-microfluidics.com*. URL: https://darwin-microfluidics.com/blogs/tools/syringe-needle-gauge-table

[43] Danielle Dresden.(2019). What to know about angioplasty. *MedicalNewsToday.com*. URL: https://www.medicalnewstoday.com/articles/327154

[44] Benedetto Marelli, Chiara E. Ghezzi, Mark James-Bhasin, Showan N. Nazhat. (2015). Fabrication of injectable, cellular, anisotropic collagen tissue equivalents with modular fibrillar densities. *Biomaterials 37 (2015) pp 183-193*

[45] Eleif.Photo measure. *eleif.net*. URL: https://eleif.net/photo_measure.html

[46] Rachel H. Coy , Owen R. Evans, James B. Phillips and Rebecca J. Shipley .(2018). An integrated theoretical-experimental approach to accelerate translational tissue engineering. *J Tissue Eng Regen Med 2018; 12: e53–e59*

[47] R. Coy, G. Al-Badri, C. Kayal, C. O'Rourke, P. J. Kingham, J. B. Phillips and R. J. Shipley. (2020).Combining in silico and in vitro models to inform cell seeding strategies in tissue engineering. *J. R. Soc. Interface.1720190801.20190801*

[48] Arnold Verruijt.(2016). Theory and problems of poroelasticity. *Delft University of Technology*

[49] Esther Reina-Romo, Sourav Mandal, Paulo Amorim, Veerle Bloemen, Eleonora Ferraris and Liesbet Geris. (2021). Towards the Experimentally-Informed In Silico Nozzle Design Optimization for Extrusion-Based Bioprinting of Shear-Thinning Hydrogels. *Front. Bioeng. Biotechnol. 9:701778. doi: 10.3389/fbioe.2021.701778*

[50] Faith A. Morrison. (2001). UNDERSTANDING RHEOLOGY. *OXFORD UNIVERSITY PRESS*

[51] Hans Petter Langtangen, Anders Logg.(2016). Solving PDEs in Python The FEniCS Tutorial I. *Simula SpringerBriefs on Computing*

[52] Anders Logg, Kent-Andre Mardal, Garth N. Well.(2010). Automated Solution of Differential Equations by the Finite Element Method, The FEniCS Book. *Springer, Mathematics Subject Classification: 65M60, 65N30, 65F08, 68N19, 74S05*

[53] TJeremy Bleyer.(2016). Numerical tours of continuum mechanics using FEniCS: Time-integration of elastodynamics equation. *Creative Commons Attribution-ShareAlike 4.0 International License* URL: https://comet-fenics.readthedocs.io/en/latest/demo/elastodynamics/demo_elastodynamics.py.html

[54] J.P. PONTHOT. (2021). Introductory Finite Element Method (FEM) course. *Lecture notes from Liège University course, LTAS - Aerospace Laboratory Computational Non Linear Mechanics*

[55] Welcome to ParaView.(2022). *Paraview website*, URL: https://www.paraview.org/

[56] Claudia Wittkowske, Gwendolen C. Reilly, Damien Lacroix, Cecile M. Perrault. (2016). In Vitro Bone Cell Models: Impact of Fluid Shear Stress on Bone Formation. *Front Bioeng Biotechnol. 2016 Nov 15;4:87. doi: 10.3389/fbioe.2016.00087. PMID: 27896266; PMCID: PMC5108781.*

[57] Pedersen, J. M., Shim, Y.-S., Hans, V., Phillips, M. B., Macdonald, J. M., Walker, G., et al. (2016). Fluid Dynamic Modeling to Support the Development of FlowBased Hepatocyte Culture Systems for Metabolism Studies. *Front. Bioeng. Biotechnol. 4, 72. doi:10.3389/fbioe.2016.00072*

[58] Silvani, G., Romanov, V., Cox, C. D., and Martinac, B. (2021). Biomechanical Characterization of Endothelial Cells Exposed to Shear Stress Using Acoustic Force Spectroscopy. *Front. Bioeng. Biotechnol. 9, 21. doi:10.3389/fbioe.2021.612151*

[59] Lamé constants. Encyclopedia of Mathematics. URL: http://encyclopediaofmath.org/index.php?title=Lam%C3%A9_constantsoldid=42630

[60] George B.Arfken, David F.Griffing, Donald C.Kelly and Joseph Priest. (1984). Chapter 16 - FLUID MECHANICS. *International Edition University Physics, 1984, pp 306-325*

[61] C.M.Allen, E.Drauglis. (1969). Boundary layer lubrication: monolayer or multilayer. *Wear Volume 14, Issue 5, pp363-384*

[62] O Bäumchen, Karin Jacobs. (2010). Slip effects in polymer thin films. *Journal of Physics Condensed Matter 22(3):033102* DOI:10.1088/0953-8984/22/3/033102

[63] Votta Emiliano. (2021). Advanced modeling approaches for cardiovascular surgery. *Lecture support material. Politecnico di Milano*

[64] (2022).FEM for Two-Dimensional Solids (Finite Element Method) Part 1. *what-when-how.com* URL: http://what-when-how.com/the-finite-element-method/fem-for-two-dimensional-solids-finite-element-method-part-1/

[65] Ajay Harish. (2020). Implicit vs Explicit Finite Element Method (FEM): What Is the Difference?. *Simscale blog.* URL:https://www.simscale.com/blog/2019/01/implicit-vs-explicit-fem/

[66] Ajay Harish. (2020).Finite Element Method – What Is It? FEM and FEA Explained. *Simscale blog.* URL: https://www.simscale.com/blog/2016/10/what-is-finite-element-method/

[67] King H. Yang. (2018). Modal and Transient Dynamic Analysis. *Basic Finite Element Method as Applied to Injury Biomechanics*

[68] (2022).Explicit and implicit methods. *Wikipedia.com.* URL: https://en.wikipedia.org/wiki/Explicit_and_implicit_methods

[69] Łukasz Skotny. (2019).Difference Between Implicit vs Explicit Analysis. *enterfea blog.* URL: https://enterfea.com/implicit-vs-explicit/

[70] Christine Obbink-Huizer.(2021). Implicit vs explicit finite element analysis: when to use which?. *Simuleon FEA Blog.* URL: https://info.simuleon.com/blog/implicit-vs-explicit-finite-element-analysis

[71] Di Miao.(2018).Camparison of Newmark-beta method and Generalized-alpha method. *PhD candidate in Computational Mechanics website- Orem UT* URL: https://miaodi.github.io/finite%20element%20method/newmark-generalized/

[72] (2022). BDF, Generalized Alpha, and Runge-Kutta Methods.*Comsol.com.* URL: https://www.comsol.com/support/knowledgebase/1062

[73] Hoss Belyadi, Ebrahim Fathi and Fatemeh Belyadi. (2019). Chapter Thirteen - Rock mechanical properties and in situ stresses. *Hydraulic Fracturing in Unconventional Reservoirs (Second Edition) Theories, Operations, and Economic Analysis, pp 215-231*

[74] (2022).Principal Stresses Strains. *continuummechanics.org.* URL: https://www.continuummechanics.org/principalstressesandstrains.html

[75] Huiquan Jiang, Yun Qian, Cunyi Fan and Yuanming Ouyang.(2020). Polymeric Guide Conduits for Peripheral Nerve Tissue Engineering. *Front. Bioeng. Biotechnol.* DOI: https://doi.org/10.3389/fbioe.2020.582646

[76] Ajay Harish. (2020). What is Convergence in Finite Element Analysis?. *Simscale.come.* URL: https://www.simscale.com/blog/2017/01/convergence-finite-element-analysis/

Appendix A

Introduction on Peripheral Nerve Repair

A.1 Five steps of the nerve regeneration in the hollow NGC

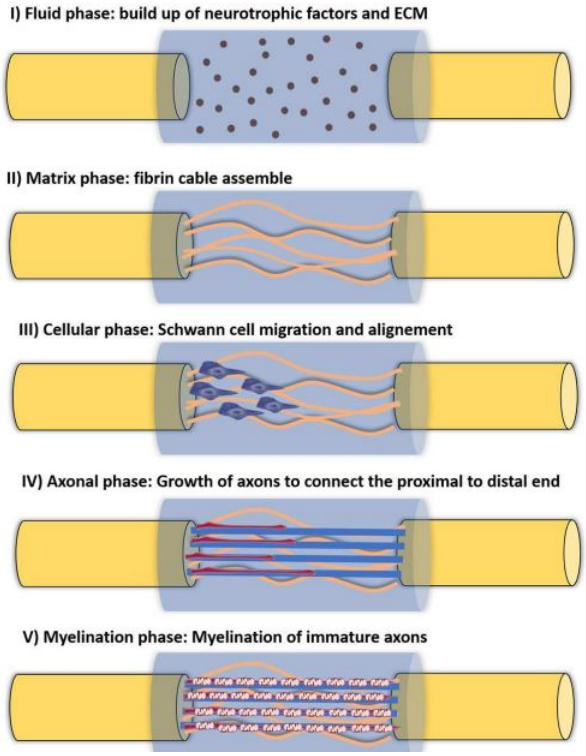

A.2 Peripheral nerve injury process

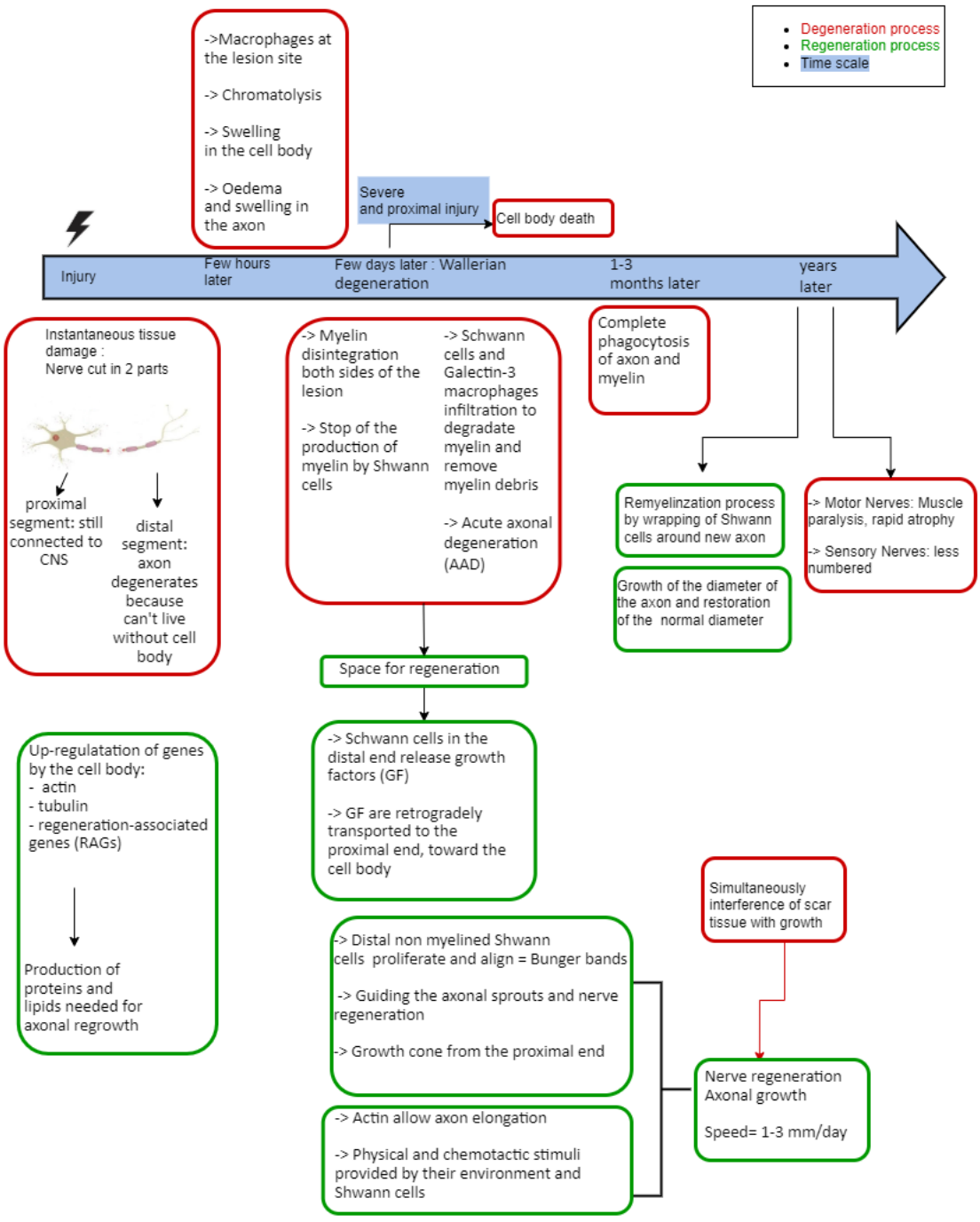

Appendix B

Reported properties of the GAE-EngNT construct

B.1 Length of GAE-EngNT constructs

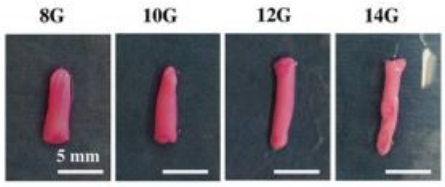

B.2 Collagen Fiber Density of GAE-EngNT construct

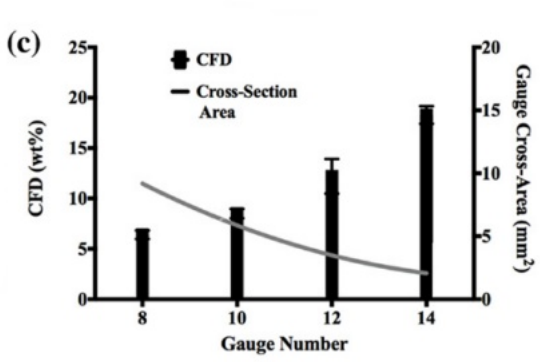

Appendix C

Construct density computation: Matlab code

```
%% ------------------------------------------------------------------------%
% Master thesis - Mathematical model of GAE method
% Academic year 2021-2022
% Authors: Estelle Pitti
% Volume fold and contruct density computation
%   Volume folds computation which is the ratio between the initial and
%   final volume after the GAE process
%   Density computation based on the collagen concentration and CFD
%% ------------------------------------------------------------------------%

clear all
close all
clc

%%% Volume folds
% Initial volumes
Vi_canada=1.5E+3;
Vi_UCL = 1E+3;

% Geometry properties of the construct for different needle sizes
length = [8 8.75 9.58 10.33 12];
diameters= [3.429 2.692 2.159 1.6 1.194];
areas = pi.* (diameters/2).^2;
Vf = areas.* length;

% Volume fold computation
for i= 1:5
```

```
27      if i<5
28          folds(i) =  Vi_canada/Vf(i);
29      else
30          folds(i) =  Vi_UCL/Vf(i);
31      end
32  end
33  Vf
34  folds
35
36  %%% Density of the construct
37
38  % Initial collagen density
39  Collagen_c_initial = 3; %4.5*75%
40
41  % Final collagen density
42  Collagen_c_final = zeros(1,5);
43  Collagen_c_final(1)=Collagen_c_initial;
44  Collagen_c_final(2:5)= folds(1:4)*Collagen_c_initial;
45
46  % Density of the construct
47  CFD = [0.8 6 8 12.5 18];
48  Density_gel = 100*Collagen_c_final./CFD;
49  Density_gel
```

Appendix D

Young's modulus parameter identification

D.1 Stress-strain curves data

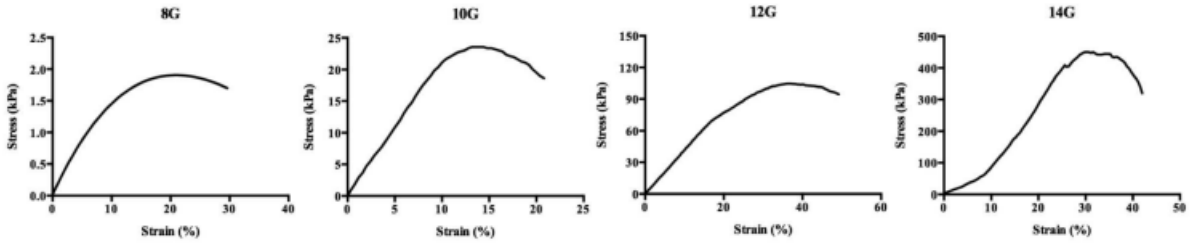

D.2 Data extraction matlab code

```
%% ------------------------------------------------------------------------%
% Master thesis - Mathematical model of GAE method
% Academic year 2021-2022
% Authors: Marco Stevanella
% Data extraction
%   Extraction of the data from a graph in a picture
%   Converting into a matlab plot generating a x and y data vector
%% ------------------------------------------------------------------------%

clear all;
close all;
```

```
12 [filename, pathname] = uigetfile('*.jpg','Select the image file:
       ');
13 nomefile=strcat(pathname,filename);
14 image=imread(nomefile);
15 hfig=figure;
16 him=imshow(image,[]);
17 hsp=imscrollpanel(hfig,him);
18 apisp=iptgetapi(hsp);
19 h=msgbox('Select the origin of the reference frame');
20 waitfor(h);
21 [x0,y0,P0] = impixel;
22 prompt={'X-value at the origin:','Y-value at the origin:'};
23 titolo='Origin XY coordinates';
24 numlines=1;
25 defaultanswer={'1','0'};
26 answer=inputdlg(prompt,titolo,numlines,defaultanswer);
27 x0value=str2double(cell2mat(answer(1,1)));
28 y0value=str2double(cell2mat(answer(2,1)));
29 h=msgbox('Select the last tick mark on the x-axis');
30 waitfor(h);
31 [x1,y1,P1] = impixel;
32 prompt={'What is the value on the last tick mark on the x-axis?'
       };
33 titolo='X-range extent';
34 numlines=1;
35 defaultanswer={'0'};
36 answer=inputdlg(prompt,titolo,numlines,defaultanswer);
37 deltax=str2double(cell2mat(answer(1,1)));
38 h=msgbox('Select the last tick mark on the y-axis');
39 waitfor(h);
40 [x2,y2,P2] = impixel;
41 prompt={'What is the value on the last tick mark on the y-axis?'
       };
42 titolo='Y-range extent';
43 numlines=1;
44 defaultanswer={'0'};
45 answer=inputdlg(prompt,titolo,numlines,defaultanswer);
46 deltay=str2double(cell2mat(answer(1,1)));
47 h=msgbox('Select points on the relevant plot');
48 waitfor(h);
49 [xi,yi,Pi] = impixel;
50 % translate pixel coordinates
51 xn=xi-x0;
52 yn=y0-yi;
53 % rotate pixel coordinates
54 m1=(y1-y0)/(x1-x0);
55 m2=(x2-x0)/(y0-y2);
56 xrot=xn-yn*m1;
```

```
yrot=yn+xn*m2;
% from pixels to axes' scales
x=xrot.*((deltax-x0value)/(sqrt((x1-x0)^2+(y1-y0)^2)));
y=yrot.*((deltay-y0value)/(sqrt((x2-x0)^2+(y2-y0)^2)));
% account for the fact that the origin may be not at (0,0)
x=x+x0value;
y=y+y0value;
close all;
figure;
hold on;
plot(x,y,'.b');
set(gca,'xlim',[x0value deltax],'ylim',[y0value deltay]);
t=linspace(min(x),max(x),100);
p=pchip(x,y,t);
plot(t,p,'-r');

Data=table(x,y);
filename='Stress_strain_curves.xlsx';
writetable(Data,filename,'Sheet','14G');
```

D.3 Matlab code for the Young's modulus data extraction

```
%%-------------------------------------------------------------------------%

% Master thesis - Mathematical model of GAE method
% Academic year 2021-2022
% Authors: Estelle Pitti
% Young's modulus computation
%   Isolating the linear part by observation of the entire stress-strain
%   curve
%   Linear interpolation
%   Computation of the slope of the interpolated line
%   Save the data in the excel file where the x and y data from the
%   stress-strain curves were stored after extraction
%   Plot of the Young's modulus obtained and the diameter of the needle
%   Find the best fit for the curve
%   Extract the Young's modulus value for 16G
%%-------------------------------------------------------------------------%


```

```
%%% Isolating the linear part
% Limit values for 8G, 10G, 12G, 14G and 16G
values_up = [10 12 30 30 55];
values_down = [0 0 0 10 15];
limit_linear_up = values_up(4);
limit_linear_down = values_down(4);
j=1;
for i=1:length(x)
    if x(i)<limit_linear_up && x(i)>limit_linear_down
        X_elastic(j)=x(i);
        Y_elastic(j)=y(i);
        j=j+1;
    end
end

%%% Linear interpolation
% Fiting the data with a polynom of first order
p=polyfit(X_elastic,Y_elastic,1);
% Computing the slope
b = p(1);
% Finding the interpolated line
yCalc1 = b.*X_elastic+ p(2);
figure(2)
scatter(X_elastic,Y_elastic)
grid on
hold on
plot(X_elastic,yCalc1)
xlabel('Strain [%]')
ylabel('Stress [kPa]')
title('Linear part of the stress-strain curve 8G needle')
legend('Data','Linear regression')

%%% Save the result in the excel file
filename='Stress_strain_curves.xlsx';
xlswrite(filename, 'b', '14G', 'C1');
xlswrite(filename, b, '14G', 'C2');

%%% Interpolation for the 16G
% Young's modulus and diameters for 8G to 14G
E= [0.14E+3, 2.06E+3, 3.6E+3, 2E+4];
Di= [3.429E-3, 2.692E-3, 2.159E-3, 1.6E-3];
figure()
hold on
plot(Di, E)

% Fiting the curve with a polynome of second order (best by
    observation)
p=polyfit(Di,E,2);
```

```
64 E_interp= p(1)*Di.^2+p(2)*Di+p(3);
65 plot(Di, E_interp)
66
67 %Extraction of the Young's modulus value for 16G
68 Di_16G=1.194E-3;
69 E_16G = p(1)*Di_16G^2+p(2)*Di_16G+p(3)
```

D.4 Interpolation for the 16G Young's modulus

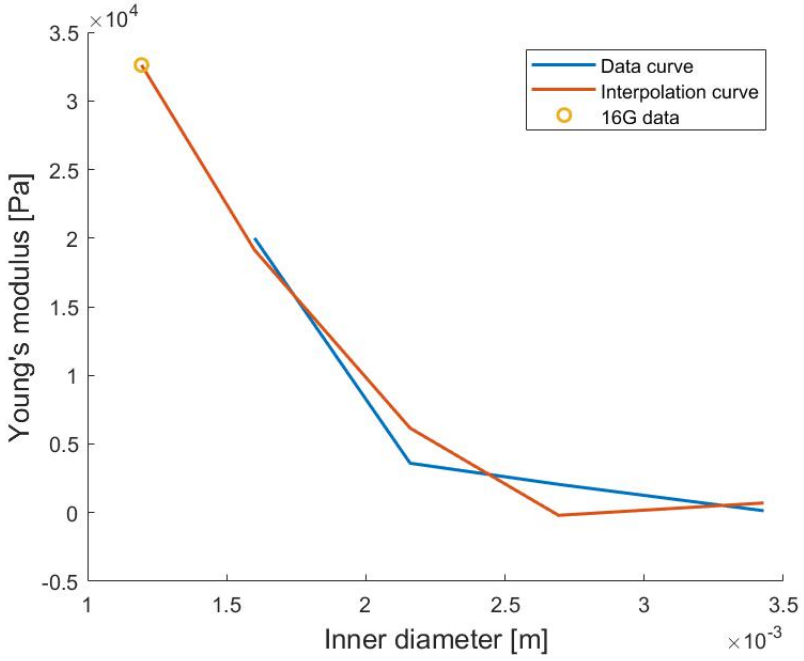

Appendix E

Plastic Compression primary model in FEniCS

The model represented in figure E.1, aim at representing the collagen gel in a 48 well-plate which is used as a mould for for the PC. The geometry is therefore cylindrical in 3D and rectangular in 2D initiating the asymmetry problem. A compression stress is applied on the top boundary. The theoretical framework of the model is statics solid mechanics looking at the instantaneous deformation of the material by applying the stress and constrains. However, in order to add some complexity, the applied stress is defined linearly increasing with time as it can be seen in figure E.2. Therefore, the outcome is obtained by successive static mechanics resolution with a value of the applied stress given a higher value at each new static resolution. A 2D and 3D model is computed in a confined or unconfined material condition.
The equations of static solid mechanics considering a linear elastic material are given as follow [51]:

$$-\nabla \cdot \sigma = f \tag{E.1}$$

$$\sigma = \lambda \ \ trc(\epsilon) \ \ \mathbf{I} + 2\mu\epsilon \tag{E.2}$$

$$\epsilon = \frac{1}{2}(\nabla u + (\nabla u)^T) \tag{E.3}$$

Beforehand, a 1D analytical resolution has been computed as well as the system of equation in terms of the unknown variable $\mathbf{u} = (u_x, u_y)$. Before, generating the set of results for the model, the convergence was performed finding the minimum mesh size for convergent

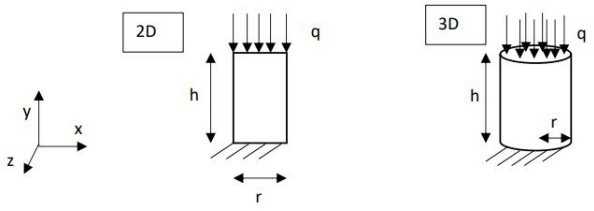

Figure E.1: Primary model for the PC method

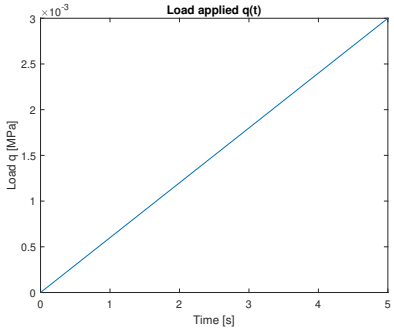

Figure E.2: Linearly increasing applied stress

results. Afterwards, the 2D and 3D models has been run for the confined and unconfined boundary conditions. The overall amplitude and field of deformation distribution in the material can be observed over time, also looking at the time evolution of the deformation at specific nodes of the mesh. A graph of the displacement over the load can also be obtained. In addition, the stress distribution over the material can be observed for the 4 components of the stress tensor. The stress-strain curve at different nodes can also be derived. Another interesting feature to compute is the principal stress values. Concerning the 3D model in the confined case, the results obtained were faulty as a coarse mesh was used in order to work at a low computation time. Obviously, this model is not representative enough of the PC model to be exposed entirely in the next chapter. Naturally, the PC method doesn't have a linearly increasing applied load, the hyper hydrated gel is not linear elastic and the targeted deformations are plastic. The aim of this primary model was to train building a model from scratch targeting the PC framework.

Appendix F

Dynamic problem: FEniCS code

```
# cd ../../mnt/c/Users/User/Documents
# python3 GAE_elastodynamics.py

from __future__ import print_function
from fenics import *
from dolfin import *
import numpy as np
import time
import csv
import math


# Spacial and temporal convergence assessment
# for count_conv in range(10):
    # print(count_conv)

# Start of time measure
time0 = time.time()

# Form compiler options
parameters["form_compiler"]["cpp_optimize"] = True
parameters["form_compiler"]["optimize"] = True

# Parameters of the model:
Diameter = [3.429E-3, 2.692E-3, 2.159E-3, 1.6E-3, 1.194E-3] # Diameter of the construct for 8G,10G,12G,14G and 16G [m]
Length = [8E-3, 8.75E-3, 9.58E-3, 10.33E-3, 12E-3]          # Length of the construct for 8G,10G,12G,14G and 16G [m]
nx = 150    #10+20*count_conv                                # Number of elements in the mesh on the x-direction [-]
ny =150     #10+20*count_conv                                # Number of elements in the mesh on the y-direction [-]
rho = Constant(1.1E+3)                                       # Mass density [kg/m^3]
```

```
30 Modulus = [0.14E+3, 2.06E+3, 3.6E+3, 2E+4, 3.26E+4]          #
       Young's modulus [Pa]
31 nu = 0.3                                                      #
       Poisson's ratio [-]
32 eta_GAE = 0.2                                                 #
       Viscous damping coefficient [0-1]
33 eta_lu = 6E+4                                                 #
       Viscosity of the lubrification layer [Pa.s]
34 T        = 270.                                               #
       Duration of the GAE process- Maximum time of the simulation [
       s]
35 Nsteps   = 100    #5+20*count_conv                            #
       Number of time steps [-]
36 p0 = 5E+3                                                     #
       Applied aspiration pressure [Pa]
37 alpha_m = Constant(0.2)                                       #
       Generalized-alpha parameter for the update formula of u
38 alpha_f = Constant(0.4)                                       #
       Generalized-alpha parameter for the update formula of v,a and
        p
39 Cv = 5.5E+6                                                   #
       Damping coefficient for the fluid friction dissipation [N.s/m
       ^3]
40
41 # Mesh Definition
42 Di = Diameter[4]
43 Aire= (Di/2)**2*math.pi
44 l = Length[4]
45 mesh = RectangleMesh(Point(0,0), Point(Di, l), nx, ny)
46
47 # Elastic parameters computation
48 E = Modulus[4]
49 mu     = Constant(E / (2.0*(1.0 + nu)))
50 lmbda = Constant(E*nu / ((1.0 + nu)*(1.0 - 2.0*nu)))
51
52 # Time-stepping parameter
53 dt = Constant(T/Nsteps)
54
55 # Stress application as Neumann conditions
56 p = Constant((0,p0)) # Pressure applied on the top of the
       construct
57 pb = Constant((0,0)) # Pressure applied on the bottom of the
       construct
58 print('h:', eta_lu/Cv) # lubrification layer width [m]
59
60 # Generalized-alpha parameters definition
61 gamma    = Constant(0.5+alpha_f-alpha_m)
62 beta     = Constant((gamma+0.5)**2/4.)
```

```
63
64 # Define function spaces
65 V = VectorFunctionSpace(mesh, "P", 1) # Define function space
       for displacement, velocity and acceleration
66 Vsig = TensorFunctionSpace(mesh, "P", 1) # Define function space
       for tensor of stresses and strains
67 V_bis = FunctionSpace(mesh, 'P', 1) # Define function space for
       principal stress values
68
69 # Define functions
70 du = TrialFunction(V)# Trial function
71 u_ = TestFunction(V) # Test function
72 u = Function(V, name="Displacement") # Current (unknown)
       displacement
73 # Fields from previous time step (displacement, velocity,
       acceleration)
74 u_old = Function(V)
75 v_old = Function(V)
76 a_old = Function(V)
77
78 # Definition of the BC domain
79 def walls(x, on_boundary):
80     return on_boundary and near(x[0], 0.) or near(x[0], Di)
81
82 def top(x, on_boundary):
83     return near(x[1], l) and on_boundary
84
85 def bottom(x, on_boundary):
86     return near(x[1], 0) and on_boundary
87
88 # Create mesh function over the cell facets
89 boundary_subdomains = MeshFunction("size_t", mesh, mesh.topology
       ().dim() - 1)
90 boundary_subdomains.set_all(0)
91 force_t_boundary = AutoSubDomain(top)
92 force_t_boundary.mark(boundary_subdomains, 1)
93 force_w_boundary = AutoSubDomain(walls)
94 force_w_boundary.mark(boundary_subdomains, 2)
95 force_w_boundary = AutoSubDomain(bottom)
96 force_w_boundary.mark(boundary_subdomains, 3)
97 # Define measure tool for boundary condition integrals
98 dss = ds(subdomain_data=boundary_subdomains)
99 # Set up Dirichlet boundary conditions
100 zero = Constant(0.0)
101 bc = DirichletBC(V.sub(0), zero, walls)
102
103 # Definition of each term of the equation
104 def sigma(u,v):
```

```
105     return 2.0*mu*sym(grad(u)) + (lmbda*tr(grad(u))+ eta_GAE*tr(
            grad(v)))*Identity(len(u))
106
107 def epsilon(u):
108     return 0.5*(nabla_grad(u) + nabla_grad(u).T)
109
110 def sigma_principal_max(sigma_x, sigma_y, tau_xy):
111     return((sigma_x+sigma_y)/2 + sqrt(((sigma_x-sigma_y)/2)**2 +
            tau_xy**2))
112
113 def orientation(sigma_x, sigma_y, tau_xy):
114     return atan(2*tau_xy/(sigma_x-sigma_y))/2
115
116 def m(u, u_):
117     return rho*inner(u, u_)*dx
118
119 def k(u, v, u_):
120     return inner(sigma(u,v), sym(grad(u_)))*dx
121
122 def c(v, u_):
123     return (Cv*inner(v, u_))*dss(2)
124
125 def Wext(u_):
126     return dot(u_, p)*dss(1) + dot(u_, pb)*dss(3)
127
128 # Update formula for displacement, velocity and acceleration at
        the end of each time step
129 # Update formula for acceleration
130 # a = 1/(2*beta)*((u - u0 - v0*dt)/(0.5*dt*dt) - (1-2*beta)*a0)
131 def update_a(u, u_old, v_old, a_old, ufl=True):
132     if ufl:
133         dt_ = dt
134         beta_ = beta
135     else:
136         dt_ = float(dt)
137         beta_ = float(beta)
138     return (u-u_old-dt_*v_old)/beta_/dt_**2 - (1-2*beta_)/2/
            beta_*a_old
139
140 # Update formula for velocity
141 # v = dt * ((1-gamma)*a0 + gamma*a) + v0
142 def update_v(a, u_old, v_old, a_old, ufl=True):
143     if ufl:
144         dt_ = dt
145         gamma_ = gamma
146     else:
147         dt_ = float(dt)
148         gamma_ = float(gamma)
```

```
149     return v_old + dt_*((1-gamma_)*a_old + gamma_*a)
150
151 def update_fields(u, u_old, v_old, a_old):
152
153     # Get vectors (references)
154     u_vec, u0_vec  = u.vector(), u_old.vector()
155     v0_vec, a0_vec = v_old.vector(), a_old.vector()
156
157     # use update functions using vector arguments
158     a_vec = update_a(u_vec, u0_vec, v0_vec, a0_vec, ufl=False)
159     v_vec = update_v(a_vec, u0_vec, v0_vec, a0_vec, ufl=False)
160
161     # Update (u_old <- u)
162     v_old.vector()[:], a_old.vector()[:] = v_vec, a_vec
163     u_old.vector()[:] = u.vector()
164
165
166 def avg(x_old, x_new, alpha):
167     return alpha*x_old + (1-alpha)*x_new
168
169 # Solving
170 # Residual
171 a_new = update_a(du, u_old, v_old, a_old, ufl=True)
172 v_new = update_v(a_new, u_old, v_old, a_old, ufl=True)
173 res = m(avg(a_old, a_new, alpha_m), u_)+ c(avg(v_old, v_new,
       alpha_f), u_,) + k(avg(u_old, du, alpha_f), avg(v_old, v_new,
        alpha_f), u_,) - Wext(u_)
174 a_form = lhs(res)
175 L_form = rhs(res)
176 # Define solver for reusing factorisation
177 K, res = assemble_system(a_form, L_form, bc)
178 solver = LUSolver(K, "mumps")
179 solver.parameters["symmetric"] = True
180
181 # Time-stepping
182 time_code = np.linspace(0, T, Nsteps+1)
183
184 # Generation of the results
185 u_top = np.zeros((Nsteps+1,))
186 u_bottom = np.zeros((Nsteps+1,))
187 energies = np.zeros((Nsteps+1, 5))
188 t_record = np.zeros((Nsteps+1,))
189 E_damp = 0
190 E_ext = 0
191 sig = Function(Vsig, name="sigma")
192 epsi = Function(Vsig, name="epsilon")
193 p_stress = Function(V_bis, name="principal stress")
194 ori = Function(V_bis, name="orientation p_stress")
```

```
195 p_field_x = Function(V_bis, name="p_field_x")
196 p_field_y = Function(V_bis, name="p_field_y")
197 p_field_z = Function(V_bis, name="p_field_z")
198 xdmf_file = XDMFFile("GAE_elastodynamics-results.xdmf")
199 xdmf_file.parameters["flush_output"] = True
200 xdmf_file.parameters["functions_share_mesh"] = True
201 xdmf_file.parameters["rewrite_function_mesh"] = False
202
203
204 def local_project(v, V, u=None):
205
206     #Element-wise projection using LocalSolver
207     dv = TrialFunction(V)
208     v_ = TestFunction(V)
209     a_proj = inner(dv, v_)*dx
210     b_proj = inner(v, v_)*dx
211     solver = LocalSolver(a_proj, b_proj)
212     solver.factorize()
213     if u is None:
214         u = Function(V)
215         solver.solve_local_rhs(u)
216         return u
217     else:
218         solver.solve_local_rhs(u)
219         return
220
221 for (i, dt) in enumerate(np.diff(time_code)):
222
223     t = time_code[i+1]
224     print("Time: ", t)
225     t_record[i+1]=t
226
227     # Solve for new displacement
228     res = assemble(L_form)
229     bc.apply(res)
230     solver.solve(K, u.vector(), res)
231
232     E_ext += assemble(Wext(u-u_old))
233
234     # Update old fields with new quantities
235     update_fields(u, u_old, v_old, a_old)
236
237     # Save solution u to XDMF format
238     xdmf_file.write(u, t)
239
240     # Compute stress tensor and save to XDMF format
241     local_project(sigma(u,v_old), Vsig, sig)
242     xdmf_file.write(sig, t)
```

```
243
244         # Compute strain tensor and save to XDMF format
245         local_project(epsilon(u), Vsig, epsi)
246         xdmf_file.write(epsi, t)
247
248         # Compute major principal stress and save to XDMF format
249         [s11, s12, s21, s22] = sig.split(True)
250         local_project(sigma_principal_max(sig[0,0], sig[1,1], sig
                [0,1]), V_bis, p_stress)
251         xdmf_file.write(p_stress, t)
252         local_project(orientation(s11, s22, s12), V_bis, ori)
253         xdmf_file.write(ori, t)
254
255         # Compute 3 components of the major principal stress field
                and save to XDMF format
256         local_project(cos(orientation(s11, s22, s12))*
                sigma_principal_max(s11, s22, s12),V_bis, p_field_x)
257         xdmf_file.write(p_field_x, t)
258         local_project(sin(orientation(s11, s22, s12))*
                sigma_principal_max(s11, s22, s12),V_bis, p_field_y)
259         xdmf_file.write(p_field_y, t)
260         local_project(Constant(0),V_bis, p_field_z)
261         xdmf_file.write(p_field_z, t)
262
263         # Compute difference between top surface displacement and
                bottom surface displacement
264         u_top[i+1] = u(Di/2, l)[1]
265         u_bottom[i+1] = u(Di/2,0.)[1]
266
267         # Compute enery balance components
268         E_elas = assemble(0.5*k(u_old, v_old, u_old))
269         E_kin = assemble(0.5*m(v_old, v_old))
270         E_damp += dt*assemble(c(v_old, v_old))
271         E_tot = E_elas+E_kin+ E_damp -E_ext
272         energies[i+1, :] = np.array([E_elas, E_kin, E_damp, E_ext,
                E_tot])
273
274
275 # Mesh refinement: total number of element in the mesh
276 Nbe= Nsteps  #nx*ny
277
278 # CPU time evaluation
279 time1=time.time()
280 CPU= time1-time0
281 print('CPU time:', CPU)
282
283 # Average u_y value at the last time step
284 print('avg uy:', np.mean(u.vector()[1]))
```

```
285 u_avg=np.mean(u.vector()[1])
286
287 # Maximum u_y value at the last time step
288 print('max uy:', np.amax(u.vector()[1]))
289 u_max=np.amax(u.vector()[1])
290
291 # Maximum major principal stress at the last time step
292 print('max major principal stress:',
293           p_stress.vector().max())
294 p_stress_max=p_stress.vector().max()
295
296 # Maximum shear stress at the last time step
297 print('max shear stress:',
298           s12.vector().max())
299 shear_stress_max=s12.vector().max()
300
301 # Maximum of the difference between the vertical displacement of
      the top and the bottom surface at the middle point
302 print('max diff uy:',
303             np.amax(u_top-u_bottom))
304
305 u_diff_max=np.amax(u_top-u_bottom)
306
307
308
309 # Export data in excel to assess the convergence
310 # data_header = ['Nx','Ny','Nb_t','CPU_time', 'Tot_eng', '
      max_principal_stress']
311 # data = [{'Nx': nx, 'Ny': ny, 'Nb_t': Nbe ,'CPU_time': CPU, '
      Tot_eng':energies[Nsteps, 4] ,'max_principal_stress':
      p_stress.vector().max()}]
312
313 # name = 'convergence_t_%d.csv' % count_conv
314 # print(name)
315 # with open(name, 'w') as file_writer:
316     # dict_writer = csv.DictWriter(file_writer, data_header)
317
318     # dict_writer.writeheader()
319     # for item in data:
320         # dict_writer.writerow(item)
321
322
323 # Extract data for energy balance and difference of displacement
      between the top and the bottom surface over time
324 file= open('visc_adapt.csv', 'w')
325 dict_writer = csv.writer(file)
326
327 for w in range(Nsteps):
```

```
328         dict_writer.writerow([t_record[w], energies[w, 0], energies
                [w, 1], energies[w, 2], energies[w, 3], energies[w, 4],
                u_top[w], u_bottom[w]])
329
330 file.close()
```

Appendix G

Spacial and temporal convergence: Matlab code

```
%% ------------------------------------------------------------------------%
% Master thesis - Mathematical model of GAE method
% Academic year 2021-2022
% Authors: Estelle Pitti
% Spacial and temporal convergence data
%   Extraction of the excel data obtained by the FEniCS simulations
%   Ploting the main properties of the model and the CPU time in function
%   of the number of elements or of time steps
%% ------------------------------------------------------------------------%


clear all
close all
clc

% Space convergence
for i=1:10
    filename=sprintf('convergence_%d.csv',i-1);
    conv=readtable(filename);
    Nbe(i)=conv.Nb_elements;
    CPU(i)=conv.CPU_time;
    tot_eng(i)=conv.Tot_eng;
    stress(i)=conv.max_principal_stress;
end
figure()
subplot(1,3,1)
plot(Nbe,stress, 'LineWidth',1.5)
grid on
```

```
28 xlabel('Number of elements', 'FontSize',13)
29 ylabel('Maximum principal stress [Pa]', 'FontSize',13)
30 subplot(1,3,2)
31 plot(Nbe,tot_eng, 'LineWidth',1.5)
32 grid on
33 xlabel('Number of elements', 'FontSize',13)
34 ylabel('Total energy in the system [J]', 'FontSize',13)
35 subplot(1,3,3)
36 plot(Nbe,CPU, 'LineWidth',1.5)
37 grid on
38 ylabel('CPU time [s]', 'FontSize',13)
39 xlabel('Number of elements', 'FontSize',13)
40
41 % Time convergence
42 for i=1:10
43     filename=sprintf('convergence_t_%d.csv',i-1);
44     conv=readtable(filename);
45     Nbe(i)=conv.Nb_t;
46     CPU(i)=conv.CPU_time;
47     tot_eng(i)=conv.Tot_eng;
48     stress(i)=conv.max_principal_stress;
49 end
50 figure()
51 subplot(1,3,1)
52 plot(Nbe,stress, 'LineWidth',1.5)
53 grid on
54 xlabel('Number of time steps', 'FontSize',13)
55 ylabel('Maximum principal stress [Pa]', 'FontSize',13)
56 subplot(1,3,2)
57 plot(Nbe,tot_eng, 'LineWidth',1.5)
58 grid on
59 xlabel('Number of time steps', 'FontSize',13)
60 ylabel('Total energy in the system [J]', 'FontSize',13)
61 subplot(1,3,3)
62 plot(Nbe,CPU, 'LineWidth',1.5)
63 grid on
64 ylabel('CPU time [s]', 'FontSize',13)
65 xlabel('Number of time steps', 'FontSize',13)
```

Appendix H

Post-processing using Matlab to generate the model results

H.1 Energy balance and difference of top and bottom vertical displacement

```
%% ------------------------------------------------------------------------%
% Master thesis - Mathematical model of GAE method
% Academic year 2021-2022
% Authors: Estelle Pitti
% Energy balance plot over time
% Difference of displacement between the top and the
% bottom part of the construct at the middle point plot over
    time
%
%% ------------------------------------------------------------------------%


clear all
close all
clc

%%% Energy balance computation
filename='visc_adapt.csv';
conv=readtable(filename);
Time= conv.Var1;
E_elas= conv.Var2;
E_kin = conv.Var3;
E_damp = conv.Var4;
E_ext = conv.Var5;
E_tot = conv.Var6;
figure()
```

```
hold on
plot(Time,E_elas, 'LineWidth',1.5)
plot(Time,E_kin, 'LineWidth',1.5)
plot(Time,E_damp, 'LineWidth',1.5)
plot(Time,E_ext, 'LineWidth',1.5)
plot(Time,E_tot, 'LineWidth',1.5)
xlabel('Time [s]', 'FontSize',12)
ylabel('Energies [J]', 'FontSize',12)
legend('Elastic energy','Kinetic energy','Damping energy', '
    External energy','Total energy')

%%% Difference of displacement computation
u_top = conv.Var7;
u_bottom = conv.Var8;
figure()
plot(Time, u_top-u_bottom, 'LineWidth',1.5)
xlabel('Time [s]', 'FontSize',12)
ylabel('u\_top - u\_bottom [m]', 'FontSize',12)
```

H.2 Aspiration pressure and viscous coefficient double Y plot generation

```
%% ------------------------------------------------------------------------%

% Master thesis - Mathematical model of GAE method
% Academic year 2021-2022
% Authors: Estelle Pitti
% Double Y axis graph of the aspiration pressure and viscous
    coefficient to
% garantee the minimum success of the aspiration without elastic
    rupture
%
%% ------------------------------------------------------------------------%


close all
clear all
clc

Needle_gauge_nb = [8 10 12 14 16];
p0 = [10, 2E+2, 3E+2, 2E+3, 5E+3 ];
Cv = [7E+4, 1E+6, 1E+6, 4E+6, 5.5E+6 ];
h= [0.8, 0.06, 0.06, 0.015, 0.011];
du = [0.2E-3, 0.3E-3, 0.3E-3,0.3E-3, 0.7E-3 ];
```

```
yyaxis right
plot(Needle_gauge_nb, Cv,'-o', 'LineWidth',1.5)
grid on
ylabel('Viscous coefficient [Pa.s/m]', 'FontSize',12)
yyaxis left
plot(Needle_gauge_nb, p0,'-o', 'LineWidth',1.5)
ylabel('Applied aspiration pressure [Pa]', 'FontSize',12)
xlabel('Needle gauge number')
```

H.3 Maximum shear stress and major principal stress for different needle gauge numbers

```
%% ------------------------------------------------------------------------%

% Master thesis - Mathematical model of GAE method
% Academic year 2021-2022
% Authors: Estelle Pitti
% Maximum shear stress and major principal stress for different needle
% gauge numbers
%
%% ------------------------------------------------------------------------%


clear all
close all
clc

Needle_gauge_nb = [8 10 12 14 16];
max_shear_stress = [2.31,32.96,35.86, 162.096,256.389];
max_major_princ_stress = [10.11, 203.236, 304.617,2022.91,5031.787];

figure()
plot(Needle_gauge_nb,max_major_princ_stress ,'-o', 'LineWidth',1.5)
hold on
grid on
plot(Needle_gauge_nb, max_shear_stress,'-o', 'LineWidth',1.5)
ylabel('Maximum stress level [Pa]', 'FontSize',12)
xlabel('Needle gauge number')
legend('Major principal stress','Shear stress')
```

Appendix I

Non-linear stress-strain curve

I.1 Strain-strain curve computation: Matlab code

```
%% ------------------------------------------------------------------------%
% Master thesis - Mathematical model of GAE method
% Academic year 2021-2022
% Authors: Estelle Pitti
% Stress-strain curve computation at the node 437 and vertical normal
% components of the stress and strain tensor
%  linear interpolation of the curve is provided to show the degree of
%  non-linearity of the strain-strain curve
%
%% ------------------------------------------------------------------------%

clear all
close all
clc

% Extracting the stress and strain data
file = readtable('stress-strain.csv');
E=file.Epsilon;
S=file.Sigma;
% Converting the strain in percentage
E_= E*100;
%Linear interpolation
p = polyfit(E_,S,1);
S_fit = p(1)*E_ +p(2);
% Strain-strain curve
figure()
plot(E_,S)
% Linear interpolation to check the degree of non-linearity of
```

```
    the
% stress-strain curve
hold on
plot(E_,S_fit)
grid on
xlabel('Strain [%]')
ylabel('Stress [Pa]')
legend('Node 437','Linear interpolation')
```

I.2 Strain-strain curve non-linearity evaluation

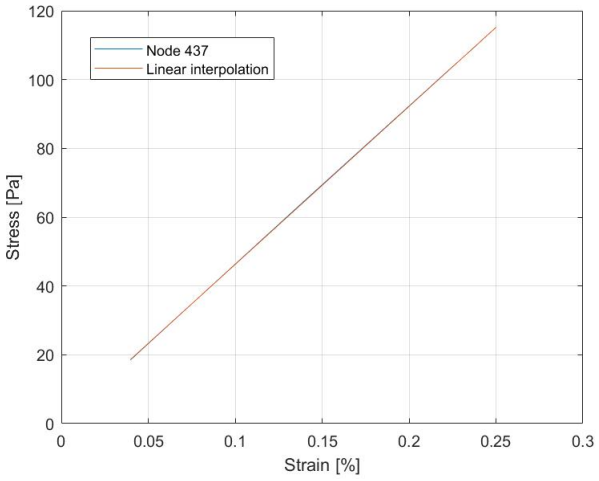

Figure I.1: Stress-strain curve at the node 432 with the vertical normal component of the stress and strain tensor and the linear interpolation of the curve

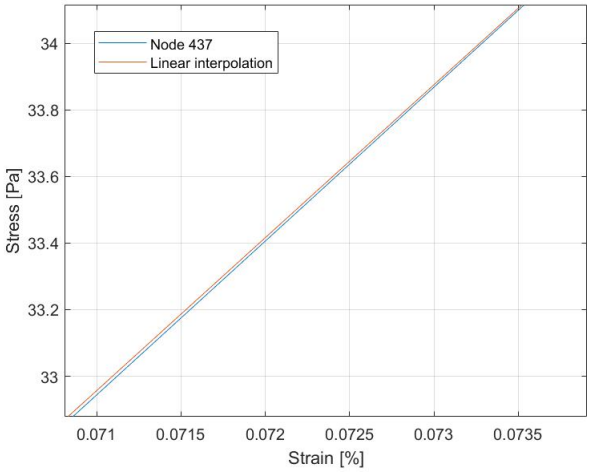

Figure I.2: Zoom on the linear interpolation and stress-strain curve to show the non linearity